Coordination Chemistry Reviews, 68 (1985) 169–278
Elsevier Science Publishers B.V., Amsterdam – Printed in The Netherlands

THE NUCLEAR MAGNETIC RESONANCE PROPERTIES OF CHROMIUM, MOLYBDENUM AND TUNGSTEN COMPOUNDS

MARTIN MINELLI and JOHN H. ENEMARK

Department of Chemistry, University of Arizona, Tucson, Arizona 85721 (U.S.A.)

ROBERT T.C. BROWNLEE, MAXWELL J. O'CONNOR† and ANTHONY G. WEDD

Department of Chemistry, La Trobe University, Bundoora, Victoria 3083 (Australia)

(Received 2 January 1985)

CONTENTS

† Deceased 18 March 1985; this review is dedicated to his memory.

0010-8545/85/$38.50

ABBREVIATIONS

[12]aneN$_3$	1,5,9-triazacyclododecane
[9]aneN$_3$	1,4,7-triazacyclononane
[9]aneS$_3$	1,4,7-trithiacyclononane
acacH	acetylacetone
acamH	*N*,*N*-diethylacetoacetamide
B(pz)$_4$	tetrakis(1-pyrazolyl)borate
bpy	2,2′-bipyridine
Br$_4$-cat	3,4,5,6-tetrabromocatechol
Bu^i	isobutyl
Bu^n	n-butyl
Bu^s	s-butyl
Bu^t	t-butyl
Bz	benzyl
cat	catechol
cht	cycloheptatriene
Cp	cyclopentadienide, $C_5H_5^-$
Cy	cyclohexyl
cystH	L-cysteine
depe	1,2-bis(diethylphosphino)ethane
dien	diethylenetriamine
dpmH	dipivaloylmethane
dppe	1,2-bis(diphenylphosphino)ethane
dppm	bis(diphenylphosphino)methane
dppp	1,3-bis(diphenylphosphino)propane
dptpe	1,2-bis(di-*p*-tolylphosphino)ethane
dtne	1,2-bis(1,4,7-triaza-1-cyclononyl)ethane
dttdH$_2$	2,3,8,9-dibenzo-1,4,7,10-tetrathiadecane
edtaH$_4$	$\{(HO_2CCH_2)_2NCH_2\}_2$
eedtaH$_4$	$O\{CH_2CH_2N(CH_2CO_2H)_2\}_2$
egtaH$_4$	$\{CH_2OCH_2CH_2N(CH_2CO_2H)_2\}_2$
Et	ethyl
HB(Me$_2$pz)$_3$	hydrotris(3,5-dimethyl-1-pyrazolyl)borate

$HB(pz)_3$	hydrotris(1-pyrazolyl)borate
$hbdabH_2$	*N*,*N*′-bis(2-hydroxybenzyl)-1,2-diaminobenzene
$hbdaeH_2$	*N*,*N*′-bis(2-hydroxybenzyl)-1-diaminoethane
$hedtaH_3$	$(HO_2CCH_2)_2NCH_2CH_2N(CH_2CO_2H)CH_2CH_2OH$
$hpdtaH_4$	$(HO_2CCH_2)_2NCH_2CH(OH)CH_2N(CH_2CO_2H)_2$
$idaH_2$	$NH(CH_2CO_2H)_2$
L-cysORH	L-cysteine-R-ester (R = Me, Et)
m-xyl	*m*-xylene
$mabH_2$	2,3-bis(2-mercaptoanilino)butane
$maeH_2$	1,2-bis(2-mercaptoanilino)ethane
Me	methyl
MepenH	*O*-methyl-(*S*)-penicillamine
mes	mesitylene
Me_2bpy	4,4′-dimethyl-2,2′-bipyridine
$Me_3[9]aneN_3$	*N*,*N*′,*N*″-trimethyl-1,4,7-triazacyclononane
Me_5Cp	pentamethylcyclopentadienide
$mpeH_2$	*N*,*N*′-bis(2-mercapto-2-methylpropyl)ethylenediamine
mqH	8-mercaptoquinoline
NMP	*N*-methylpyrrole
$ntaH_3$	$N(CH_2CO_2H)_3$
ox	oxalate
o-xyl	*o*-xylene
p-xyl	*p*-xylene
$pdtaH_4$	(R,S)-$(HO_2CCH_2)_2NCH_2CHMeN(CH_2CO_2H)_2$
$penH_2$	α-penicillamine
Ph	phenyl
phen	1,10-phenanthroline
phobb	1-n-propyl-2-α-hydroxylbenzylbenzimidazole
pip	piperidine
pn	1,2-diaminopropane
Pr^i	isopropyl
Pr^n	n-propyl
py	pyridine
qH	8-hydroxyquinoline
$RidaH_2$	$RN(CH_2CO_2H)_2$, (R = Me, Et, Bz)
$smaH_2$	*N*-(salicylidene)-2-mercaptoaniline
THF	tetrahydrofuran
tol	toluene
triphos	bis(2-diphenylphosphinoethyl)phenylphosphine
3,5-Bu^thbdacH_2	*N*,*N*′-bis(3,5-di-t-butyl-2-hydroxybenzyl)-*cis*-1,2-diaminocyclohexane
5-X-saeH_2	*N*-(5-X-salicylidene)-2-aminoethanol
5-X-sapH_2	*N*-(5-X-salicylidene)-2-aminophenol

A. INTRODUCTION

The chemistry of the Group 6 * metals chromium, molybdenum, and tungsten is exceedingly versatile [1–7]. Ten oxidation states, VI(d^0) to −III(d^9) are known, and there is a tendency in the higher oxidation states (II–VI) for condensation to occur giving polynuclear species such as the polyoxometallates [6]. The organometallic chemistry [3] of the lower oxidation states is particularly well developed. In addition to the intrinsic interest of such intriguingly complex chemistry, a further stimulus arises from the use of the metals in technologies such as steelmaking and electroplating and in catalyst systems employed by the petrochemical industry. The biological role of these metals (especially that of molybdenum [7] in the nitrogenase and other enzyme systems) is also an area of intense interest.

One incentive for development of the nuclear magnetic resonance (NMR) spectroscopy of the Group 6 metals is the lack of a direct spectroscopic probe for diamagnetic metal sites to complement the role of electron spin resonance as a direct probe for paramagnetic centers. The development of an increasing accessibility to X-ray absorption spectroscopy [8] and the structural information available from the associated fine structure (EXAFS) is another aspect of this quest for a direct spectroscopic probe.

(i) History

Certain aspects of the NMR properties of the Group 6 metals have been reviewed [9–14], and a convenient starting point for the present detailed review is the article by Kidd and Goodfellow [9], which covered the literature to 1976. At that time, only ^{183}W of the four magnetic nuclei ^{53}Cr, ^{95}Mo, ^{97}Mo and ^{183}W (Table 1) had attracted any attention, because of the relatively high sensitivity of ^{1}H–{^{183}W}, ^{19}F–{^{183}W} and ^{31}P–{^{183}W} double-resonance and ^{1}H–{^{183}W, ^{31}P} triple-resonance experiments. The lack of interest in direct observation of the four Group 6 nuclei was because they are among the least sensitive of NMR nuclei. The reasons for this low sensitivity include:

(a) Low receptivities. In general terms, signal intensity (receptivity, D) is proportional to $\gamma^3 NI(I+1)$, where γ is the magnetogyric ratio, N the natural abundance of the isotope and I the nuclear spin quantum number. The low receptivities relative to ^{1}H(D^{P}) and ^{13}C(D^{C}) listed in Table 1 are a consequence of the low absolute magnitudes of γ ($1.1–1.8 \times 10^7$ rad T^{-1} s^{-1}

* This group notation is in accord with recent action by the IUPAC and ACS nomenclature committees.

TABLE 1

Nuclear properties [a]

Nucleus	Spin I, $\hbar$	Natural abundance N, atom %	Magnetic moment μ, μ_N	Magnetogyric ratio γ, 10^7 rad T^{-1} s^{-1}
^{53}Cr	3/2	9.55	−0.6113	−1.5120
^{95}Mo	5/2	15.72	−1.081 [e]	−1.750 [e]
^{97}Mo	5/2	9.46	−1.104	−1.787
^{183}W	1/2	14.40	0.2025	1.120

[a] Data from R.K. Harris, Nuclear Magnetic Resonance, Spectroscopy, Pitman, London, 1983, pp. 230–233. [b] Resonance frequency corrected to the field strength at which the protons of tetramethylsilane resonate at exactly 100 MHz. [c] Ref. 41. [d] R.T.C. Brownlee, M.J.

compared with the range for known nuclei of 0.4–29 × 10^7 rad T^{-1} s^{-1}) and with the low values of N (9–16 atom %).

(b) Low resonance frequencies. Resonance frequencies are proportional to γ and so the reference standards $[MO_4]^{2-}$ listed in Table 1 resonate in the low frequency range (4–7 MHz) in a magnetic field in which the protons of tetramethylsilane resonate at exactly 100 MHz. The fact that low receptivities and low frequencies normally go hand in hand provided little incentive for the early development of low-frequency multinuclear NMR probes.

(c) Nuclear electric quadrupole moments. ^{53}Cr, ^{95}Mo and ^{97}Mo have $I > 1/2$ and possess nuclear quadrupole moments, Q, which can couple to the local electric field gradient, q, providing a mechanism of rapid relaxation. This leads to large linewidths and low resolution. The quadrupole relaxation mechanism normally dominates the relaxation processes of quadrupolar nuclei. For rapidly rotating molecules whose motion is isotropic with correlation time τ_c, the linewidth is given by eqn. (1) [15]

$$W_{1/2} = (\pi T_{2q})^{-1} = (\pi T_{1q})^{-1} = \frac{3\pi}{10}\left(\frac{(2I+3)}{I^2(2I-1)}\right)\left(\frac{e^2 q_{zz} Q}{h}\right)^2\left(1+\frac{\eta^2}{3}\right)\tau_c \quad (1)$$

where η is the asymmetry parameter for q and

$$\eta = (q_{yy} - q_{xx})/q_{zz} \quad (2)$$

Note that an increase in the electric field gradient q (due to lowering of

Quadrupole moment Q, 10^{-28} m^2	NMR frequency [b] Ξ, MHz	Reference sample	Relative receptivity	
			D^P	D^C
−0.15(5) [c]	5.642510 [d]	2 M $Na_2[CrO_4]$ D_2O, apparent pH 11, 20°C	8.62×10^{-5}	0.489
−0.015(4) [f]	6.516926 [g]	2 M $Na_2[MoO_4]$ D_2O, apparent pH 11, 20°C	5.14×10^{-4}	2.92
0.17(4) [f]	6.653692 [d]	as for ^{95}Mo	3.29×10^{-4}	1.87
0	4.166388 [d,h]	2 M $Na_2[WO_4]$ D_2O, apparent pH 11, 20°C	1.06×10^{-5}	0.0599

O'Connor, unpublished observation. [e] The sign given in the reference of footnote a is in error. [f] M. Dubke, W. Jitschin, G. Meisel, and W.J. Childs, Phys. Lett. A, 65 (1978) 109. [g] Ref. 16. [h] Ref. 138.

symmetry: "quadrupolar broadening") or in τ_c ("correlation time broadening") both lead to an increase in linewidth.

(ii) Current status

Until recently these technical and theoretical difficulties limited NMR studies of Group 6 nuclei to NMR specialists and dissuaded most chemists from applying the technique to current research problems. The advent of commercially-available Fourier transform (FT) spectrometers equipped with superconducting magnets of moderately high field and multinuclear low-frequency probes has encouraged chemists to examine the insensitive Group 6 nuclei more closely. Rapid relaxation of the quadrupolar nuclei allows rapid data collection in the FT mode, permitting an improvement in signal intensity which can compensate partially for large linewidths. Practical experience for Group 6 [16] and other nuclei (e.g. ^{17}O, ^{43}Ca) [17,26b] is leading to the development of tactics to improve sensitivity further (see Section C(vi)). The prospects for using commercially available multinuclear Fourier transform NMR spectrometers to probe the chemistry of Group 6 metals directly are summarized in the next paragraphs.

For ^{53}Cr ($I = 3/2$) a combination of low receptivity and a quadrupole moment of intermediate magnitude (note the dependence of $W_{1/2}$ on Q^2 in eqn. 1) ensures that direct observation remains difficult except for sites of very high point symmetry (i.e. of low q). Section D reviews the limited NMR data for ^{53}Cr.

About 70% of the NMR results for Group 6 metals involve ^{95}Mo, and the great majority of such studies have appeared since 1980. This quadrupolar nucleus ($I = 5/2$) has the highest receptivity of the Group 6 nuclei and a reasonably small Q (Table 1). The resonance frequency is low, but higher than either ^{53}Cr or ^{183}W and is accessible by commercially-available low-frequency broadband probes (Section C). The dependence of $W_{1/2}$ on the components of q (eqn. 1) means that ^{95}Mo resonances can be narrow (0.3 Hz for $[MoS_4]^{2-}$ [19]) or broad (1900 Hz for $Mo_2(O_2CBu^n)_4$ [20]) depending upon the point symmetry of the site. The linewidths of a large number of compounds are sufficiently narrow (< 1000 Hz) for convenient measurement by current commercial instrumentation, and ^{95}Mo NMR data available to the authors through July 1984 for over 450 compounds are tabulated and discussed in Section E.

^{97}Mo($I = 5/2$) has a similar receptivity and resonance frequency to ^{95}Mo, but $Q(^{97}Mo)/Q(^{95}Mo) = 11.4$. Such a large difference between the quadrupole moments of two isotopes of one element with identical spin is exceptional [18] and arises from the fact that ^{95}Mo has an outer half-filled $d_{5/2}$ neutron shell, which makes no contribution to the permanent quadrupole moment. The addition of two neutrons to this shell to create ^{97}Mo results in a relatively large change in Q. The dependence of $W_{1/2}$ on Q^2 (eqn. 1) means that ^{97}Mo NMR linewidths are two orders of magnitude greater than those of corresponding ^{95}Mo resonances (Fig. 1), and therefore ^{95}Mo is usually the nucleus of choice for chemical studies. However, if the ^{97}Mo

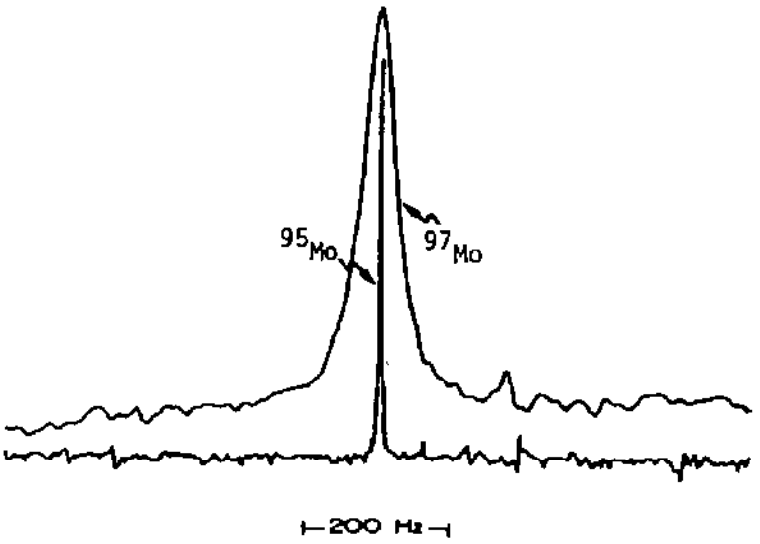

Fig. 1. ^{95}Mo and ^{97}Mo NMR spectra of $Na_2[MoO_4]$ (1 M in 3 M NaCl, pH 12). From ref. 18, with permission.

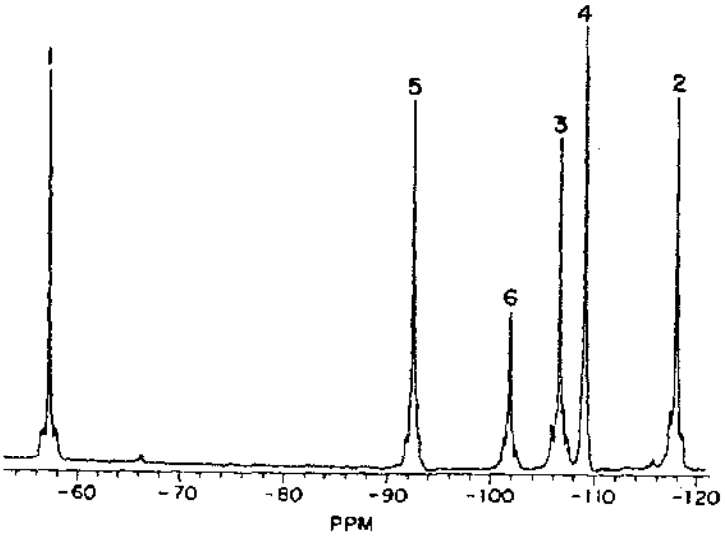

Fig. 2. ^{183}W NMR spectrum of α-$(Bu^n_4N)_5[TiPW_{11}O_{40}]$ in MeCN/MeCN-d_3. Concentration, 0.23 M (11.4 g in 12.5 ml); accumulation time, 113.8 h (195 000 scans with repetition time, 2.1 s). Adapted from ref. 151 with permission. See Fig. 27(b) for numbering system.

resonances are observable, the existence of two isotopes with different relaxation rates can allow convenient investigation of chemical exchange reactions [18].

Direct observation of ^{183}W ($I = 1/2$) can be difficult and time-consuming because of long relaxation times (e.g. T_1 for $W(CO)_6$ is > 80 s). Figure 2 gives an indication of the commitment needed to record a multi-line spectrum of good quality for a polyoxotungstate. However, the narrow linewidths associated with ^{183}W NMR allow the resolution of ^{183}W–^{183}W spin–spin coupling, which provides key structural information for these complex molecules in solution (Section F). The low frequency of ^{183}W is near the lower limit of most commercially available broadband probes.

B. REFERENCE STANDARDS

The NMR frequencies listed in Table 1 refer to 2M solutions of $Na_2[MO_4]$ (M = Cr, Mo, W) in D_2O at an apparent pH of 11. All chemical shifts quoted in this review are referenced to these standards as 0 ppm. Chemical shifts previously referenced to a saturated solution of $M(CO)_6$ in THF or to neat WF_6 have been referenced to the above standards by using $\delta(^{95}Mo)$ for $Mo(CO)_6 = -1856$ ppm [50], $\delta(^{183}W)$ for $W(CO)_6 = -3483$ ppm and $\delta(^{183}W)$ for $WF_6 = -1117$ ppm. The standards of Table 1 are easy to observe, indefinitely stable and resonate towards the center of the known chemical shift scales. Compounds which resonate at a higher frequency than

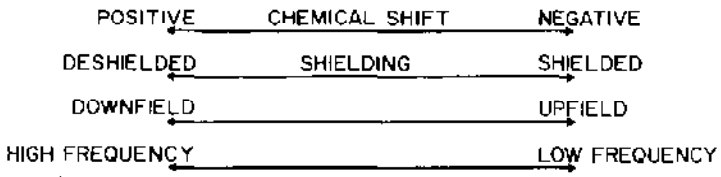

Fig. 3. NMR terminology.

the $[MO_4]^{2-}$ reference have positive chemical shifts, and the metal nucleus is deshielded relative to that of the reference complex. In this review chemical shift changes will be described exclusively as shielding changes. Thus a decrease in the metal chemical shift means that the shielding at the metal nucleus has increased. The relationships between chemical shift, shielding and the older notations (upfield/downfield and high frequency/low frequency) are illustrated in Fig. 3.

C. EXPERIMENTAL TECHNIQUES

Direct observation of the insensitive Group 6 nuclei by FT NMR requires carefully planned and executed experiments in order to obtain chemically-useful information in a reasonable amount of time. The quadrupolar Group 6 nuclei, ^{53}Cr, ^{95}Mo and ^{97}Mo, exhibit wide variations in chemical shift and linewidth. The relaxation times, T_{1q} and T_{2q}, for a quadrupolar nucleus of spin I are given by eqn. (1), and it can be seen that broad lines correspond to short relaxation times. Sections C(i)–(vi) discuss factors relevant to observation of the quadrupolar nuclei. The ^{183}W ($I = 1/2$) nucleus normally has very sharp ($W_{1/2}$, 1 Hz) resonance signals and correspondingly long relaxation times. Section C(vii) highlights observation of ^{183}W NMR.

(i) Spectrometer properties

The requirements and characteristics of a modern multinuclear NMR spectrometer have recently been reviewed [21]. Briefly, such an instrument must be capable of generating a wide range of frequencies, selecting and amplifying a frequency, and detecting the absorption of the chosen frequency by the sample. The key component for flexible and sensitive performance by a multinuclear NMR spectrometer is the probe itself. Most standard multinuclear spectrometers now meet the above requirements.

(a) Probe pulse characteristics

The inherently low sensitivity of the Group 6 metals implies that the exciting pulse should be close to 90° in order to maximize the signal from

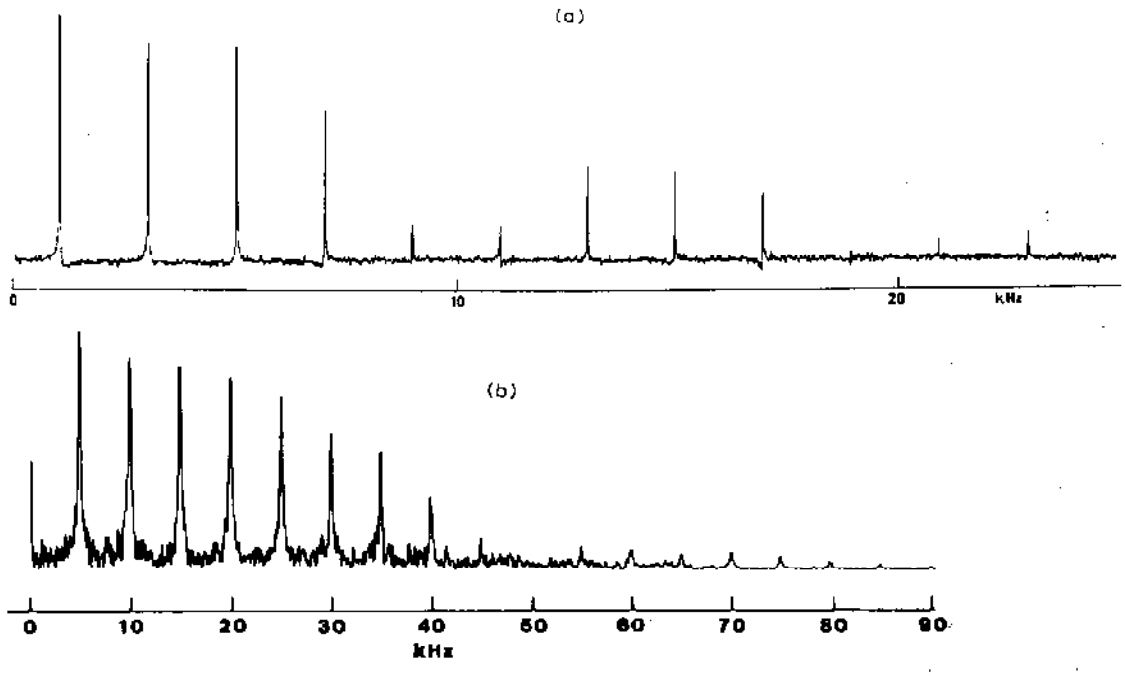

Fig. 4. Nodes in ^{95}Mo NMR power spectra: (a) 100 μs sample pulse using a probe with a 125 μs 90° pulse; (b) 20 μs sample pulse using probe with a 31 μs 90° pulse; note different scale.

the sample. However, the large chemical shift ranges of Group 6 metals can easily result in an absorption frequency for the sample which is 30 kHz or more away from the carrier frequency. It is recognized that there is a severe fall off in the power transmitted at frequencies outside the reciprocal of the pulse width from the carrier frequencies [22] and accurate intensities should thus be determined fairly near the carrier frequency. Clearly, increasing the pulse power and decreasing the 90° pulse width will increase the frequency range which can be sampled in a single experiment. Figures 4(a) and 4(b) illustrate the fall off in transmitted power for two probes with vastly different 90° pulses.

The pulse characteristics of commercially-available broadband probes have improved rapidly in recent years. Early broadband probes with variable capacitors had 90° pulses as long as 125 μs [23]! In addition the 90° pulse increased with decreasing frequency. Contemporary digitally-selected broadband probes have 90° pulses as short as 35–40 μs, and the pulses are nearly constant over the entire frequency range of the probe [21,24].

(b) Acoustic ringing and probe ringing

The electromagnetic generation of ultrasonic waves in metallic materials leads to a spurious signal known as "acoustic ringing" which is coherent with the exciting pulse [21,25]. Accumulation of this spurious signal in the

free induction decay (FID) can completely obliterate the signals from the sample, especially those of low concentrations requiring extended accumulation. Acoustic ringing is most severe under conditions of high magnetic field, high pulse power and low exciting frequencies (20 MHz and below), and is highly dependent upon the materials used to construct the probe, especially the probe body. Aluminum, which is commonly used in probe construction, shows one of the largest acoustic ringing responses of any metal, and therefore is a poor material to use for low frequency probes. Lead is one of the most effective metals for reducing acoustic ringing [25].

The ringing of the electronic circuitry of a sensitive probe (high probe Q factor) also contributes to the total spurious signal which is coherent with the pulse. For the remainder of this review acoustic ringing and the ringing of the probe circuitry will be collectively called "probe ringing".

Probe ringing appears as a sharp peak (Fig. 5(a)) at the beginning of the FID and is transformed to a broad peak (rolling baseline) (Fig. 5(b)) unless special precautions are taken. A rolling baseline makes it especially difficult to detect broad resonances, and consequently probe ringing is the limiting factor in observing broad signals at low concentration [26].

A convenient compound for evaluating the performance of an NMR spectrometer for ^{95}Mo NMR (Figs. 4 and 5) is $MoO_2(ONC_5H_{10})_2$. This compound is easily synthesized [27] and is soluble in a variety of organic solvents. The linewidth (160 Hz in $HCONMe_2$) is more representative of low-symmetry complexes than $[MoO_4]^{2-}$, but is still sufficiently small to enable good signal-to-noise data to be acquired in a few minutes.

(ii) Observation of narrow signals

According to eqn. 1, a linewidth of 30 Hz corresponds to a relaxation time of 11 ms. When using the JEOL FX-200 spectrometer a 90° pulse with a spectral width of 10 kHz is used to acquire 4K data points, resulting in an acquisition time of 205 ms. This results in a digital resolution of 5 Hz and hence defines the line position with reasonable accuracy. A preacquisition delay (dead time) of 750 μs is sufficient to allow for acoustic ringing to decay, and the base line is very flat even for long accumulation on dilute solutions. Signal loss over this first 750 μs is insignificant for narrow signals. In general, observation of ^{95}Mo resonances of this linewidth is relatively easy.

(iii) Observation of broad signals

A linewidth of 1000 Hz corresponds to a relaxation time (T_{2q}) of 318 μs. With a preacquisition delay of 700 μs only 11% of the signal remains to

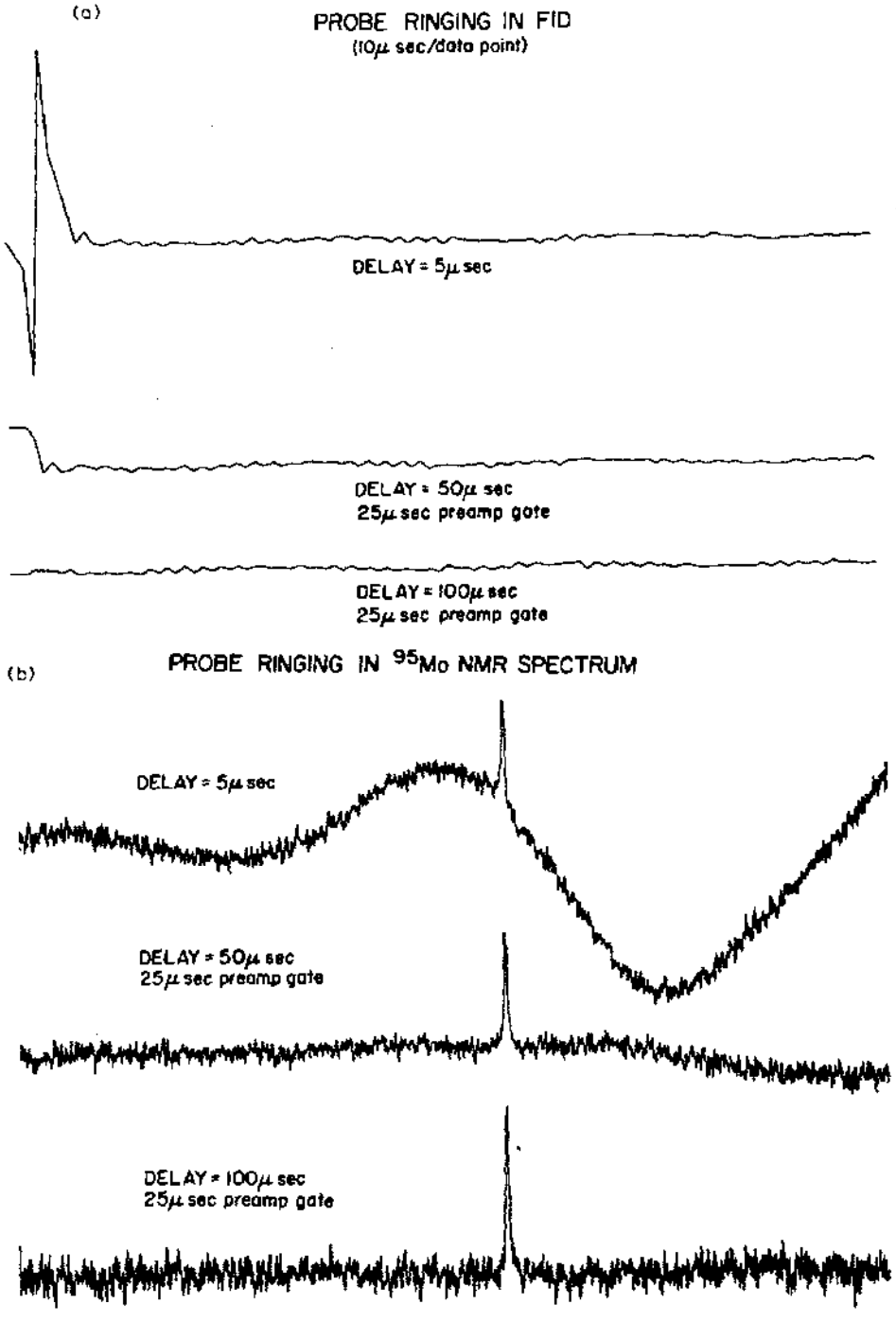

Fig. 5. Probe ringing from modified Bruker WM-250 spectrometer described in text, $MoO_2(ONC_5H_{10})_2$ in CH_2Cl_2: (a) FID, 10 μs/data point, pre-acquisition delays of 5, 50, 100 μs; (b) transformed spectra from (a).

detect. Thus, broad line species are hard to observe, both because a broad signal results in low amplitude and because the fast relaxation rate makes the signal difficult to distinguish from probe ringing and its resultant rolling baseline. Consequently, a minimum preacquisition delay consistent with an acceptable baseline is needed, and the data must be acquired at the fastest possible rate. For example, if the preacquisition delay can be reduced to 100 μs (Fig. 5), 73% of the signal will remain. In a typical experiment, a 20–30 μs pulse with a 50 kHz spectral width is digitized into 4K data points to give a resolution of 24 Hz. Clearly, the observation of broad lines is also facilitated by a short 90° pulse which permits a large frequency range (50 kHz) to be sampled in a single experiment with a tip angle close to 90° (Section C(i), Fig. 4). It is our experience that dilute samples of molecules having broad lines are difficult to observe.

(iv) Chemical shifts

As is the case for all nuclei where a single line spectrum is produced, extreme care must be taken to check that the signal is not folded. For quadrature detection, repeating the spectrum with a different spectral width is necessary. A relatively long preacquisition delay can result in phasing problems when two or more peaks are present, and care must be taken to phase each peak separately in order to determine accurate chemical shifts.

The actual chemical shifts are measured by comparing the absolute frequency of the unknown sample with the absolute frequency of the external standard. The frequency difference is then converted to ppm from the standard frequency. Positive chemical shifts are "downfield" and correspond to shifts to higher frequency (Fig. 3).

Normal experimental procedure is to lock and shim the spectrometer on the deuterium resonance of the standard reference, before running all other samples unlocked, without altering the field or shim controls. However, when very long accumulations (> 24 h) are necessary, deuterated solvents or an internal capillary tube containing D_2O are used to maintain the lock signal. The errors associated with measured chemical shifts are ± 1 ppm for linewidths less than 200 Hz; ± 3 ppm for linewidths in the range 200 to 500 Hz; and ± 8 ppm for linewidths greater than 500 Hz.

(v) Linewidths

Exponential broadening is usually employed to improve the signal-to-noise ratio, and it is normally necessary to correct the measured half width for exponential broadening. The error in measuring linewidths is ± 5 Hz for linewidths less than 100 Hz; ± 20 Hz for linewidths between 100 and 400 Hz; and ± 60 Hz for linewidths in excess of 400 Hz.

(vi) Methods of improving sensitivity

It is evident that the observation of dilute samples with broad lines is difficult. A number of methods can be used to increase the possibility of observing such signals.

(a) Increasing the number of NMR-active nuclei in the sample

This can be achieved by increasing the concentration of the sample in solution, by increasing N (the fraction of NMR-active nuclei) through isotopic enrichment, or by increasing the size of the sample. Increasing the sample size requires a larger diameter probe. However, larger probes generally have longer 90° pulses. Thus, a typical exciting pulse (20–30 μs) will produce a smaller tip angle (lower sensitivity) which partially negates the increased volume of a larger probe. For ^{95}Mo the net sensitivity for a 20–30 μs exciting pulse using a standard 10 mm broadband probe is often better than for a standard 15 mm broadband probe, and the 10 mm probe requires only about half as much sample [23,24,28].

(b) Decreasing the molecular correlation time (τ_c)

Equation 1 shows that the relaxation time, and hence the linewidth, is related to the molecular correlation time (τ_c). By assuming a spherical solute molecule in a medium of viscosity η', the rotational correlation time τ_c is given by eqn. 3

$$\tau_c = \eta' V f / kT \tag{3}$$

where f is a microviscosity factor (0.16 for liquids) and V is the volume of the solute molecule. It is evident [16,17] that either lowering the viscosity of the solvent (Fig. 6), or measuring the sample at a higher temperature, will reduce the molecular correlation time and thereby decrease the spectral half width ($W_{1/2}$) of the signal.

(c) Increasing the sensitivity of the spectrometer

High resolution superconducting Fourier transform NMR spectrometers are primarily designed for studies of sensitive or commonly-studied nuclei with $I = 1/2$, e.g. ^{1}H and ^{13}C, rather than for low-frequency quadrupolar nuclei such as ^{95}Mo. The sensitivity of commercial NMR spectrometers such as the Bruker WM-250 for ^{95}Mo can be enhanced by several modifications and additions.

A fixed-frequency 10 mm probe specifically tuned for ^{95}Mo (16.3 MHz) has a somewhat shorter 90° pulse than a digitally selected broadband probe and can accept more power without arcing [24]. Fixed-frequency probes also seem less prone to ringing. The ringing is further reduced by shielding the probe with lead rather than with aluminum.

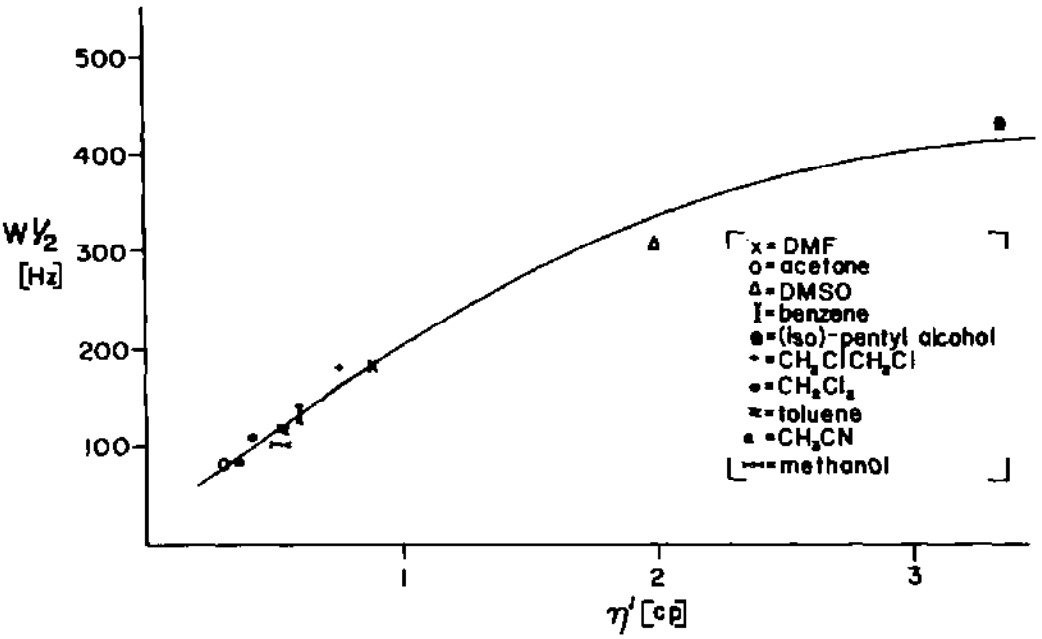

Fig. 6. Dependence of linewidth ($W_{1/2}$) on solvent viscosity (η') for $Mo(NO)_2(acac)_2$. Adapted from ref. 28, with permission.

The materials and circuitry of the probe are not the only source of ringing in the spectrometer. Ringing can be further decreased by inserting a fixed-frequency duplexer and preamplifier between the probe and the broadband preamplifier [29]. The arrangement allows the preacquisition delay to be reduced from 200 to 100 μs with no loss of spectral quality. For a 1000 Hz line this will increase the sensitivity by 60%.

The output of low-frequency power from a broadband spectrometer is often low and can be contaminated with overtones and other frequencies [24]. If the transmitter output is passed through a narrow-band linear amplifier then the quality of the low-frequency power is improved, and the 90° pulse is reduced from 35 to 26 μs [30]. This changes the tip angle for an exciting pulse of 20 μs from 51° to 69°, which in turn increases the overall sensitivity by about 20%, provided that the increased power does not significantly increase the ringing (Section C(i)(b)).

The spectra in Figs. 5(a) and 5(b) were obtained on a modified Bruker WM-250 system using a Bruker fixed-frequency 10 mm ^{95}Mo probe (16.3 MHz) with lead shielding. A Doty Scientific duplexer and preamplifier with a 16 MHz frequency center was inserted between the probe and the Bruker broadband preamplifier. The transmitter output was amplified with a Heathkit SB-201 (1 kW) linear amplifier, with input attenuated to give a 26 μs 90° pulse [30].

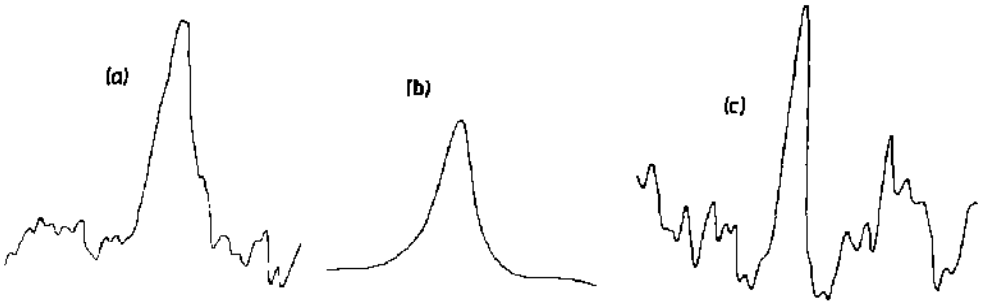

Fig. 7. ^{95}Mo NMR spectra. (a) [Mo] = 1 M; 1.36×10^6 transients; pre-acquisition delay 800 μs; FX200 multilow probe. (b) [Mo] = 1 M; 1×10^4 transients; pre-acquisition delay 100 μs; transverse probe. (c) [Mo] = 5×10^{-3} M; 9.6×10^6 transients; pre-acquisition delay 350 μs; transverse probe. Reproduced from ref. 20, with permission.

(d) Using a transverse probe to increase sensitivity

In superconducting magnets, the sample tube axis is parallel to the principal magnetic field axis and this leads to inefficient transmitter/receiver coil design. This problem is overcome by using a probe in which the sample tube is aligned horizontally and the transmitter coil is wound around the sample tube. A threefold increase in signal to noise over the normal probe configuration is expected [31] for equivalent sample volumes. An inconvenience of the transverse probe is that it must be removed from the magnet each time a sample is changed.

A ^{95}Mo transverse probe constructed from copper wire has been used recently [20]. Figure 7 provides an example of the improved sensitivity of this new probe for $Mo_2(O_2CBu^n)_4$ in tetrahydrofuran ($W_{1/2}$, ca. 1500 Hz). Part of the increased sensitivity of the probe results from the transverse design. However, substantial sensitivity enhancement was realized because the decreased acoustic ringing (Section C(i)–(iii)) of the new probe (which was shielded with lead rather than aluminum or copper) enabled the pre-acquisition delay to be reduced. With this probe a preacquisition delay of 350 μs for a JEOL FX-200 spectrometer provided flat base lines after 10^7 transients, permitting convenient detection of solutions of [Mo] of 0.01 M with linewidths greater than 1500 Hz. A reduction in the preacquisition delay from 800 to 350 μs for a signal of $W_{1/2}$ of 1000 Hz represents a sensitivity enhancement of four, which provides an overall twelve-fold increase in sensitivity for this experiment with this transverse probe.

(e) Using multiple pulse sequences to reduce probe ringing

Since probe ringing is coherent with the exciting pulse (Section C(i)(b)) several multiple pulse sequences have been designed to subtract the ringing

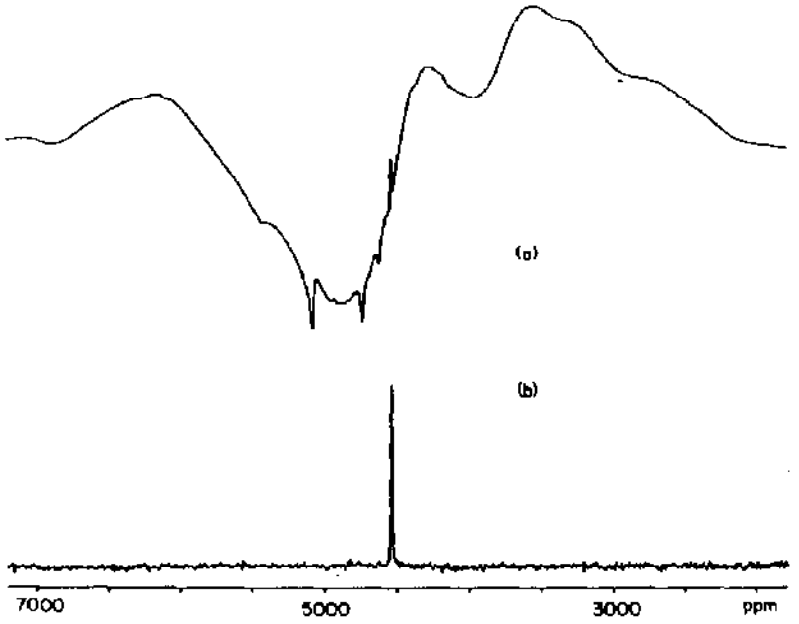

Fig. 8. ^{99}Ru spectrum of $[Ru(bpy)_3]^{2+}$: (a) normal acquisition with 5 μs pre-acquisition delay; (b) acquisition with multiple pulse sequence described in ref. 21. Reproduced from ref. 21, with permission.

signal from the accumulating FID [21]. Spectacular sensitivity enhancements with a preacquisition delay of only 5 μs have been achieved for systems in which relatively sharp lines are pulsed near the carrier frequency [21] (Fig. 8). However, the multiple pulse technique does not necessarily make it easier to detect broad signals or signals which are far from the carrier frequency. Several 180° pulses are used in the multiple pulse sequence. The duration of these pulses and the fall off of transmitted power away from the exciting frequency (Fig. 4) become critical to the success of the method. A probe with a 90° pulse of 20 μs or less is probably necessary if this technique is to be generally useful for obtaining ^{95}Mo NMR signals from new compounds or from solutions containing several different molybdenum centers with diverse chemical shifts.

(f) Conclusions

There is an urgent need for the development of high power (90° pulse < 20 μs), large volume (> 10 mm i.d.), low-frequency probes with satisfactory probe ringing characteristics. Such probes, together with the development of suitable pulse sequence techniques, will facilitate examination of low-frequency NMR nuclei such as ^{53}Cr and ^{95}Mo.

(vii) Observation of ^{183}W resonances

Direct observation can be very time-consuming (Fig. 2), but is being increasingly utilized (Section F). A valuable compilation of ^{183}W chemical shifts and spin–spin coupling constants has been obtained by McFarlane et al. [32,33] utilizing indirect heteronuclear $^{1}H-\{^{183}W\}$, $^{19}F-\{^{183}W\}$, $^{13}C-\{^{183}W\}$ double resonance and, in certain cases, $^{1}H-\{^{183}W, ^{31}P\}$ triple resonance. Such methods can provide chemical shifts in a few minutes provided additional decoupling channels are available to the spectrometer, but are restricted to species in which ^{183}W is coupled to a nucleus of high receptivity. Another approach is to take advantage of coupling to a second nucleus to enhance the ^{183}W signal by J-polarization transfer between the coupled spins, making use of the INEPT pulse sequence train [34].

The shiftless relaxation agent $Cr(acac)_3$ has been used to shorten the relaxation time, T_1, and allow faster acquisition of data. The ^{183}W resonances were not broadened under the conditions employed [35].

D. CHROMIUM-53 NMR

Resonances for only two compounds [36–39] have been reported with that of $Cr(CO)_6$ ($W_{1/2}$, 17 Hz) [37] being shielded by 1795 ppm relative to $[CrO_4]^{2-}$ ($W_{1/2}$, 11 Hz).

The $[CrO_4]^{2-}$ resonance was first reported [36] in 1969 when the pH-dependence of its linewidth was followed. The signal broadens upon acidification due to exchange with the generated $[Cr_2O_7]^{2-}$. The chemical shift shows a concentration dependence (increased shielding with increased concentration) which is itself cation dependent: $Na^+ < K^+ < Rb^+ < NH_4^+ < Cs^+$ [37]. The magnitude is ca. -1 ppm molal^{-1} for Na^+ and ca. -20 ppm molal^{-1} for Cs^+.

Poorly-resolved satellite peaks are seen [39] at the base of the central ^{53}Cr resonance in aqueous solutions of $[CrO_4]^{2-}$ enriched to 35 atom % in ^{17}O ($I = 5/2$). Computer analysis yields $J(^{53}Cr-^{17}O) = 10 \pm 2$ Hz. A linear dependence of $J(M-^{17}O)$ upon the atomic number of M was noted for the series $[VO_4]^{3-}$, $[CrO_4]^{2-}$ and $[MnO_4]^{-}$.

Relaxation times have been measured [38] in aqueous solutions of $K_2[CrO_4]$ (0.5–3.0 molal). A slight increase in T_1 (determined by the inversion-recovery method) occurred as the concentration decreased and extrapolation to zero concentration gave $T_1 = 55 \pm 5$ ms. The T_1 values at the lower concentrations were similar in magnitude to the T_2 values determined from the linewidths which suggests (eqn. 1) that the quadrupole relaxation mechanism determines the observed linewidths. The magnitudes of q and η for $[CrO_4]^{2-}$ and $Cr(CO)_6$ will be small [40] because of the high

point symmetries of these molecules and so the observed linewidths (11 and 17 Hz, respectively [37]) are a function of a substantial quadrupole moment Q [41]. There is an uncertainty of at least a factor of four in the reported magnitudes of Q (Table 1) [41]. However, use of eqn. (1) to calculate $W_{1/2}(^{53}Cr)/W_{1/2}(^{95}Mo)$ suggests that the linewidths of ^{53}Cr resonances will be between two and three orders of magnitude greater than the equivalent ^{95}Mo resonances, which can themselves be very broad (Section E). This point, augmented by the low receptivity, highlights the problem of direct detection of ^{53}Cr resonances with currently available instrumentation.

E. MOLYBDENUM-95 AND -97 NMR

Prior to 1975, measurements of $^{95,97}Mo$ NMR concentrated on the determination [42–46] of μ, Q and the Knight shift by observation of the metal or of aqueous molybdate, although $^{95,97}Mo$ resonances were used to study electronic interactions in cobalt–molybdenum alloys [47] and were detected in solid $Na_2[MoO_4]$ [48]. Study of chemical phenomena in solution commenced in 1975 when Vold and Vold [18] nicely exploited the different relaxation times of the ^{95}Mo and ^{97}Mo nuclei in $[MoO_4]^{2-}$ to study the protonation and condensation of that ion as a function of pH. In 1976, as part of a series of papers [19,39,49–53], Lutz and co-workers [19,50] started to define a chemical shift scale by examination of some systems of high symmetry ($Mo^0(CO)_6$, $[Mo^{IV}(CN)_8]^{4-}$ and $[Mo^{VI}O_{4-n}S_n]^{2-}$ ($n = 0$–4)) for which quadrupolar line-broadening was expected to be minimal. In 1980, the potential of ^{95}Mo NMR for study of organometallic systems was demonstrated [54], and this area has developed rapidly. Many areas of complex polyoxo and cluster chemistry of molybdenum feature metal sites of low symmetry, and their ^{95}Mo NMR properties are of considerable interest. The many active research areas in molybdenum chemistry and the role of molybdenum in enzymes [7] have further stimulated the rapid development of ^{95}Mo NMR spectroscopy in the past five years.

For convenience the ^{95}Mo NMR data are tabulated and discussed by oxidation state. Within a given oxidation state complexes with similar chemical or structural features are grouped together to illustrate the effects of systematic changes on the ^{95}Mo NMR spectra. The ^{95}Mo chemical shift scale covers a range of 7000 ppm and is schematically represented in Fig. 9. It is apparent that the ^{95}Mo chemical shift cannot be used to distinguish, a priori, between mononuclear Mo(0), Mo(II) and Mo(IV) species. However, the ^{95}Mo chemical shift is highly sensitive to structural and electronic variations within a series of closely-related mononuclear compounds. For example, molybdenum(VI) complexes show large increases in the chemical

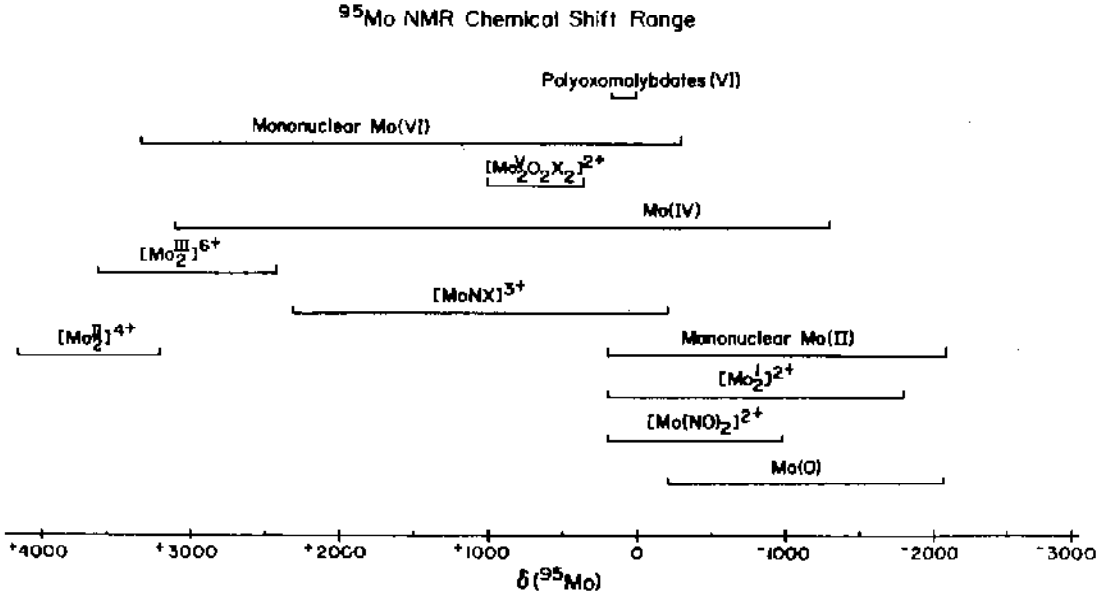

Fig. 9. ^{95}Mo NMR chemical shift range.

shift when an oxo group is replaced by a sulfido group. (Sections E(i)(b), E(i)(d)). Sequential coordination of Cu^{I} units to MoS_4^{2-} results in stepwise decreases in the chemical shift (Section E(i)(c)). Polynuclear species exhibiting strong intermetallic bonding (e.g. $[Mo_2^{II}]^{4+}$ species [16,20], Section E(v)(e)) can resonate in ranges far removed from those observed for mononuclear species in the same oxidation state (Fig. 9).

^{95}Mo NMR has also been used to follow reactions (Section E(i)(d)), to detect diastereomeric metal centers (Section E(v)(c)) and to identify compounds in reaction mixtures before separation and purification of products [33,112]. Spin–spin coupling (Section E(xi)) to other nuclei (especially ^{31}P) often enables solution stereochemistries to be determined unambiguously.

The ^{95}Mo NMR data for the compounds reviewed in Section E were relatively easy to assemble because almost every report mentioned molybdenum NMR in the title. In addition a substantial fraction of the data are from the authors' laboratories. Subsequent reviewers of ^{95}Mo NMR will face a more difficult task. The technique is rapidly becoming another routine tool used by chemists doing research on molybdenum, and the ^{95}Mo NMR parameters for new compounds may be partially obscured among data from other measurements used for characterization and identification [84,87,127]. The authors hope that the tabulation and discussion of the existing ^{95}Mo NMR data in Section E will further encourage those studying molybdenum chemistry to consider applying ^{95}Mo NMR to their own research problems.

(i) Molybdenum(VI) compounds

(a) Molybdate and the polyoxomolybdates

The relaxation rates of molybdate solutions in water are independent of pH in the range 9–12 [18] and the $[MoO_4]^{2-}$ ion can be examined free of complicating chemical effects because the rate of oxygen exchange is slow (0.02–0.05 s^{-1}) [55] and protonation and condensation processes are unimportant. The ^{95}Mo and ^{97}Mo relaxation times of 840 ± 20 and 6.5 ± 0.2 ms translate (eqn. 1) to half-widths of 0.38 and 49 Hz respectively for the particular samples (1 M $Na_2[MoO_4]$, 3 M NaCl) examined (see Table 28). Directly-observed ^{95}Mo NMR linewidths are greater than 0.5 Hz (Fig. 1, Table 2) and accurate estimates are restricted by magnetic field inhomogeneity. The much broader ^{97}Mo linewidths ($^{97}Q/^{95}Q = 11.4$) can be determined accurately and use of eqn. 1 and an estimate of τ_c provides electric quadrupole coupling constants $e^2q_{zz}^{97}Q/h$ and $e^2q_{zz}^{95}Q/h$, of 3.3 and 0.29 MHz, respectively [40]. These are small, but significantly greater than the value of zero expected for idealised tetrahedral site symmetry ($q_{zz} = 0$). The symmetry of the solvation shell is apparently lower than tetrahedral as it seems that ion-pair formation is ruled out by the insensitivity of the linewidths to salt concentration [40].

However, the chemical shift does exhibit a concentration dependence which is itself cation dependent. The Li^+ and NH_4^+ salts show increasing shielding (ca. -2.4 ppm $molal^{-1}$) with increasing concentration compared with a deshielding (ca. $+1$ ppm $molal^{-1}$) for the Na^+ and K^+ analogues

TABLE 2

$[MoO_{4-n}X_n]^{2-}$ (X = S, Se; $n = 0$–4) complexes [a]

Anion	Solvent [b]			
	Water			MeCN [c]
	δ, ppm	$W_{1/2}(^{95}Mo)$, Hz	$W_{1/2}(^{97}Mo)$, Hz	δ, ppm
$[MoO_4]^{2-}$	0	0.5 [d] (0.38 [d])	35 (48.9 [f])	[e]
$[MoO_3S]^{2-}$	497	10 [d]	[e]	[e]
$[MoO_2S_2]^{2-}$	1067	2.8 [d]	85	964
$[MoOS_3]^{2-}$	1654	0.7 [d]	35	1587
$[MoS_4]^{2-}$	2259	0.3 [d]	25	2207
$[MoO_3Se]^{2-}$	656	[e]		[e]
$[MoO_2Se_2]^{2-}$	1450	[e]		1335
$[MoOSe_3]^{2-}$	2272	[e]		2171
$[MoSe_4]^{2-}$	3145	[e]		3339

[a] Data from refs. 19, 53, 56, 57. [b] Nominal conc., 0.1–0.5 M. [c] Linewidth <10 Hz. [d] Spinning sample. [e] Not observed. [f] Calculated from the data of ref. 18 for a sample of Na_2MoO_4 (1 M) in aqueous NaCl (3 M).

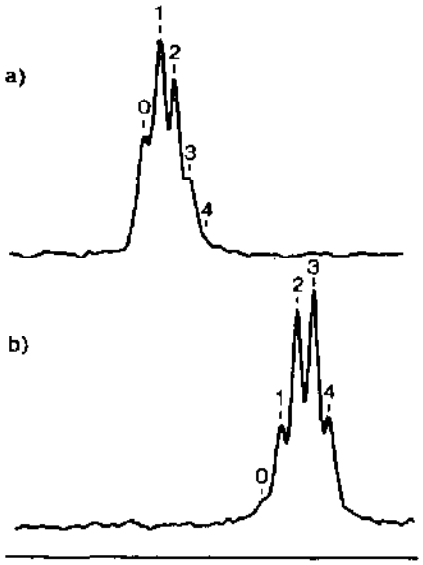

Fig. 10. ^{95}Mo NMR spectra of basic $Na_2[MoO_4]$: (a) 1 molal solution in H_2O (relative atom %: $^{16}O:^{17}O:^{18}O = 61.4:10.9:27.7$); (b) 0.87 molal solution in D_2O (relative atom %: $^{16}O:^{18}O = 27.5:72.5$). The indices n mark absorption due to $[Mo^{16}O_{4-n}{}^{18}O_n]^{2-}$. Taken from ref. 51, with permission.

[11,49]. This contrasts with $[CrO_4]^{2-}$ where increasing shielding is observed uniformly (Section D) [37].

The sensitivity of the ^{95}Mo chemical shift to the fine details of its environment is highlighted further by intramolecular isotope effects. Fine structure due to individual isotopomers $[Mo^{16}O_{4-n}{}^{18}O_n]^{2-}$ ($n = 0$–4) are resolved (Fig. 10) in $Na_2[MoO_4]$ solutions of varying oxygen isotope content [51]. The isotope effect is -0.25 ± 0.01 ppm for replacement of ^{16}O by ^{18}O and lineshape analysis indicates a statistical distribution of oxygen isotopes within 5 min, consistent with the rate of oxygen exchange [55]. The difference in chemical shift of the two patterns in Fig. 10 is due to a solvent hydrogen isotope effect of about -1.9 ppm when D_2O substitutes for H_2O, and a very minor concentration shift [39].

Below pH 9, the linewidths of molybdate solutions increase as chemical exchange processes affect the relaxation rate [18]. Above pH 7.7, protonation of molybdate dominates the chemistry (eqn. 4).

$$H^+ + [MoO_4]^{2-} \rightleftharpoons [MoO_4H]^- \quad \log K = 3.5 - 3.9 \text{ [18]} \tag{4}$$

Application of two-site exchange equations allows determination of the rate constant for protonation, $k_H = 4.8 \times 10^9$ l mol^{-1} s^{-1}. This number is in excellent agreement with that determined by ultrasonic relaxation. The availability of two isotopes with intrinsically different relaxation rates allows

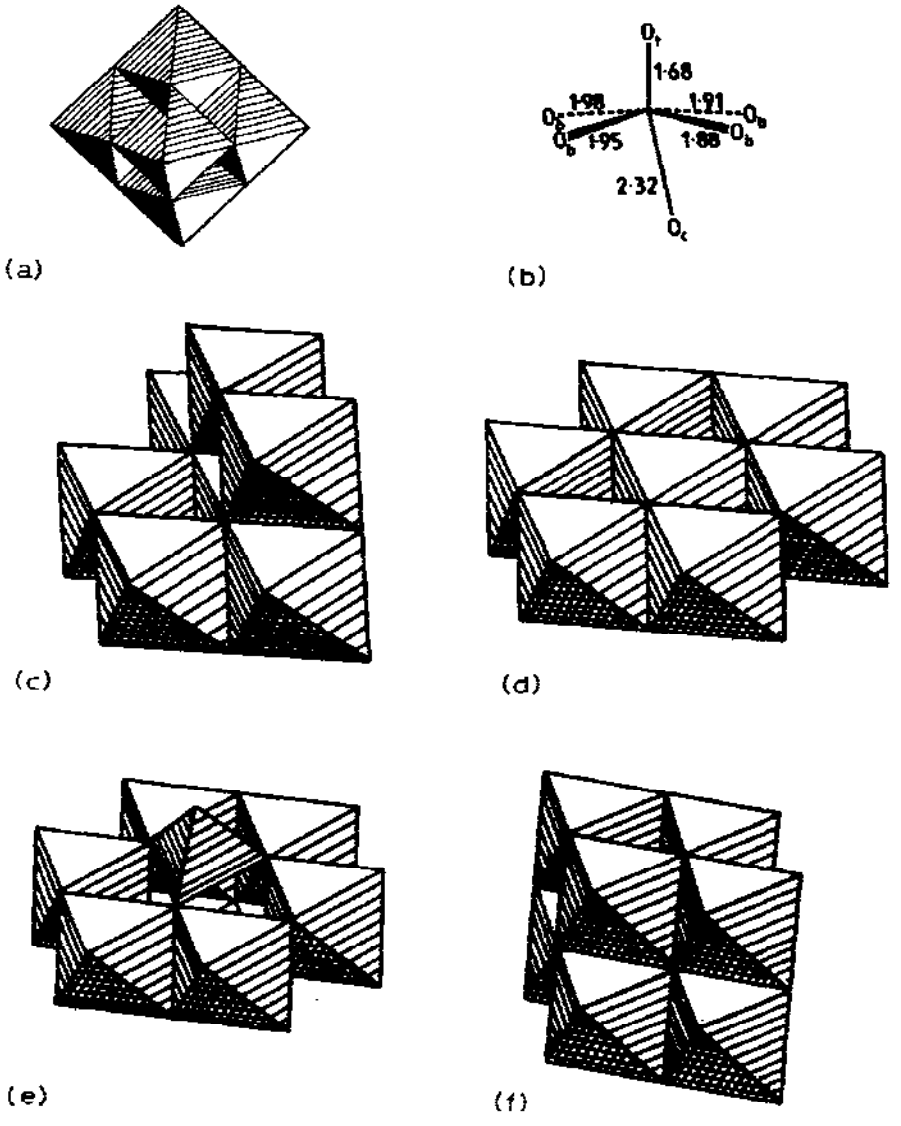

Fig. 11. Idealized condensed polyhedron models of polyoxomolybdate structures observed in the solid state. (a) $[Mo_6O_{19}]^{2-}$; (b) Bond lengths observed for each molybdenum site in (a); (c) $[Mo_7O_{24}]^{6-}$; (d) $[XMo_6O_{24}]^{n-}$; (e) α-$[Mo_8O_{26}]^{4-}$; (f) β-$[Mo_8O_{26}]^{4-}$. Adapted from ref. 60, with permission.

separation of the kinetic parameters at a single temperature and removes the need for temperature or magnetic field variation. The relaxation time, T_1, for the protonated form drops to 0.2–0.3 ms from 840 ms for $[MoO_4]^{2-}$ and reflects the increased field gradient at ^{95}Mo.

As molybdate solutions are acidified below pH 7.7, the molybdate signal broadens and a second, broad resonance, assigned to $[Mo_7O_{24}]^{6-}$ (Fig. 11(c) depicts the solid state structure) appears at about pH 6.5 [49,59,60]. These

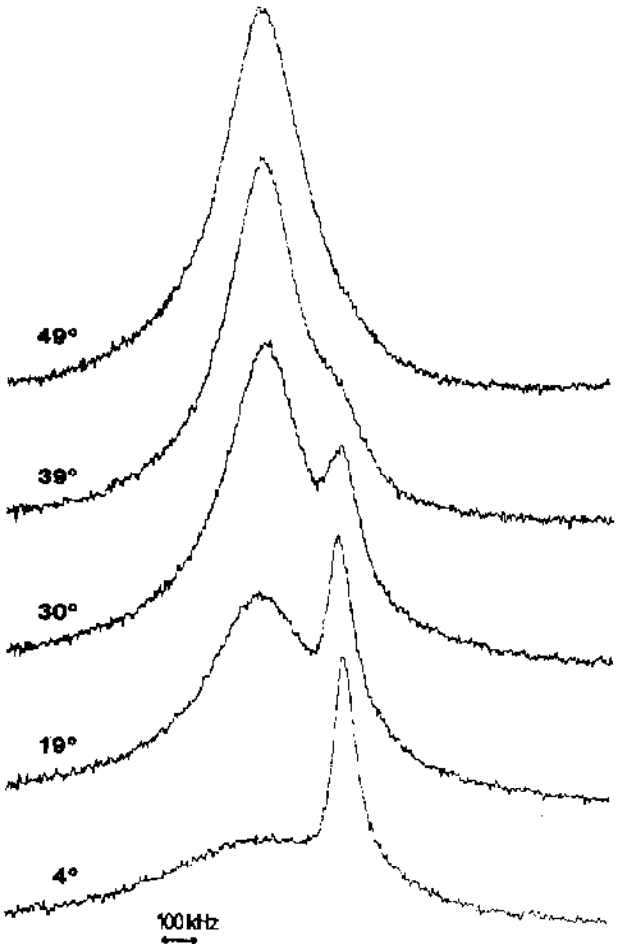

Fig. 12. Temperature variation of the ^{95}Mo NMR spectrum of $Na_6[Mo_7O_{24}]\cdot 4\ H_2O$ (96.47 atom % ^{95}Mo) in H_2O ([Mo] = 2.8 M; pH 6.1; no. of pulses, 4–5000; pulse repetition time, 0.86 s; spectral bandwidth, 2500 Hz). Reproduced from ref. 60, with permission.

general assignments are reasonable, as available equilibrium data indicate that for [Mo] = 10^{-3} M, the predominant species present will be $[MoO_4]^{2-}$ and its mono- and di-protonated forms and $[Mo_7O_{24}]^{6-}$ and its mono- and tri-protonated forms [58]. A 0.4 M solution of $Na_6[Mo_7O_{24}]\cdot 4\ H_2O$ (96.47 atom % ^{95}Mo) in H_2O (pH 6.1) also exhibits the two resonances at lower temperatures (Fig. 12) [60]. These coalesce as the temperature is increased progressively to 49°C and it is apparent that the Mo- and Mo_7-based species are exchanging rapidly on the ^{95}Mo NMR time-scale. The ^{17}O NMR spectrum of $[Mo_7O_{24}]^{6-}$ also shows reversible, temperature-dependent changes and at 90°C, only a very broad water resonance is observed [61]. The detailed nature of the rapid exchange reactions seen in the ^{95}Mo and ^{17}O NMR spectra cannot be discerned from the present limited data.

TABLE 3

Polyoxomolybdates [a]

Compound	[Mo] (M)	Solvent	Temperature (°C)	δ, (ppm)	Linewidth (Hz)
$(Bu^n_4N)_2[Mo_2O_7]$	0.15	MeCN	20	−7	16
$(Bu^n_4N)_2[Mo_6O_{19}]$	0.1	MeCN	20	122	88
	1.4	$HCONMe_2$	20	125	240
$(Bu^n_4N)_3[VMo_5O_{19}]$	0.2	MeCN	20	140	230
$Na_6[Mo_7O_{24}]\cdot 4\ H_2O$	2.8 [a]	H_2O (pH 6.1)	20	−1.2	ca. 120
				34	ca. 500
$Na_3[AlH_6Mo_6O_{24}]\cdot 4\ H_2O$	0.9	H_2O (pH 5.5)	50	−18	290
$Na_6[TeMo_6O_{24}]\cdot 2\ H_2O$	2.0	H_2O (pH 5.5)	50	10	200
$Na_5[IMo_6O_{24}]\cdot 3\ H_2O$	2.5	H_2O (pH 5.5)	50	−11	370
α-$(Bu^n_4N)_4[Mo_8O_{26}]$	0.15 [b,c]	MeCN	20	16	23
β-$(Bu^n_4N)_3K[Mo_8O_{26}]\cdot 2\ H_2O$	0.05 [b,c]	MeCN	20	19	240
				109	ca. 220
α-$(Bu^n_4N)_4[SiMo_{12}O_{40}]$	0.2	MeCN	50	27	520
α-$(Bu^n_4N)_3[PMo_{12}O_{40}]$	0.2	MeCN	50	25	720
$[H_8CeMo_{12}O_{42}]\cdot 18\ H_2O$	2.5	H_2O (pH 5.5)	20	2	460

[a] Data from ref. 60. [b] Enriched to 96.47 atom % ^{95}Mo. [c] Enriched to 21.7 atom % ^{17}O.

A preliminary survey is available for a range of polyoxomolybdates(VI) (Table 3) which contain one, two or three terminal oxo ligands [60,62]. The chemical shifts fall into the range presently defined for mononuclear $[Mo^{VI}O]^{4+}$, *cis*-$[Mo^{VI}O_2]^{2+}$ and *fac*-$[Mo^{VI}O_3]$ species with peripheral ligands possessing O or N donor atoms (Fig. 9; see Tables 5–8). This might be expected for polynuclear species which feature minimal interaction between $Mo^{VI}(d^0)$ sites.

In contrast to the polyoxotungstates (Section F) where the number of ^{183}W resonances observed is usually that expected for the static structures, ^{95}Mo NMR does not provide direct structural information. Linewidths generally exceed 100 Hz for six-coordinate sites but can be narrow (ca. 20 Hz at 20°C) for four-coordinate sites. Important influences include low site symmetries (high q_{zz}, eqn. 1), relatively high molecular radii (high τ_c, eqns. 1 and 3) and chemical exchange (Fig. 12). For example, both $[Mo_6O_{19}]^{2-}$ and the Keggin anions such as α-$[PMo_{12}O_{40}]^{3-}$ exhibit high point group symmetries (O_h and T_d respectively: Figs. 11(a) and 27(a)) in the solid state [6] and solution [61], but the site symmetry of the equivalent molybdenum atoms is low (Fig. 11(b)).

An interesting case is that of α-$[Mo_8O_{26}]^{4-}$ (Fig. 11(e)) which exhibits a single ^{95}Mo resonance (Fig. 13(a)). The simplest interpretation is that this narrow signal is due to the two tetrahedral capping Mo atoms (site symmetry

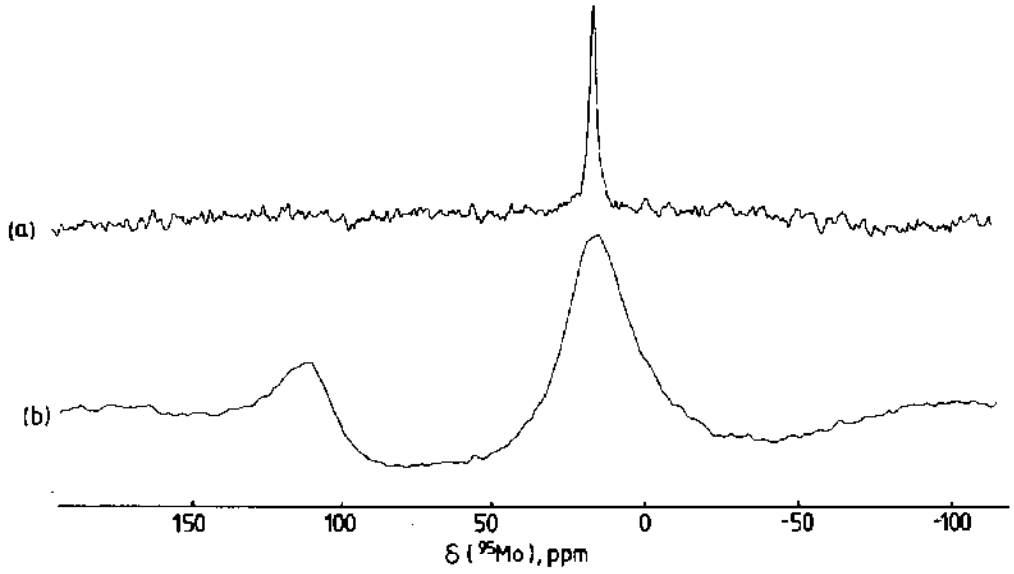

Fig. 13. ^{95}Mo NMR spectra of samples (atom %: ^{95}Mo 96.47; ^{17}O 21.72) in MeCN at 20°C (pulse repetition time, 0.55 s; spectral bandwidth, 4000 Hz). (a) α-$(Bu^n_4N)_4[Mo_8O_{26}]$ ([Mo] = 0.15 M; number of pulses, 1000); (b) β-$(Bu^n_4N)_4[Mo_8O_{26}]$ ([Mo] = 0.05 M; number of pulses, 6700). Reproduced from ref. 60, with permission.

C_{3v}; note the narrow linewidth of $[Mo_2O_7]^{2-}$ (Table 3)) and that the resonances of the ring Mo atoms are too broad to be detected under the present conditions. Note that the six-ring Mo atoms of $[XMo_6O_{24}]^{n-}$ (Fig. 11(d)) exhibit linewidths greater than 200 Hz, even at 50°C (Table 3). Alternatively, all eight Mo atoms could be involved in a fast exchange process. In contrast the β-isomer of $[Mo_8O_{26}]^{4-}$ features three inequivalent Mo sites in the ratio 2:1:1 (Fig. 11(f)), but two broad resonances are present in the ^{95}Mo spectrum (Fig. 13(b)).

Low temperature ^{17}O NMR spectra of $[Mo_7O_{24}]^{6-}$, and α- and β-$[Mo_8O_{26}]^{4-}$ exhibit the number of resonances expected from the solid state structures (Fig. 11), but chemical exchange processes are observed in both aqueous and nonaqueous solutions and especially at elevated temperatures. It is apparent that a systematic integrated study of ^{95}Mo and ^{17}O NMR properties of polyoxomolybdates is warranted as they may have markedly different time scales. In particular, low temperature ^{17}O NMR can be used to confirm the integrity of sample solutions. For example, an early communication reported that α- and β-$[Mo_8O_{26}]^{4-}$ exhibited the same single narrow ^{95}Mo signal in MeCN [62]. This error resulted from examination of a sample of β-isomer containing < 10 mol % of α-isomer. The very narrow α-signal (Fig. 13) has a chemical shift close to that of a broad β-signal and dominated the observed spectrum. Contributing difficulties included use of a

less sensitive spectrometer, the presence of "rolling baseline" due to probe ringing and the low solubility ([Mo] = 0.05 M) of β-$(Bu^n_4N)_3K[Mo_8O_{26}]$ in MeCN. The problem of detecting broad signals in the presence of contaminating narrow ones is highlighted by this case.

(b) Molybdate derivatives

Data [19,53,56,57] for the thio- and selenido-molybdates(VI), $[MoO_{4-n}X_n]^{2-}$ ($n = 0$–4, X = S, Se) in H_2O and MeCN solutions are listed in Table 2 and depicted schematically in Fig. 14. These solutions are reactive and interconversion of species is facile in the presence of protons [63,64]. Consequently, assignments are based upon the internal consistency of the results and those for $[WO_{4-n}S_n]^{2-}$ complexes (Section F). For example, the anions exhibit uniformly narrow (< 10 Hz) linewidths, a similar solvent dependence of the chemical shift, and a systematic decrease in shielding with successive substitution of O atoms by S or Se atoms. The decrease is 497–604 ppm per S atom and 656–873 ppm per Se atom in aqueous solution. Similar behavior is found in $[PO_{4-n}S_n]^{3-}$ [65].

The isotopomers $[Mo(^{32}S)_4]^{2-}$ and $[Mo(^{32}S)_3{}^{34}S]^{2-}$ can be resolved in naturally-abundant $[MoS_4]^{2-}$ (cf. $[MoO_4]^{2-}$, Fig. 10) [52]. The cation dependence of the chemical shift is slight, but the solvent dependence of the chemical shift of $[MoS_4]^{2-}$ is pronounced, being over 70 ppm in the solvents examined [56]. The chemical basis of this solvent dependence is not understood, but it may be related to expansion of the coordination sphere promoted by protonation of the sulfido ligands in protic solvents.

The ^{97}Mo NMR linewidths of the thiomolybdates are between one and two orders of magnitude greater than those of the corresponding ^{95}Mo

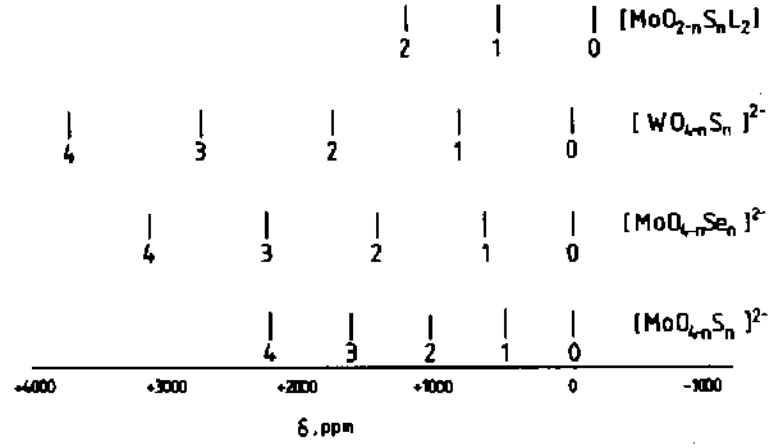

Fig. 14. Chemical shift scale for thio and selenido species (LH = R_2NOH). Reproduced from ref. 64, with permission.

resonances [53], consistent with quadrupolar relaxation (Section E(xii) and eqn. 1: $W_{1/2} \propto Q^2$).

(c) Copper–molybdenum–sulfur clusters

An important facet of the chemistry of the thiomolybdate anions is their ligand properties [63,64]. They bond to a wide variety of metal centers via the sulfur atoms while maintaining the physical integrity of the $[MoO_{4-n}S_n]^{2-}$ moiety. A series of Cu–Mo–S clusters has been examined [56,66,67] by ^{95}Mo NMR (Table 4), and the data for the simpler bi- and trinuclear derivatives of $[MoS_4]^{2-}$ demonstrate that equilibrium (5) lies essentially to the left.

$$2[XCuS_2MoS_2]^{2-} \rightleftharpoons [XCuS_2MoS_2CuX]^{2-} + [MoS_4]^{2-} \quad (X = CN, SPh) \qquad (5)$$

All resonances for $[(XCu)_nMoS_4]^{2-}$ complexes are shielded relative to $[MoS_4]^{2-}$ and the ^{95}Mo chemical shift decreases by 200–400 ppm upon addition of each Cu^IX (X = Cl, Br, I, SPh, CN) unit to the $[MoS_4]^{2-}$ core [67]. Smaller variations in the molybdenum chemical shift result from changing the nature of the X ligand attached to the Cu atom: SPh < I < Br < Cl ~ CN [67]. Substitution of Cu^I by Ag^I in $[(NCCu)MoS_4]^{2-}$ deshields the molybdenum nucleus by 57 ppm [56].

The data in Table 4 also permit several direct comparisons among $[(XCu)_nMoS_4]^{2-}$, $[(XCu)_nMoOS_3]^{2-}$ and $[(XCu)MoO_2S_2]^{2-}$ (n = 0, 1, 2, 3)

TABLE 4

Thiomolybdate(VI) cluster compounds [a]

Compound	Solvent	δ (ppm)	Linewidth (Hz)	Ref.
$[(NCCu)MoS_4]^{2-}$	MeCN	1864	30	56, 66
$[(NCAg)MoS_4]^{2-}$	MeCN	1921	15	56
$[(NCCu)MoOS_3]^{2-}$	MeCN	1199	25	56
$[(PhSCu)MoS_4]^{2-}$	MeCN	1903	50	66
$[(PhSCu)MoO_2S_2]^{2-}$	$HCONMe_2$	611	70	67
$[(NCCu)_2MoS_4]^{2-}$	MeCN	1616	220	56, 66
$[(PhSCu)_2MoS_4]^{2-}$	MeCN	1700	630	66
$[(PhSCu)_2MoOS_3]^{2-}$	$HCONMe_2$	892	100	67
$[(ClCu)_2MoS_4]^{2-}$	$HCONMe_2$	1618	250	67
$[(BrCu)_2MoS_4]^{2-}$	$HCONMe_2$	1632	600	67
$[(ClCu)_3MoS_4]^{2-}$	$HCONMe_2$	1234	200	67
$[(ClCu)_3MoOS_3]^{2-}$	CH_2Cl_2	474	20	67
$[(BrCu)_3MoS_4]^{2-}$	$HCONMe_2$	1272	250	67
$[(ICu)_3MoS_4]^{2-}$	MeCN	1282	170	67
$[(ClCu)_4MoS_4]^{2-}$	$HCONMe_2$	886	1400	67
$[(BrCu)_4MoS_4]^{2-}$	$HCONMe_2$	910	1400	67

[a] 20–25°C.

complexes. The pair $[(NCCu)MoS_4]^{2-}$ (**1**) and $[(NCCu)MoOS_3]^{2-}$ (**2**) shows an increased shielding of 665 ppm for the oxo-containing anion, [56] similar to the 605 ppm difference between the free $[MoS_4]^{2-}$ and $[MoOS_3]^{2-}$ anions (Table 2). For $[(PhSCu)MoS_4]^{2-}$ (**1**) and $[(PhSCu)MoO_2S_2]^{2-}$ (**3**), the oxo-containing anion is 1290 ppm more shielded [67], compared with a difference of 1190 ppm between the free $[MoS_4]^{2-}$ and $[MoO_2S_2]^{2-}$ anions (Table 2). Complexes of structural types **1**, **2**, and **3** display similar linewidths for a given X group, and are all < 100 Hz.

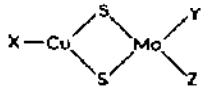

1 Y=Z=S
2 Y=S, Z=O
3 Y=Z=O

The $[(XCu)_nMoS_4]^{2-}$ anions with $n = 2$, 3 undergo a structural change when the molybdenum core changes from $[MoS_4]^{2-}$ to $[MoOS_3]^{2-}$. For the pair $[(PhSCu)_2MoS_4]^{2-}$ (**4**) and $[(PhSCu)_2MoOS_3]^{2-}$ (**5**), the shielding of the molybdenum nucleus is 808 ppm larger in **5** [67] (Table 4).

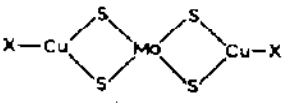

4

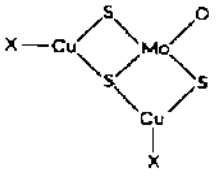

5

The linewidth of **5** (100 Hz) is smaller than that of **4** (250 Hz) even though **4** exhibits a higher Mo site symmetry.

The anions $[(ClCu)_3MoS_4]^{2-}$ (**6**) and $[(ClCu)_3MoOS_3]^{2-}$ (**7**) show similar chemical shift differences to **4** and **5**, with compound **7** being 760 ppm more shielded than **6**.

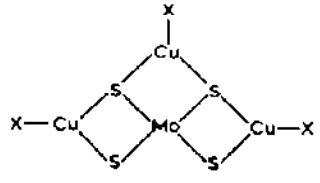

6

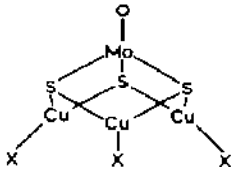

7

An examination of Table 4 suggests that other factors beside quadrupolar and correlation time broadening (eqn. 1) can contribute to the linewidths. For example, in MeCN an order of magnitude increase in linewidth is observed by lowering the symmetry from T_d in $[MoS_4]^{2-}$ (< 1 Hz) to C_{2v} in $[(NCAg)MoS_4]^{2-}$ (15 Hz) and this parallels that observed (Table 2) for a similar progression from $[MoS_4]^{2-}$ (0.3 Hz) to $[MoO_2S_2]^{2-}$ (2.8 Hz) in H_2O. However, correlation broadening will make some contribution for the larger $[(NCAg)MoS_4]^{2-}$ anion and the presence of unresolved ^{95}Mo–$^{107,109}Ag$ ($I =$

1/2) coupling should not be discounted. An increase in the ^{95}Mo relaxation rate caused by coupling to a rapidly relaxing neighboring quadrupolar nucleus (^{63,65}Cu, $I = 3/2$) is a plausible explanation of the increased linewidth of $[(NCCu)MoS_4]^{2-}$ (30 Hz) over that of the Ag analogue. The larger linewidth for $[(PhSCu)MoS_4]^{2-}$ (50 Hz) is consistent with correlation time broadening due to the bulky phenyl group.

For $[(XCu)_2MoS_4]^{2-}$ complexes the linewidths range from 200–600 Hz. The importance of correlation time broadening is illustrated by the decrease of the linewidth of $[(NCCu)_2MoS_4]^{2-}$ in $HCONMe_2$ from 900 to 140 Hz as the temperature is increased from 20 to 100°C [56]. The $[(XCu)_3MoS_4]^{2-}$ complexes (**6**) show linewidths of ~ 200 Hz. Conversion of **6** to **7** decreases the linewidth substantially [67]. The presence of trigonal symmetry (as in **7**) often leads to relatively narrow lines.

(d) Hydroxylamidomolybdenum(VI) compounds

The dialkyl(hydroxylamido) complexes, $Mo^{VI}O_2(ONR_2)_2$ (**8**), first isolated by Wieghardt [27], are another group of complexes in which sulfido and selenido ligands can be systematically substituted for a terminal oxo ligand. In one sense, these six-coordinate species might be regarded as pseudo-tetrahedral due to the small bite angle of the R_2NO ligand [27,68,69] but their geometry is more accurately described as skew trapezoid bipyramidal [81,82]. The magnitude of deshielding upon replacement of an oxo ligand is somewhat larger [68,69,71] than for the simple molybdates, being about 700 ppm per S and 1000 ppm per Se atom added (Table 5). The stepwise conversion of $MoO_2(ONR_2)_2$ to $MoOS(ONR_2)_2$ and $MoS_2(ONR_2)_2$ by the action of the sulfiding reagent $(Me_3Si)_2S$ can be followed conveniently by ^{95}Mo NMR (Fig. 15, [71]). ^{95}Mo NMR can also be used to follow the slow interconversion of these compounds in the presence of protons [72].

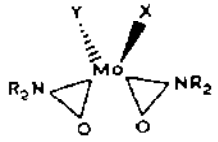

8

Another feature of the systematic replacement of oxo groups by sulfido groups in $MoO_2(ONR_2)_2$ complexes is the decrease in linewidth that accompanies incorporation of sulfur. For $MoO_{2-n}S_n(ONC_5H_{10})_2$ the linewidths (Hz) are 160($n = 0$), 100($n = 1$) and 70($n = 2$) [71]. This suggests that in these complexes the asymmetry parameter (eqn. 2) decreases as sulfur replaces oxygen. Alternatively, the more polar Mo–O bonds may interact more strongly with the solvent, resulting in correlation time broadening for the oxo complex.

(e) cis-*Dioxomolybdenum(VI) compounds*

The ^{95}Mo NMR spectra of many six-coordinate complexes containing the *cis*-$[Mo^{VI}O_2]^{2+}$ unit have been examined (Tables 5 and 6) because such units are thought to occur at the molybdenum sites of certain enzymes [78,79]. The point group symmetry of such species can be no higher than C_2. The *cis*-stereochemistry of the oxo ligands is imposed electronically [4], but the detailed molecular structure is determined by non-bonded repulsions between donor atoms [80–82]. Consequently, ^{95}Mo chemical shifts in this stereochemically-flexible system are sensitive to apparently minor ligand variations. For example, the chemical shifts of $MoO_2(SCMe_2CMe_2NHR)_2$ (R = H, Me) differ by 129 ppm [23]. Few simple correlations are apparent in Tables 5 and 6. The total chemical shift range covers about 900 ppm, and the shifts of two general coordination spheres appear to be reasonably well-defined:

$[MoO_2(\text{thiolate-S})_2N_2]$: 400 → 700 ppm

$[MoO_2(O, N)_4]$: −230 → +100 ppm

TABLE 5

Hydroxylamidomolybdenum(VI) compounds

Compound	Solvent	Chemical shift (ppm)	Linewidth (Hz)	Ref.
$MoO_2(ONHMe)_2$	$HCONMe_2$	−219	200	71
$MoO_2(ONHMe)_2$	MeCN	−230	65	68
$MoO_2(ONHBu^t)_2$	$HCONMe_2$	−218	150	71
$MoO_2(ONMe_2)_2$	$HCONMe_2$	−165	120	71
$MoO_2(ONEt_2)_2$	$HCONMe_2$	−169	160	68, 71
$MoOS(ONEt_2)_2$	$HCONMe_2$	544	140	71
$MoOS(ONEt_2)_2$	CH_2Cl_2	541	70	68
$MoOSe(ONEt_2)_2$	$HCONMe_2$	865	120	71
$MoS_2(ONEt_2)_2$	$HCONMe_2$	1234	100	68, 71
$MoO_2(ONC_5H_{10})_2$	$HCONMe_2$	−184	160	71
$MoO_2(ONC_5H_{10})_2$	$CDCl_3$	−177	[a]	69
$MoOS(ONC_5H_{10})_2$	$HCONMe_2$	531	100	71
$MoOS(ONC_5H_{10})_2$	$CDCl_3$	537	[a]	69
$MoOSe(ONC_5H_{10})_2$	$HCONMe_2$	855	70	71
$MoS_2(ONC_5H_{10})_2$	$HCONMe_2$	1219	70	71
$MoS_2(ONC_5H_{10})_2$	$CDCl_3$	1229	[a]	69
$MoO_2(ONBz_2)_2$	$HCONMe_2$	−161	260	68, 71
$MoOS(ONBz_2)_2$	$CHCl_3$	565	340	68
$MoS_2(ONBz_2)_2$	$CHCl_3$	1282	530	68

[a] Linewidth not reported.

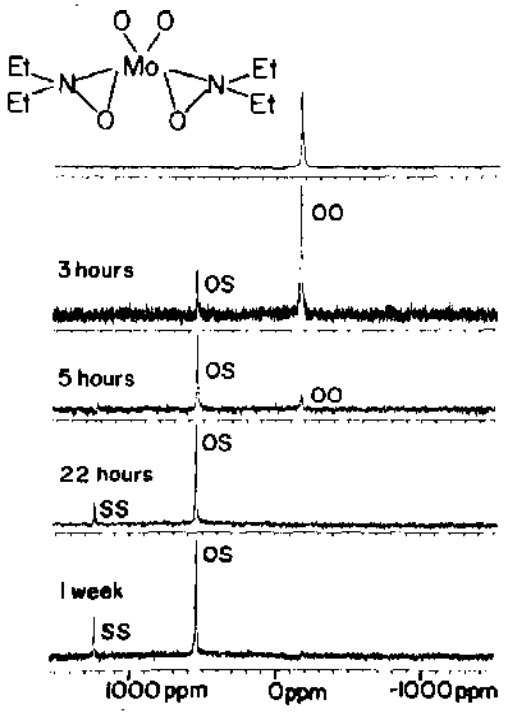

Fig. 15. Conversion of $MoO_2(ONEt_2)_2$ (0.6 M in $CHCl_3$) to $MoOS(ONEt_2)_2$ and $MoS_2(ONEt_2)_2$ by incubation with $(Me_3Si)_2S$ (2 equivalents).

Replacement of an O or N donor atom of a ligand by a thiolate sulfur leads to a deshielding of 200–400 ppm; the most clear-cut comparison is between MoO_2(sap)(HCONMe$_2$) (34 ppm) and MoO_2(sma)(HCONMe$_2$) (231 ppm) [23]. On the other hand, thioether sulfur appears [73] to be more shielding than amine nitrogen, and so ^{95}Mo shielding in these systems increases in the order $RS^- < RO^-$, $R_3N < R_2S$.

The chemical shifts of $MoO_2Br\{HB(Me_2pz)_3\}$ (129 ppm) and $MoO_2Cl\{HB(Me_2pz)_3\}$ (85 ppm) [73] demonstrate that six-coordinate *cis*-$[MoO_2]^{2+}$ complexes show inverse halogen dependence of the chemical shift [11] (Section G(i)(c)).

Factors which contribute to the wide range of linewidths (24–1170 Hz) are also difficult to discern. Although quadrupolar broadening is the major factor, species with no formal symmetry (e.g. $MoO_2\{(SCH_2CH_2)_2NCH_2CH_2NMe_2\}$, 45 Hz) can have relatively narrow lines. The effects of correlation time broadening are apparent. The linewidths of MoO_2(hbdae) derivatives in CH_2Cl_2 increase progressively from 50 to 220 Hz as the number of t-butyl substituents increases progressively from 0 to 4 [73]. For $MoO_2(S_2CNR_2)_2$ complexes the linewidth increases smoothly from 140 to 570 Hz in the expected order R = Me < Et < Pr^n < Bu^n [30]. In addition, the

TABLE 6

cis-Dioxomolybdenum(VI) compounds [a]

Compound	Ligand donor atoms	Solvent	Chemical shift (ppm)	Linewidth (Hz)	Ref.
$(Et_4N)_2[MoO_2(NCS)_4]$	N_4	Me_2CO	−155	330	73
$MoO_2(OMe)\{HB(Me_2pz)_3\}$	ON_3	CH_2Cl_2	−35	100	73
MoO_2(3-Bu^{t}hbdae)	O_2N_2	CH_2Cl_2	−19	120	73
MoO_2(3,5-Bu^{t}hbdae)	O_2N_2	CH_2Cl_2	−15	220	73
MoO_2(3,5-Bu^{t}hbdac)	O_2N_2	CH_2Cl_2	−11	140	73
$MoO_2(NCS)\{HB(Me_2pz)_3\}$	N_4	$HCONMe_2$	−5	250	73
$MoO_2(acam)_2$	O_4	$HCONMe_2$	−4	160	23
$MoO_2(dpm)_2$	O_4	CH_2Cl_2	−4	120	68
MoO_2(hbdae)	O_2N_2	CH_2Cl_2	0	50	73
$MoO_2(acac)_2$	O_4	$HCONMe_2$	3	130	28, 68
MoO_2(hbdab)	N_2O_2	CH_2Cl_2	7	100	68
MoO_2(5-H-sae)(Me_2SO)	O_3N	Me_2SO	26	430	74
MoO_2(5-Br-sae)(Me_2SO)	O_3N	Me_2SO	29	470	74
MoO_2(5-NO_2-sae)(Me_2SO)	O_3N	Me_2SO	31	450	74
MoO_2(5-NO_2-sap)(Me_2SO)	O_3N	Me_2SO	31	160	74
MoO_2(5-Cl-sae)(Me_2SO)	O_3N	Me_2SO	32	500	74
MoO_2(5-CH_3O-sae)(Me_2SO)	O_3N	Me_2SO	34	860	74
MoO_2(sap)($HCONMe_2$) [b]	O_3N	$HCONMe_2$	34	350	23
MoO_2(sap)(Me_2SO)	O_3N	Me_2SO	38	470	74
MoO_2(5-Br-sap)(Me_2SO)	O_3N	Me_2SO	39	1170	74
MoO_2(5-Cl-sap)(Me_2SO)	O_3N	Me_2SO	40	280	74
MoO_2(5-CH_3O-sap)(Me_2SO)	O_2N	Me_2SO	47	860	74

MoO_2q_2	O_2N_2	$HCONMe_2$	58	100	23
$MoO_2Cl\{HB(Me_2pz)_3\}$	N_3Cl	$HCONMe_2$	85	400	73
$MoO_2Br\{HB(Me_2pz)_3\}$	N_3Br	CH_2Cl_2	129	270	73
$MoO_2(S_2CNMe_2)_2$	S_4	CH_2Cl_2	151	140	30
$MoO_2(S_2CNEt_2)_2$	S_4	CH_2Cl_2	176	280	23
$MoO_2(S_2CNPr^n_2)_2$	S_4	CH_2Cl_2	173	430	30
$MoO_2(S_2CNBu^n_2)_2$	S_4	CH_2Cl_2	175	570	30
$MoO_2(sma)(HCONMe_2)$	O_2NS	$HCONMe_2$	231	360	23
$MoO_2(dttd)$	S_4	CH_2Cl_2	409	65	73
$MoO_2(Mepen)_2$	N_2S_2	$HCONMe_2/Me_2SO$	131, 451 [c]	[d]	75
$MoO_2(SCMe_2CMe_2NH_2)_2$	N_2S_2	CH_2Cl_2	452	270	23
$MoO_2(mq)_2$	N_2S_2	$HCONMe_2$	460	145	68
$MoO_2(SCH_2CH_2NH_2)_2$	N_2S_2	Me_2SO	467	275	76
MoO_2(L-cysOEt)$_2$	N_2S_2	$NCONMe_2$	469	[d]	77
MoO_2(L-cysOMe)$_2$	N_2S_2	$HCONMe_2$	467, 495 [c]	[d]	77
$MoO_2(mae)$	N_2S_2	$HCONMe_2$	491	500	23
$MoO_2(mab)$	N_2S_2	$HCONMe_2$	499	550	73
$MoO_2(mpe)$	N_2S_2	$HCONMe_2$	543	270	23
$MoO_2(SCMe_2CMe_2NHMe)_2$	N_2S_2	CH_2Cl_2	581	320	23
$MoO_2\{(-CH_2NMeCH_2CH_2S)_2\}$	N_2S_2	MeCN	599	55	68
$MoO_2\{(SCH_2CH_2)_2NCH_2CH_2NMe_2\}$	N_2S_2	CH_2Cl_2	604	45	23
		$HCONMe_2$	604	50	68
$MoO_2\{(-CH_2NEtCH_2CH_2S)_2\}$	N_2S_2	MeCN	629	40	68
$[MoO_2(phobb)]_2O$	[e]	CH_2Cl_2	47, 76	[d]	128

[a] For ligand abbreviations, see pp. 171, 172 [b] Abbreviated as sip in ref. 23. [c] Separate resonances assigned to two diastereomeric molybdenum centers. [d] Linewidth not reported. [e] The binuclear complex contains a five-coordinate (O_2, N)MoO_2 unit and a six-coordinate (O_3, N)MoO_2 unit.

linewidth of the $MoO_2(acac)_2$ resonance in MeOH varies linearly from 73 Hz at 41°C to 270 Hz at −34°C [68].

Individual resonances for MoO_2(L-cysOMe)$_2$ in $HCONMe_2$ are resolved at 495 and 467 ppm and may be assigned a to the Δ and Λ diastereomers in relative concentrations of about 1 : 5 [77]. An approximate $\Delta G^{\neq}$ value, 64 kJ mol^{-1} can be estimated for their interconversion.

(f) Oxo, nitrido and imido complexes

Although the coodination chemistry of Mo^{VI} is dominated by the *cis*-$[MoO_2]^{2+}$ unit, several compounds containing the $[Mo^{VI}O]^{4+}$, $[Mo^{VI}N]^{3+}$, and $[Mo^{VI}(NPh)]^{4+}$ units have been examined by ^{95}Mo NMR (Table 7). Seven-coordinate $[MoO]^{4+}$ complexes with the general formula $[MoO(S_2CNR_2)_3]BF_4$ and $MoOX_2(S_2CNR_2)_2$ (R = Me, Et, Pr^n, Bu^n; X = Cl^- or Br^-; $X_2 = S_2^{2-}$) have chemical shifts ranging from 55 to 182 ppm with the dimethyldithiocarbamato complexes being more shielded than their dialkyl analogues [30]. For the $MoOX_2(S_2CNR_2)_2$ complexes, replacement of Cl by Br causes deshielding of the ^{95}Mo nucleus, i.e. this type of complex shows an inverse halogen dependence. The corresponding nitrido complexes, $MoN(S_2CNR_2)_3$ (R = Me, Et), exhibit ^{95}Mo NMR resonances at ca. −100 ppm, which are shielded in comparison with the monooxo complexes and also in comparison with the other $[MoN]^{3+}$ complexes studied ($MoNX_3$, X = Cl, OBu^t; $[MoNCl_4]^-$ and $[MoNCl_5]^{2-}$). The nitrido complexes cover a chemical shift range of 1200 ppm. The phenylimido complex, $[Mo(NPh)(S_2CNEt_2)_3]BF_4$, is even more shielded than the corresponding nitrido complex. Replacement of a dithiocarbamato ligand in $[Mo(NPh)(S_2CNEt_2)_3]BF_4$ by two Cl^- or Br^- ligands deshields the ^{95}Mo nucleus, as also occurs for the corresponding monooxo complexes. These halide complexes exhibit an inverse halogen dependence. The novel carbyne compound $Mo(CCMe_3)(CH_2CMe_3)_3$ has $\delta = 1404$ ppm, $W_{1/2} = 10$ Hz [102].

The $MoO_2(ONR_2)_2$ complexes (**8**, Section E(i)(d)) react with catechols to form seven-coordinate $[MoO]^{4+}$ complexes [83] with a general formula $MoO(ONR_2)_2$(cat), with only N and O donor atoms. The ^{95}Mo resonances occur from −42 to +17 ppm (Table 7(a)) and are more shielded than the $[MoO(S_2CNR_2)_3]^+$ complexes [30] described above. The most shielded $[MoO]^{4+}$ complex known is $[MoO(O_2)(CN)_4]^{2-}$ with $\delta = -610$ ppm [84].

(g) fac-*Trioxomolybdenum(VI) compounds*

A few six-coordinate *fac*-MoO_3 complexes have been studied by ^{95}Mo NMR (Table 8). All feature one tertiary amine and two carboxylate ligands and resonate at 66 ± 4 ppm [59,68]. Interestingly, while $[(MoO_3)_2(pdta)]^{4-}$ exhibits a single resonance at 22°C, two resonances are resolved [85] at higher temperatures and may be assigned to the inequivalent sites *Mo*NCH_2–

TABLE 7

Monooxo, nitrido and phenylimido Mo(VI) compounds

(a) Monooxo compounds	Solvent	Chemical shift (ppm)	Linewidth (Hz)	Ref.
$[MoO(S_2CNMe)_3]BF_4$	CH_2Cl_2	55	20	30
$[MoO(S_2CNEt_2)_3]BF_4$	CH_2Cl_2	80	40	30
$MoOCl_2(S_2CNMe_2)_2$	CH_2Cl_2	117	30	30
$MoOBr_2(S_2CNMe_2)_2$	CH_2Cl_2	163	20	30
$MoOCl_2(S_2CNEt_2)_2$	CH_2Cl_2	137	30	30
$MoOBr_2(S_2CNEt_2)_2$	CH_2Cl_2	182	30	30
$MoO(S_2)(S_2CNEt_2)_2$	CH_2Cl_2	139	50	30
$MoO(S_2)(S_2CNEt_2)_2$	CH_2Cl_2	148	70	30
$MoO(ONC_5H_{10})_2$(cat)	$CHCl_3$	−5	300	83
$MoO(ONC_5H_{10})_2$(4-Bu^t-cat)	$CHCl_3$	17	500	83
$MoO(ONC_5H_{10})_2$(3,5-Bu^t-cat)	$CHCl_3$	−28	400	83
$MoO(ONC_5H_{10})_2$(4-NO_2-cat)	$CHCl_3$	−40	450	83
$MoO(ONC_5H_{10})_2$(Br_4-cat)	$CHCl_3$	−42	450	83
$[MoO(O_2)(CN)_4]^{2-}$	CH_2Cl_2	−610	[a]	84
(b) Nitrido compounds	**Solvent**	**δ (ppm)**	**Linewidth (Hz)**	**Ref.**
$MoNCl_3$	MeCN	952	80	30
$(PPh_4)[MoNCl_4]$	CH_2Cl_2	1106	< 20	30
$(PPh_4)_2[MoNCl_5]$	CH_2Cl_2	395	50	30
$MoN(OBu^t)_3$	CH_2Cl_2	55	40	30
$MoN(S_2CNMe_2)_3$	CH_2Cl_2	−121	40	30
$MoN(S_2CNEt_2)_3$	CH_2Cl_2	−103	40	30
(c) Phenylimido compounds	**Solvent**	**δ (ppm)**	**Linewidth (Hz)**	**Ref.**
$[Mo(NPh)(S_2CNEt_2)_3]BF_4$	CH_2Cl_2	−294	450	30
$Mo(NPh)Cl_2(S_2CNEt_2)_2$	CH_2Cl_2	−254	480	30
$Mo(NPh)Br_2(S_2CNEt_2)_2$	CH_2Cl_2	−218	400	30

[a] Linewidth not reported.

(68 ppm) and *Mo*NCHMe (56 ppm). Aqueous (pH 6–7) solutions of $MoO_3(H_2NCH_2CH_2NCH_2CH_2NH_2)$, $[MoO_3(L\text{-histidine})]^-$ and $[MoO_3(L\text{-aspartate})]^{2-}$ each feature [59,85] a broadened resonance close to 0 ppm, apparently characteristic of exchange between $[MoO_4]^{2-}$ and the 1 : 1 complex.

(ii) Molybdenum(V) compounds

Mononuclear Mo(V) complexes have a d^1 electron configuration, are paramagnetic and not readily amenable to NMR measurements. Most of the Mo(V) systems examined to date by ^{95}Mo NMR are diamagnetic binuclear

TABLE 8

fac-Trioxomolybdenum(VI) complexes [a,b]

Complex	Ligand atoms	δ (ppm)	Linewidth (Hz)	Ref.
$[MoO_3(Meida)]^{2-}$	NO_2	63	120	59
$[(MoO_3)_2(edta)]^{4-}$	NO_2	63	290	59, 68
$[(MoO_3)_2(eedta)]^{4-}$	NO_2	64	150	59
$[(MoO_3)_2(egta)]^{4-}$	NO_2	64	240	59
$[MoO_3(Bzida)]^{2-}$	NO_2	65	210	59
$[MoO_3(ida)]^{2}$	NO_2	66	130	59, 68
$[MoO_3(Etida)]^{2-}$	NO_2	67	160	59, 68
$[MoO_3(nta)]^{3-}$	NO_2	67	160	59, 68
$[(MoO_3)_2(pdta)]^{4-}$ (20°C)	NO_2	67	260	59, 85
(95°C)		56, 68		85
$[(MoO_3)_2(hpdta)]^{4-}$	NO_2	70	400	59
$[(MoO_3)_2(hedta)]^{3-}$	NO_2	76	500	59

[a] In H_2O, pH = 5.5–6.0. [b] For ligand abbreviations, see pp. 171, 172.

TABLE 9

Binuclear Mo(V) compounds [a]

Compound	Solvent	Chemical shift (ppm)	Linewidth (Hz)	T (°C)	Ref.
$[Mo_2O_4(H_2O)_6]^{2+}$	1–6 M $MeSO_3H$	533	500–670 [b]	20	16
		542	260–390 [b]	50	16
	1–6 M HCl	535	450	20	16
		547	230–260 [b]	50	16
$Na_2[Mo_2O_4(edta)]\cdot H_2O$	H_2O (pH 5.5)	609	490	20	16
$Na_2[Mo_2O_2S_2(edta)]\cdot 2\ H_2O$	H_2O (pH 5.0)	982	300	50	16
$Na_2[Mo_2O_4(cyst)_2]\cdot 5\ H_2O$	H_2O (pH 5.2)	434	250	50	16
$Na_2[Mo_2O_4(pdta)]\cdot 4\ H_2O$	H_2O (pH 5.5)	635	200	70	16
		ca. 590			
$Na_2[Mo_2O_4(pen)_2]$	H_2O (pH 5.3)	431	360	20	85
$Na_2[Mo_2O_4(C_2O_4)_2(H_2O)]\cdot 3\ H_2O$	4 M $H_2C_2O_4$	533	300	20	86
syn-$[Mo_2O_4([9]aneN_3)]I_2$	H_2O	588	250	20	87
anti-$[Mo_2O_4([9]aneN_3)]I_2$	H_2O	342	250	20	87
anti-$[Mo_2O_4([12]aneN_3)_2](PF_6)_2$	MeCN	320	680		87
$(Et_4N)[Mo_2O_2(4\text{-}MeC_6H_4S)_6(OMe)]$	MeCN	718	157		88

[a] For ligand abbreviations, see pp. 171, 172. [b] Increases with increasing acid concentration due to increasing viscosity of the medium.

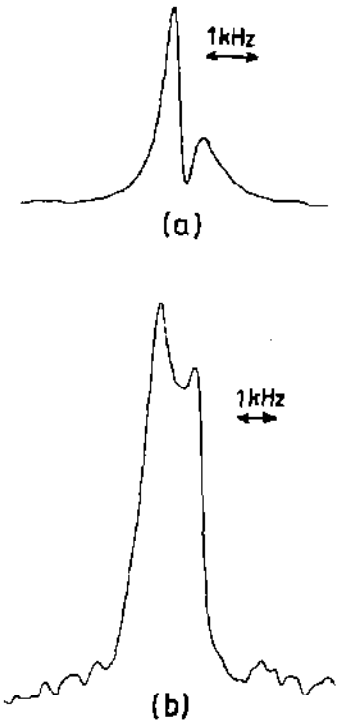

Fig. 16. ^{95}Mo NMR spectra of: (a) $Na_2[Mo_2O_4(pdta)]\cdot 4\ H_2O$ (0.5 M, pH 5.5, 70°C). The distorted line shape is due to a large phase variation across the spectrum due to a pre-acquisition delay time of 500 μs imposed to avoid a rolling base-line; (b) $Na_4[(Mo_3O_4)_2(pdta)_3]\cdot 14\ H_2O$ (ca. 0.2 M; pH 5.5, 70°C). Reproduced from ref. 16, with permission.

complexes containing the *syn*-$[(Mo^{V}O)_2(\mu\text{-}X)_2]^{2+}$ (X = O, S) structural unit (Table 9). The chemical shift observed [16] for the Mo(V) aquo-ion in $MeSO_3H$ and HCl is the same within experimental error and independent of acid concentration in the range 1–6 M. This suggests that $[Mo_2O_4(H_2O)_6]^{2+}$ is being observed in both systems.

The complexes, $[Mo_2O_4(edta)_2]^{2-}$ and $[Mo_2O_4(pdta)_2]^{2-}$ exhibit one and two ^{95}Mo NMR resonances, respectively (Fig. 16(a)) at 70°C. The methyl group on the backbone of the pdta ligand removes the C_2 symmetry axis present in the edta complex and two geometric isomers are possible. A detailed comparison of ^{1}H, ^{13}C and ^{95}Mo results allows assignment of the ^{95}Mo resonances to the inequivalent Mo–N–CHMe– and Mo–N–CH_2– sites of the so-called equatorial isomer of the *syn*-pdta compound [16]. A similar resolution was observed in the $[(Mo^{VI}O_3)_2(pdta)]^{4-}$ system (Section E(i)(g)).

The chemical shifts are again very sensitive to the electronic environment of the molybdenum atom. Note the large chemical shift difference of 246

ppm between the *syn* and *anti* isomers of $[Mo_2O_4L_2]I_2$ (**9**) [87,89], where L is 1,4,7-triazacyclononane. The *anti* isomer is more shielded even though its first electronic transition occurs at lower energy than that of the *syn* isomer. Clearly, the differences in $\Delta\epsilon$ for the first electronic transition cannot be the major factor in determining the chemical shift difference for this pair of complexes (see Section G(i)(b)).

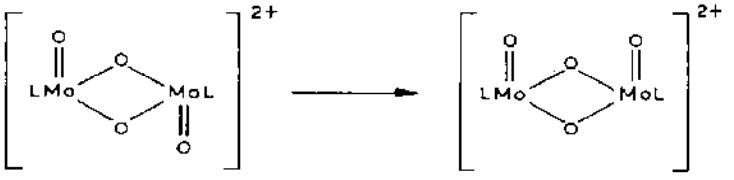

purple
342 ppm

yellow
586 ppm

9

(iii) Molybdenum(IV) compounds

The chemical shift scale for mononuclear Mo(IV) species is not well-defined (Table 10, also see Note Added in Proof and ref. 70). However, trinuclear systems based upon the $[Mo_3O_4]^{4+}$ structural unit **10** have been

TABLE 10

Molybdenum(IV) compounds [a]

Compound	Solvent	δ (ppm)	Line-width (Hz)	T (°C)	Ref.
$K_4[Mo(CN)_8]$	H_2O	−1309	80	RT	19
$K_4[MoO_2(CN)_4]$	H_2O (pH 9)	1452	360	20	85
$[Mo_3O_4(H_2O)_9]^{4+}$ [b]	4 M *p*-$MeC_6H_4SO_3H$	1133	350	50	16
	4 M $MeSO_3H$	990	620	50	16
		539 [c]	350		16
	4 M HCl	1162	450	50	16
		1024	550		
		550 [c]	500		
$H_2[Mo_3O_4(C_2O_4)_3(H_2O)_3]$	sat. aq. $H_2C_2O_4$	1044	520	20	16
$Na_4[(Mo_3O_4)_2(edta)_3]\cdot 14\ H_2O$	D_2O	1083	1000	50	16
		608 [c]	500		
$Na_4[(Mo_3O_4)_2(pdta)_3]\cdot 14\ H_2O$	H_2O (pH 5.5)	1103	1400	75	16
		1025			
$Na_2[Mo_3O_4(Meida)_3]\cdot 7\ H_2O$	H_2O (pH 5.5)	1037	250	50	16

[a] For ligand abbreviations, see pp. 171, 172. [b] Enriched to 96.7 atom % ^{95}Mo. [c] These resonances appear in aerobic solutions upon storage of samples in air.

studied in detail [16] (Table 10). Resonances were detected in the chemical shift range 990–1162 ppm for solutions of Mo(IV) generated in *p*-toluenesulfonic, methanesulfonic and hydrochloric acid media and for aqueous solutions of complexes which contain the $[Mo_3O_4]^{4+}$ unit in the solid state. The narrowness of the observed range (172 ppm) indicated that the ^{95}Mo nuclei are in similar molecular and electronic environments in all the species examined. When coupled with ^{18}O transfer [90] and EXAFS [91] experiments, the results confirm that Mo(IV) solutions in acid media contain high proportions of $[Mo_3O_4(H_2O)_9]^{4+}$ or simple complexes derived from it by substitution of water ligands. For example, two resonances attributable to $[Mo_3O_4]^{4+}$ based clusters are observed in 4 M HCl solution and the simplest interpretation of the existing data is that two species are present which differ in the number of chloro ligands. It is also possible that resolution of inequivalent sites in a single species such as $[Mo_3O_4(H_2O)_8Cl]^{3+}$ is occurring. This certainly seems to be the case in $[(Mo_3O_4)_2(pdta)_3]^{4-}$ where the two resonances (Fig. 16(b)) can be assigned to inequivalent *Mo*–N–CHMe and *Mo*–N–CH_2– sites. Although this Mo(IV) system is more complicated stereochemically than the Mo(VI) and Mo(V) pdta cases discussed previously (Sections E(i)(g) and E(ii)), a similar assignment is suggested.

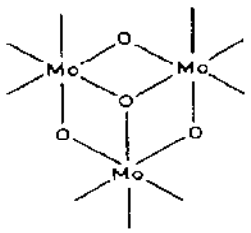

10

(iv) Molybdenum(III) compounds

Mononuclear Mo(III) species have a d^3 electron configuration and are paramagnetic, but binuclear species featuring a metal–metal triple bond are diamagnetic and can be studied by ^{95}Mo NMR [92]. The complexes Mo_2L_6 ($L = Me_2HCO^-$, Me_3CO^-, $Me_3CCH_2O^-$, Me_2N^-, $Me_3SiCH_2^-$) (Table 11) absorb between 2400 and 3700 ppm, and are among the most deshielded resonances known (Fig. 9). Only binuclear Mo(II) species with associated metal–metal quadrupole bonds have more positive chemical shifts. The shielding of the ^{95}Mo nucleus increases in the order alkyl < tertiary alkoxo < primary and secondary alkoxo < dialkylamido. The linewidths vary from 120 Hz to 630 Hz and are generally narrower than those of the Mo(II) dimers discussed in Section E(v)(e).

TABLE 11

Binuclear Mo(III) compounds [a]

Compound	Solvent	Chemical shift (ppm)	Linewidth (Hz)
$Mo_2(NMe_2)_6$	hexane	2420	630
	toluene	2430	1320
$Mo_2(OCHMe_2)_6$	toluene	2444	350
$Mo_2(OCH_2CMe_3)_6$	toluene	2447	600
$Mo_2(OCMe_3)_6$	toluene	2645	120
$Mo_2(CH_2SiMe_3)_6$	toluene	3624	500

[a] Data from ref. 92.

(v) Molybdenum(II) compounds

The wide variety of Mo(II) complexes which have been investigated by ^{95}Mo NMR includes organometallic compounds with carbonyl and cyclopentadienyl ligands, isocyanide complexes, diastereomeric complexes, and metal–metal quadruply-bonded binuclear species. Monomeric Mo(II) complexes resonate from +200 to −2100 ppm, the more shielded portion of the molybdenum chemical shift range. In contrast, the Mo(II) dimers are the most deshielded complexes known, with chemical shifts around 4000 ppm (Fig. 9).

(a) Tricarbonyl compounds

Table 12 presents ^{95}Mo NMR data for complexes with the general formula $CpMo(CO)_3X$, where X is a monodentate ligand. All of the compounds have linewidths < 200 Hz [54,93,94]. The chemical shifts show that the shielding of the $[CpMo(CO)_3]^+$ core increases in the order $-CMe{=}CMe_2$ < Cl < Br < I < $-CH_2C_6H_4R$ < Me < H < $SnMe_3$. Thus these complexes exhibit normal halogen dependence. Electron-donating ligands like $SnMe_3$ cause shielding of the molybdenum nucleus, whereas electron-withdrawing ligands such as $-CMe{=}CMe_2$ cause deshielding. It is interesting that the hydride ligand is more shielding than Me and the halogens. No ^{95}Mo–^{1}H coupling was reported for $CpMo(CO)_3H$ even though the linewidth was only 25 Hz.

A good example of the dependence of the chemical shift on ligand substituents is shown in Table 13. For $CpMo(CO)_3(CH_2C_6H_4R)$ complexes a chemical shift range of 40 ppm is observed upon variation of the R group [94]. The ^{95}Mo NMR chemical shift in these complexes is particularly sensitive to distant substituents (up to six intervening bonds). The chemical shift change is such that electron-donating substituents on the aryl ring cause shielding of the ^{95}Mo nucleus (Fig. 17). The data in Table 13 also illustrate

TABLE 12

Tricarbonylmolybdenum(II) compounds

Compound	Solvent	Chemical shift (ppm)	Line-width (Hz)	Ref.
$CpMo(CO)_3(CMe{=}CMe_2)$	$CDCl_3$	−607	110	93
$CpMo(CO)_3Cl$	$CDCl_3$	−836	120	93
$CpMo(CO)_3Br$	$CDCl_3$	−956	115	93
$CpMo(CO)_3I$	$CDCl_3$	−1248	105	93
$CpMo(CO)_3(CH_2C_6H_4R)$	$CHCl_3$ MeCN	−1551 to −1599	[a]	54, 94
$CpMo(CO)_3Me$	C_6D_6	−1736	40	93
$[CpMo(CO)_3]_2Hg$	$CDCl_3$	−1834	160	93
$CpMo(CO)_3H$	C_6D_6	−2047	25	93
$CpMo(CO)_3SnMe_3$	$CDCl_3$	−2072	60	93
$[(Me_3[9]aneN_3)Mo(CO)_3Br]PF_6$	MeCN	197	130	95, 113
$Cp(CO)Mo(\mu\text{-}SMe)_3Mo(CO)_3$	$CDCl_3$	−560	300	93

[a] See Table 13.

TABLE 13

$CpMo(CO)_3(CH_2C_6H_4R)$ compounds [a]

R	Chemical shift (ppm)	Linewidth (Hz)
H	−1599 [b]	30
	−1577	60
4-Me	−1583	50
4-OMe	−1587	70
4-F	−1577	50
4-Cl	−1566	50
$4\text{-}CF_3$	−1551	60
3-Me	−1579	60
3-OMe	−1574	70
3-F	−1562	40
3-Cl	−1559	50
$3\text{-}CF_3$	−1579 [b]	40
	−1555	60
2-Me	−1572	50
2-OMe	−1573	50
2-F	−1560	40
$2,4,6\text{-}Me_3$	−1599	60

[a] In $CHCl_3$, data from ref. 94. [b] In MeCN, data from ref. 54.

the importance of making substituent studies under identical and controlled conditions because the solvent shifts for R = H and R = $3\text{-}CF_3$ in MeCN (> 20 ppm) are larger than most substituent effects.

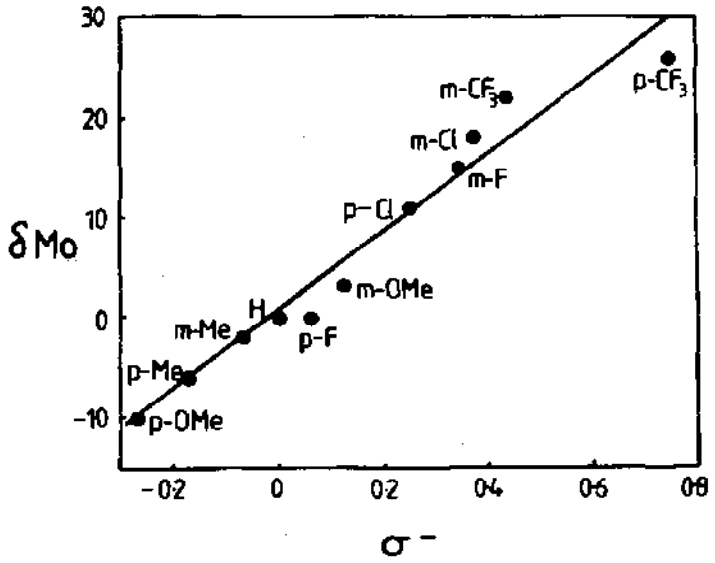

Fig. 17. Variation of $\delta(^{95}Mo)$ with Hammett σ^- constants for complexes $CpMo(CO)_3(CH_2C_6H_4R)$. Reproduced from ref. 94, with permission.

The seven-coordinate Mo(II) complex $[(Me_3[9]aneN_3)Mo(CO)_3Br]PF_6$, with a chemical shift of 197 ppm, is the most deshielded mononuclear Mo(II) complex known. Comparison of the chemical shifts of $CpMo(CO)_3Br$ (−956 ppm) and $[(Me_3[9]aneN_3)Mo(CO)_3Br]^+$ (197 ppm) shows that the

TABLE 14

Dicarbonylmolybdenum(II) compounds

Compound	Solvent	Chemical shift (ppm)	Line-width (Hz)	Ref.
$[\{HB(Me_2Pz)_3\}Mo(CO)_2]_2S$	CH_2Cl_2	+314	600	96
$\{CpMo(CO)_2(SMe)\}_2$	$CDCl_3$	−158, −213	120	93
$[CpMo(CO)_2(N,N^*)]PF_6$ [a] **(14)**	Me_2CO	−128 to −168	[a]	97
$CpMo(CO)_2(N',N^*)$ [a] **(16)**	Me_2CO	−293 to −310	[a]	97
$CpMo(CO)_2(C,N^*)$ [a] **(15)**	Me_2CO	−383 to −396	[a]	97
$CpMo(CO)_2(S_2PEt_2)$	$CDCl_3$	−340	170	93
	C_6D_6	−341	180	93
$CpMo(CO)_2(S_2CSEt)$	$CDCl_3$	−422	130	93
$CpMo(CO)_2(S_2CNEt_2)$	$CDCl_3$	−544	170	93
$CpMo(CO)_2(S_2COEt)$	$CDCl_3$	−559	100	93
$CpMo(CO)_2\{C(CF_3)=C(CF_3)C(O)SMe\}$	$CDCl_3$	−845	110	93
$CpMo(CO)\{C(O)C(CF_3)=C(CF_3)C(O)SMe\}$	$(CD_3)_2CO$	−883	185	93

[a] See Table 15.

Me_3[9]aneN$_3$ ligand deshields the $[Mo(CO)_3Br]^{2+}$ unit by 1150 ppm relative to Cp.

(b) Dicarbonyl compounds

The ^{95}Mo NMR data for several dicarbonyl complexes of general formula $CpMo(CO)_2(X, Y)$, where (X, Y) is a bidentate ligand, appear in Table 14. Linewidths are usually < 200 Hz [93,97]. These compounds provide the first direct comparison of the relative shielding effects of related ligands with sulfur donor atoms. Here the shielding increases in the order dithiophosphate < thioxanthate < dithiocarbamate < xanthate.

The most deshielded compound in Table 14 is $CpMo(CO)_2\{C(CF_3)=C(CF_3)C(O)SMe\}$ for which structure **11** has been proposed. The chemical shift of **11** (−845 ppm) is similar to that of **12** (−883 ppm, 185 Hz), an isomeric compound formed in the same reaction.

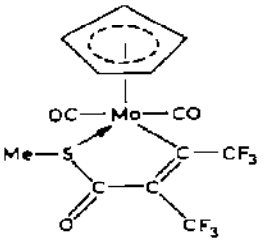

11

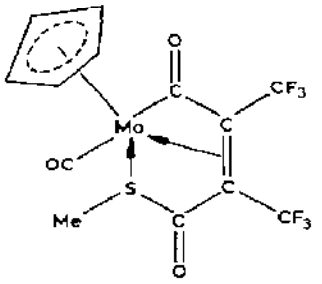

12

The binuclear complex $[CpMo(CO)_2(SMe)]_2$ shows two resonances (−158 and −213 ppm) which are deshielded relative to monomeric $CpMo(CO)_2(S, S)$ complexes. The two resonances are probably due to *syn*- and *anti*-isomers (**13**), analogous to the binuclear Mo(V) complexes (**9**, Section E(ii)).

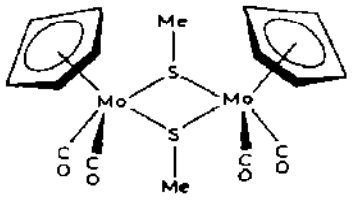

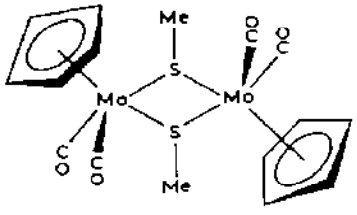

13

The binuclear complex $[\{HB(Me_2pz)_3\}Mo(CO)_2]_2S$ contains the linear $[Mo{=}S{=}Mo]^{2+}$ fragment [96] and has a very short Mo–S distance (2.200 Å). The ^{95}Mo chemical shift (314 ppm) is more deshielded than any other six- or seven-coordinate Mo(II) complex (Tables 12–16). For Mo(II) only metal–metal quadruply-bonded complexes (Section E(v)(e)) have more positive chemical shifts.

TABLE 15

Diastereomeric Mo(II) compounds [a]

General formula [b]	Structure type	Ligand groups			Chemical shift δ (ppm)	Δδ (ppm)	Linewidth (Hz)	Ref.
		R	R′	R″				
$[CpMo(CO)_2(N,N^*)]PF_6$	**14**	Me	Ph	H	−154, −168	14	<100, <100	97, 99
	14	Et	Ph	H	−145, −167	22	150, 70	97
	14	Pr^i	Ph	H	−145, −166	20	100, 70	97
	14	Me	Et	H	−186	[c]	120	97
	14	Me	COOMe	H	−169	[c]	90	97
	14	Et	COOMe	H	−159	[c]	90	97
	14	Pr^i	COOMe	H	−145	[c]	90	97
	14	CH_2Ph	COOMe	H	−160	[c]	120	97
	14	CH_2Ph	$COOCH_2Ph$	H	−156	[c]	160	97
	14	Me	Ph	Me	−141, −147	6	90, 90	97
	14	Me	Et	Me	−154	[c]	90	97
	14	Et	Ph	Ph	−128, −160	32	130, 180	97
$CpMo(CO)_2(C, N^*)$	**15**	Me	Ph	H	−383, −396	13	50, 150	97
$CpMo(CO)_2(N', N^*)$	**16**	N	–	–	−293, −310	17	70, 70	97
	16	Me	–	–	−293, −299	6	90, 120	97
$\{HB(Me_2pz)_3\}Mo(CO)(NO)(PPh_2N^*)$	**17**	H	H	Me	−339, −354	15	170, 220	97
$B(pz)_4Mo(CO)(NO)(PPh_2N^*)$	**17**	H	pz	H	−355, −370	15	160, 160	97
$B(pz)_4Mo(CO)(NO)(PPh_2N^*)$	**17**	Me	pz	H	−298, −309	11	200, 200	97

[a] In acetone solution. [b] See structural formulas **14–17** for the identities of the chiral ligands (N,N*), (C,N*), (N′,N*) and (PPh_2N^*). [c] Diastereomers not differentiated by ^{95}Mo NMR.

(c) Diastereomeric compounds

The addition of chiral bidentate ligands to the $[CpMo(CO)_2]^+$ core yields diastereomeric complexes which differ only in the configuration at the molybdenum atom [98]. A preliminary report [99] showed that ^{95}Mo NMR could be used to detect directly the two different molybdenum configurations (Fig. 18) in **14**. A wider study of diastereomeric Mo(II) complexes (**14**, **15**, **16**, Table 15) has shown that ^{95}Mo chemical shift differences of up to 32 ppm occur for diastereomers which differ only in the Mo configuration and which contain a phenyl group at the chiral carbon atom of the ligand (R′ = Ph). However, individual diastereomers could not be detected when other groups were attached to the chiral carbon atom, even relatively bulky combinations such as R = Bz, R′ = COOMe [97]. The ^{1}H NMR spectra of such complexes show separate resonances for at least one kind of proton in each diastereomeric pair [97,100].

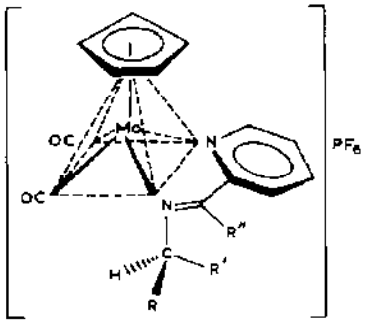

14

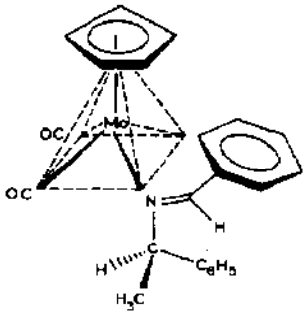

15

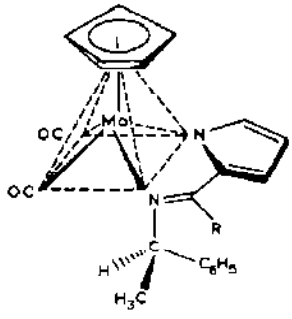

16

^{95}Mo NMR has also differentiated between the diastereomeric molybdenum centers in several polypyrazolylborato complexes containing optically-active aminophosphine ligands (**17**, Table 15),

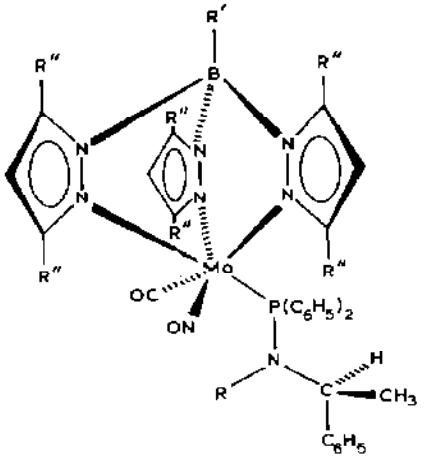

17

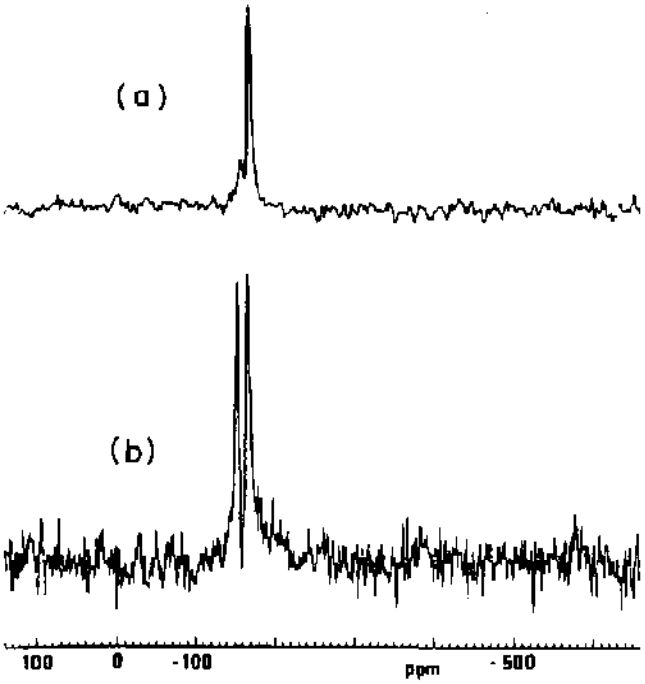

Fig. 18. ^{95}Mo NMR of diastereomers **14** (R = Me, R′ = Ph, R″ = H) in ratios (a) 4:1 and (b) 1:1. Adapted from ref. 99, with permission.

(d) Isocyanide compounds

Seven-coordinate Mo(II)-isocyanide complexes show chemical shifts from +69 to −1003 ppm (Table 16, Fig. 19) [29]. The complexes with seven

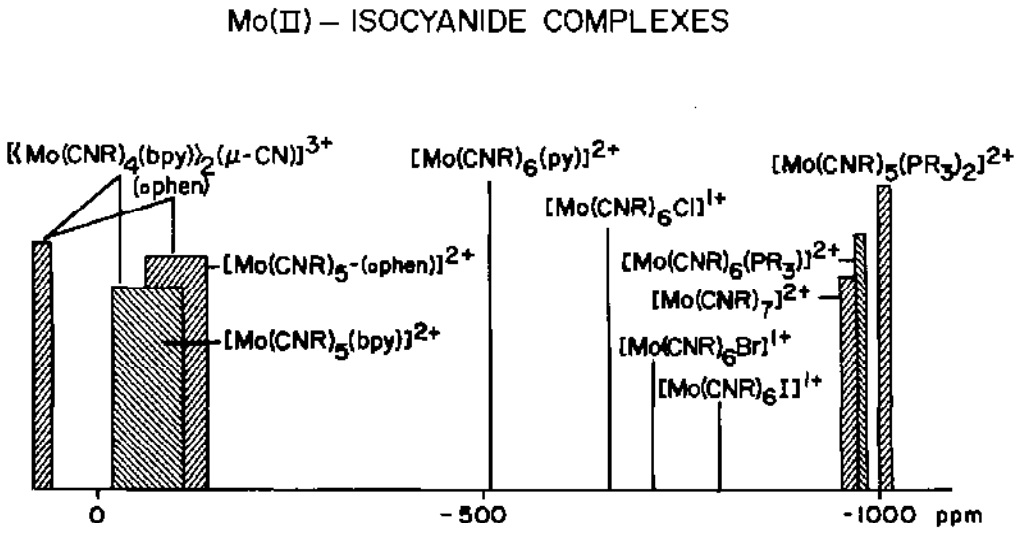

Fig. 19. Chemical shift scale for isocyanide complexes of Mo(II). Reproduced from ref. 29, with permission.

TABLE 16

Isocyanide compounds of Mo(II) [a]

Compound	Chemical shift (ppm)	Linewidth (Hz)
$[Mo(CNCH_3)_5(bpy)](PF_6)_2$	−19	130
$[Mo(CNCHMe_2)_5(bpy)](PF_6)_2$	−64	120
$[Mo(CNCMe_3)_7](PF_6)_2$	−960	35
$[Mo(CNCMe_3)_6(P\text{-}n\text{-}Bu_3)](PF_6)_2$	−970	300
$[Mo(CNCMe_3)_6I]PF_6$	−795	500
$[Mo(CNCMe_3)_6Br]PF_6$	−703	450
$[Mo(CNCMe_3)_6Cl]PF_6$	−688	450
$[Mo(CNCMe_2)_6(py)](PF_6)_2$	−508	600
$[Mo(CNCMe_3)_5(bpy)](PF_6)_2$	−57	100
$[Mo(CNCMe_3)_5(Me_2bpy)](PF_6)_2$	−86	140
$[Mo(CNCMe_3)_5(phen)](PF_6)_2$	−78	130
$[Mo(CNCMe_3)_5(dppe)](PF_6)_2$	−980	600
$[\{Mo(CNCMe_3)_4(bpy)\}_2(\mu\text{-}CN)](PF_6)_3$	+69	360
	−61	220
$[\{Mo(CNCMe_3)_4(phen)\}_2(\mu\text{-}CN)](PF_6)_3$	+59	400
	−79	170
$[\{Mo(CNCMe_3)_4(Me_2bpy)\}_2(\mu\text{-}CN)](PF_6)_3$	+46	320
	−92	200
$[Mo(CNC_6H_{11})_7](PF_6)_2$	−970	70
$[Mo(CNC_6H_{11})_5(bpy)](PF_6)_2$	−68	200
$[Mo(CNC_6H_{11})_5(phen)](PF_6)_2$	−98	260
$[Mo(CNC_6H_{11})_5(dppe)](PF_6)_2$	−1003	1100
$[Mo(CNBz)_5(bpy)](PF_6)_2$	−115	220

[a] All compounds measured in acetone at room temperature; data from ref. 29.

isocyanide ligands absorb at the shielded end of the chemical shift range around −960 ppm. Bulky R-groups on the ligand cause more shielding of the ^{95}Mo nucleus.

Replacement of the isocyanide ligands by phosphines causes shielding of about 10 ppm for every isocyanide ligand replaced. Substitution of an isocyanide ligand by an aryl nitrogen-donor ligand such as pyridine causes deshielding by over 400 ppm, and the replacement of two isocyanide ligands by two aryl nitrogen atoms, as in the *o*-phen, bpy or Me_2bpy complexes, deshields the ^{95}Mo nucleus by about 900 ppm. The $[Mo(CNCMe_3)_6X]^+$ complexes show normal halogen dependence for the chemical shift with shielding increasing in the order Cl < Br < I.

In the CN-bridged dimers, $[\{Mo(CNR)_4L\}_2(\mu\text{-}CN)]^{3+}$, the C- and N-bonded molybdenum centers can be clearly distinguished. By comparison with the corresponding monomeric $[Mo(CNR)_5L]^{2+}$ complexes, the more

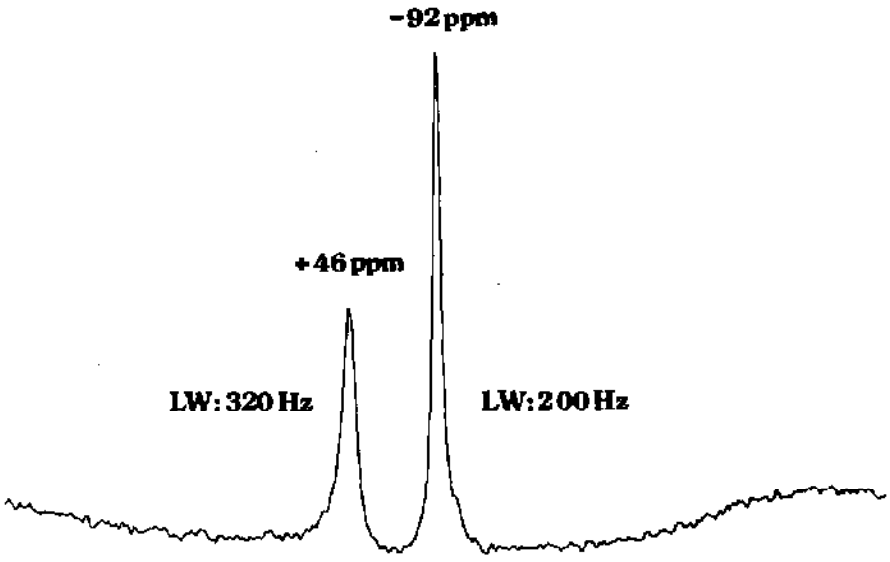

Fig. 20. ^{95}Mo NMR spectrum of $[\{Mo(CNCMe_3)_4(Me_2bpy)\}_2(\mu\text{-}CN)](PF_6)_3$ in acetone. The peak at +46 ppm is assigned to the Mo atom coordinated to the N atom of the μ-CN group. Reproduced from ref. 29, with permission.

shielded ^{95}Mo NMR signal is assigned to the C-bonded Mo and the deshielded signal to the N-bonded Mo (Fig. 20). This assignment is also consistent with the greater linewidth for the deshielded signal.

(e) Binuclear compounds

The chemical shifts for binuclear Mo(II) complexes featuring quadrupole bonds range from 3200 to 4200 ppm (Table 17) [16,20]. These complexes show the most deshielded chemical shifts known to date. Due to their large linewidths the ^{95}Mo NMR spectra of most of these complexes were measured at elevated temperatures. A good correlation between the chemical shifts of the dimers having carboxylato ligands and the pK_a values of these ligands has been found [20]. The lower the pK_a of the ligand the more deshielded is the ^{95}Mo nucleus in the dimer. Replacing Cl^- by Br^- in these complexes causes more shielding, i.e. these complexes show a normal halogen dependence like the other Mo(II) complexes mentioned above.

(vi) Molybdenum(I) compounds

Only a few Mo(I) complexes have been studied by ^{95}Mo NMR. The metal–metal singly-bonded species $[CpMo(CO)_3]_2$ (−1856 ppm, 180 Hz [101]) and $[(Me_5Cp)Mo(CO)_3]_2$ (−1701 ppm, 180 Hz [92]) are found at the shielded end of the molybdenum chemical shift range (Fig. 9). On the other

TABLE 17

Quadruply bonded Mo(II) dimers [a]

Compound	Solvent	Chemical shift (ppm)	Linewidth (Hz)	Temperature (°C)
$Mo_2(O_2CMe)_4$	THF	3702	520	55
	$HCONMe_2$	3768	670	70
$Mo_2(O_2CCHCl_2)_4$	$HCONMe_2$	4006	1070	70
$Mo_2(O_2CPr^n)_4$	THF	3682	1320	55
	$HCONMe_2$ [b]	3730	1400	70
$Mo_2(O_2CPr^i)_4$	THF	3670	950	55
	$HCONMe_2$	3719	1200	70
$Mo_2(O_2CBu^n)_4$	THF	3661	1440	55
	$HCONMe_2$	3746	1390	70
$Mo_2(O_2CBu^t)_4$	THF	3656	1040	55
	$HCONMe_2$	3696	1130	70
$Mo_2(O_2CCF_3)_4$	THF	4021	480	20
	THF [b]	4026	250	55
	$HCONMe_2$	4144	640	20
	$HCONMe_2$	4148	280	70
	MeCN	4029	320	20
	MeCN	4025	220	50
Mo_2^{4+}(aq)	1 M CF_3SO_3H	4056	430	ca. 40
$K_4[Mo_2(SO_4)_4]\cdot 2\,H_2O$	1 M CF_3SO_3H	4090	990	ca. 40
$K_4[Mo_2Cl_8]$	1 M HCl	3816	1440	20
$Cs_4[Mo_2Br_8]$	$HCONMe_2$	3227	510	20

[a] Data from ref. 20. [b] Data from ref. 16.

hand, the metal–metal triply-bonded species $[CpMo(CO)_2]_2$ (182 ppm, 100 Hz [92]) is near the center of the chemical shift range. Thus, in reaction (6) the Mo–Mo bond distance decreases from 3.235 Å to 2.448 Å and the chemical shift increases by over 2000 ppm [103,104]. Substantial deshielding of the molybdenum nucleus in metal–metal multiply-bonded complexes is also found for Mo(III) (Section E(iv)) and Mo(II) (Section E(v)(e)) and appears to be a general feature in ^{95}Mo NMR.

$$Cp(CO)_3Mo\text{–}Mo(CO)_3Cp \rightarrow Cp(CO)_2Mo{\equiv}Mo(CO)_2Cp + 2\ CO \qquad (6)$$

(vii) Molybdenum(0) compounds

The first Mo(0) complex to be measured by ^{95}Mo NMR was $Mo(CO)_6$ (−1856 ppm, 0.7 Hz) [50]. Several classes of Mo(0) complexes have since been studied including pentacarbonyl, tetracarbonyl, and tricarbonyl com-

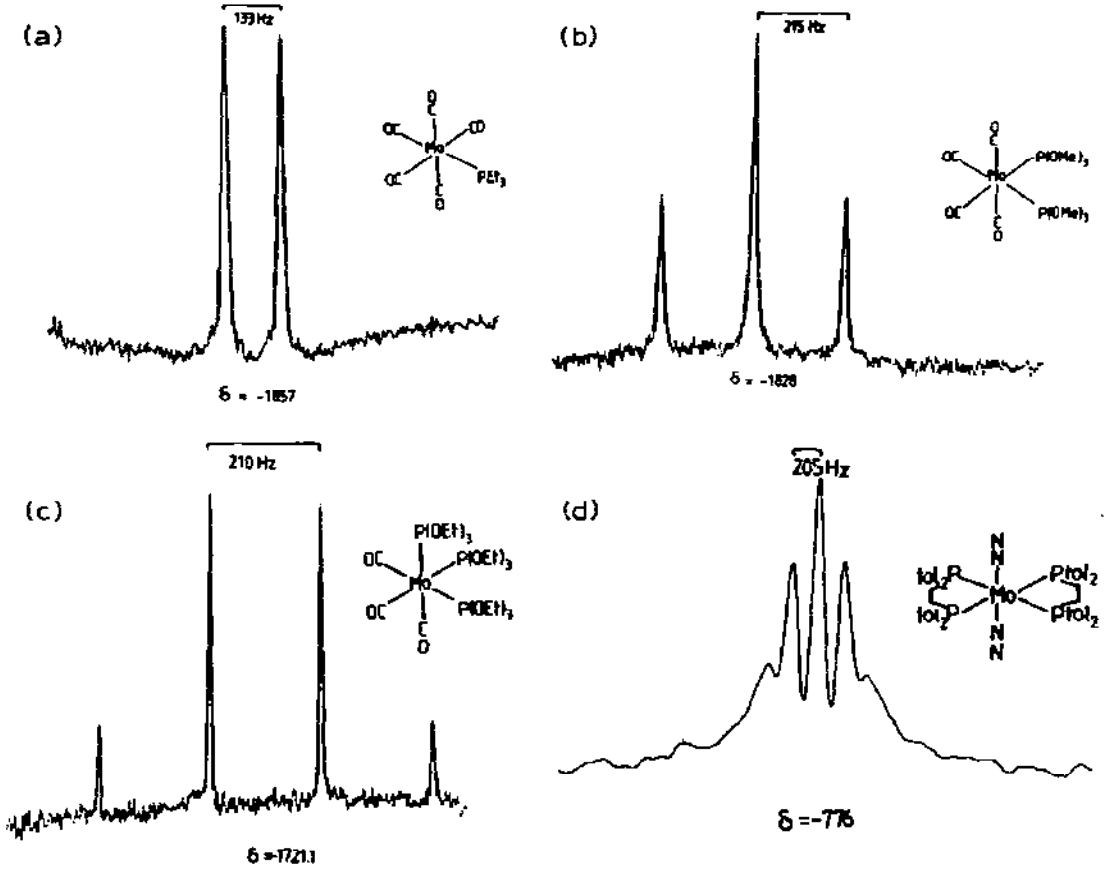

Fig. 21. ^{95}Mo NMR spectra of: (a) $Mo(CO)_5(PEt_3)$; (b) *cis*-$Mo(CO)_4\{P(OMe)_3\}_2$; (c) *fac*-$Mo(CO)_3\{P(OEt)_3\}_3$; (d) *trans*-$Mo(N_2)_2(dptpe)_2$. Reproduced from ref. 105, with permission.

plexes, and bis-dinitrogen adducts. These complexes cover the shielded part of the known ^{95}Mo NMR chemical shift range (Fig. 9). Well-resolved ^{95}Mo–^{31}P spin–spin coupling is observed for Mo(0) complexes with phosphorus-containing ligands (Fig. 21). Trends in the values of the coupling constants are discussed in Section E(xi)(a).

(a) Pentacarbonyl compounds

A large number of $Mo(CO)_5L$ complexes have been studied (Table 18). Complexes with L = phosphine absorb between −1700 and −1900 ppm, i.e. they are mostly deshielded compared to $Mo(CO)_6$. Complexes with L = phosphite absorb between −1800 and −1900 ppm. In general substitution of a CO group in $Mo(CO)_6$ by a weaker π-acceptor than CO leads to deshielding relative to $Mo(CO)_6$. The order of shielding for $Mo(CO)_5L$ complexes is $P(OR)_3 > PR_3$.

TABLE 18

Pentacarbonyl compounds

Compound	Solvent	Chemical shift (ppm)	Linewidth (Hz)	Ref.
$Mo(CO)_5(CNCMe_2Ph)$	$CDCl_3$	−1752	130	101
$(Et_4N)[HMo_2(CO)_{10}]$	THF	−1937	30	105
$Mo(CO)_5(PMe_2Ph)$	$CHCl_3$	−1788	10	105
$Mo(CO)_5(PEt_2Ph)$	CH_2Cl_2	−1815	10	105
$Mo(CO)_5(PBu^n_2Ph)$	CH_2Cl_2	−1808	20	105
$Mo(CO)_5(PPh_3)$	CH_2Cl_2	−1743	50	106, 124
$Mo(CO)_5(PEt_3)$	CH_2Cl_2	−1856	6	105
$Mo(CO)_5(PCy_3)$	CH_2Cl_2	−1825	50	106, 124
$Mo(CO)_5(PBu^n_3)$	[b]	−1842	40	105
$Mo(CO)_5(PBu^n_3)$	CH_2Cl_2	−1843	20	33, 106, 124
$Mo(CO)_5(PBu^t_3)$	CH_2Cl_2	−1711	70	106, 124
$Mo(CO)_5(AsPh_3)$	CH_2Cl_2	−1757	110	105, 106, 124
$Mo(CO)_5(SbPh_3)$	CH_2Cl_2	−1864	120	101, 105, 106, 124
$Mo(CO)_5\{P(C_6H_4\text{-}p\text{-}OMe)_3\}$	CH_2Cl_2	−1745	70	101, 106, 124
$Mo(CO)_5\{P(OMe)_3\}$	[b]	−1864	5	33, 54, 105
$Mo(CO)_5\{P(OEt)_3\}$	[b]	−1854	10	33, 54, 105
$Mo(CO)_5\{P(OPr)_3\}$	CH_2Cl_2	−1851	20	106
$Mo(CO)_5\{P(OPr^i)_3\}$	[b]	−1835	15	33, 105
$Mo(CO)_5\{P(OBu^n)_3\}$	[b]	−1854	30	105
$Mo(CO)_5\{P(OPh)_3\}$	CH_2Cl_2	−1819	40	33, 105, 106, 124
$Mo(CO)_5(CH_3CN)$	MeCN	−1440	40	106, 124
$Mo(CO)_5(pip)$	CH_2Cl_2	−1433	80	106, 124
$Mo(CO)_5(py)$	$CDCl_3$	−1387	70	101
$(Et_4N)[Mo(CO)_5Cl]$	CH_2Cl_2	−1513	110	107
$(Et_4N)[Mo(CO)_5Br]$	CD_2Cl_2	−1540	130	101, 107
$(Et_4N)[Mo(CO)_5I]$	CD_2Cl_2	−1660	190	101
$Mo(CO)_5(PPh_2Cl)$	$CDCl_3$	−1702		109

TABLE 18 (continued)

Compound	Solvent	Chemical shift (ppm)	Linewidth (Hz)	Ref.
$Mo(CO)_5(PPh_2OMe)$	$CDCl_3$	−1791		108
$Mo(CO)_5(PPh_2OEt)$	$CDCl_3$	−1788		108
$Mo(CO)_5(PPh_2OPr^n)$	$CDCl_3$	−1788		108
$Mo(CO)_5(PPh_2SPr^n)$	$CDCl_3$	−1726		109
$Mo(CO)_5(PPh_2OPr^i)$	$CDCl_3$	−1783		108
$Mo(CO)_5(PPh_2SPr^i)$	$CDCl_3$	−1723		109
$Mo(CO)_5(PPh_2OBu^n)$	$CDCl_3$	−1788		108
$Mo(CO)_5(PPh_2OBu^s)$	$CDCl_3$	−1782		108
$Mo(CO)_5(PPh_2OBu^i)$	$CDCl_3$	−1788		108
$Mo(CO)_5(PPh_2OSiMe_3)$	$CDCl_3$	−1765		109
$Mo(CO)_5(PPh_2OPh)$	$CDCl_3$	−1775	40	109, 126
$Mo(CO)_5\{PPh_2(OC_6H_4\text{-}p\text{-}Bu^t)\}$	$CDCl_3$	−1775	40	126
$Mo(CO)_5\{PPh_2(OC_6H_4\text{-}p\text{-}Ph)\}$	$CDCl_3$	−1774	47	126
$Mo(CO)_5\{PPh_2(OC_6H_4\text{-}p\text{-}OMe)\}$	$CDCl_3$	−1778	40	126
$Mo(CO)_5\{PPh_2(OC_6H_4\text{-}p\text{-}OPh)\}$	$CDCl_3$	−1774	50	126
$Mo(CO)_5\{PPh_2(OC_6H_4\text{-}p\text{-}SMe)\}$	$CDCl_3$	−1775	40	126
$Mo(CO)_5\{PPh_2(OC_6H_4\text{-}p\text{-}Cl)\}$	$CDCl_3$	−1774	40	126
$Mo(CO)_5\{PPh_2(OC_6H_4\text{-}p\text{-}COPh)\}$	$CDCl_3$	−1772	50	126
$Mo(CO)_5\{PPh_2(OC_6H_4\text{-}p\text{-}CO_2Me)\}$	$CDCl_3$	−1772	50	126
$Mo(CO)_5\{PPh_2(OC_6H_4\text{-}p\text{-}COMe)\}$	$CDCl_3$	−1772	50	126
$Mo(CO)_5\{PPh_2(OC_6H_4\text{-}p\text{-}CHO)\}$	$CDCl_3$	−1770	50	126
$Mo(CO)_5\{PPh_2(OC_6H_4\text{-}p\text{-}CN)\}$	$CDCl_3$	−1771	50	126
$Mo(CO)_5\{PPh_2(OC_6H_4\text{-}p\text{-}NO_2)\}$	$CDCl_3$	−1770	50	126

$Mo(CO)_5\{PPh_2(OC_6H_4\text{-}p\text{-}Me)\}$	$CDCl_3$	−1776	40	109, 126
$Mo(CO)_5\{PPh_2(SC_6H_4\text{-}p\text{-}Me)\}$	$CDCl_3$	−1728		109
$Mo(CO)_5\{PPh(OMe)_2\}$	CH_2Cl_2	−1816		33
$Mo(CO)_5\{P(OCH_2)_3CEt\}$	CH_2Cl_2	−1858 (40°C)	20	33
$Mo(CO)_5(PPh_2NH_2)$	$CDCl_3$	−1767		109
$Mo(CO)_5(PPh_2NHMe)$	$CDCl_3$	−1765		108
$Mo(CO)_5(PPh_2NHEt)$	$CDCl_3$	−1763		108
$Mo(CO)_5(PPh_2NHPr^n)$	$CDCl_3$	−1763		108, 109
$Mo(CO)_5(PPh_2NHPr^i)$	$CDCl_3$	−1760		108, 109
$Mo(CO)_5(PPh_2NHBu^n)$	$CDCl_3$	−1764		108
$Mo(CO)_5(PPh_2NHBu^s)$	$CDCl_3$	−1760		108
$Mo(CO)_5(PPh_2NHBu^i)$	$CDCl_3$	−1763		108
$Mo(CO)_5(PPh_2NHSiMe_3)$	$CDCl_3$	−1725		109
$Mo(CO)_5(PPh_2NHPh)$	$CDCl_3$	−1736		109
$Mo(CO)_5\{(PPh_2NHC_6H_4\text{-}p\text{-}Me)\}$	$CDCl_3$	−1737		109
$Mo(CO)_5\{PPh(NEt_2)\}_2$	CH_2Cl_2	−1801 (40°C)	30	33
$Mo(CO)_5\{P(NMe_2)_3\}$	CH_2Cl_2	−1803 (40°C)	20	33
$Mo(CO)_5(C_5H_{10}NH)$	CH_2Cl_2	−1423 (40°C)	50	33
$(NH_4)[Mo(CO)_5\{S_2P(OEt)_2\}]$	Me_2SO	−1626	90	107
$Na[Mo(CO)_5(S_2CNPh_2)]$	Me_2SO	−1596	50	107
$Na[Mo(CO)_5(S_2CNMe_2)]$	Me_2SO	−1534	100	107

[a] Compounds with coordinated phosphorus atoms usually show ^{95}Mo–^{31}P spin–spin coupling; see Section E(xi)(a) and Table 26. [b] Solvent is the ligand.

TABLE 19

Tetracarbonyl compounds [a]

Compound	Solvent	Chemical shift (ppm)	Line-width (Hz)	Ref.
$Mo(CO)_4(pn)$	$HCONMe_2$	−1311	90	54
$Mo(CO)_4(bpy)$	$HCONMe_2$	−1150	110	54, 105
cis-$Mo(CO)_4(PPh_3)_2$	CH_2Cl_2	−1556	50	106, 124
cis-$Mo(CO)_4(PBu^n_3)_2$	CH_2Cl_2	−1742	90	105, 106, 124
cis-$Mo(CO)_4(AsPh_3)_2$	CH_2Cl_2	−1577	190	106, 124
cis-$Mo(CO)_4(SbPh_3)_2$	CH_2Cl_2	−1807	250	106, 124
cis-$Mo(CO)_4\{P(C_6H_4$-*p*-$OMe)_3\}_2$	CH_2Cl_2	−1560	390	106
cis-$Mo(CO)_4(PPh_2Me)_2$	CH_2Cl_2	−1637	60	106, 124
cis-$Mo(CO)_4(PPh_2Et)_2$	CH_2Cl_2	−1657	80	106
cis-$Mo(CO)_4\{(pip)P(OPh)_3\}$	CH_2Cl_2	−1362	110	106, 124
cis-$Mo(CO)_4\{(pip)P(OPr^i)_3\}$	CH_2Cl_2	−1394	300	106
cis-$Mo(CO)_4(MeCN)_2$	MeCN	−1307	50	106
cis-$Mo(CO)_4(pip)_2$	$HCONMe_2$	−1093	90	106
trans-$Mo(CO)_4(PBu^n_3)_2$	toluene	−1741	70	106
trans-$Mo(CO)_4(AsPh_3)_2$	toluene	−1757	5	106
trans-$Mo(CO)_4(SbPh_3)_2$	toluene	−1867	150	106
trans-$Mo(CO)_4\{P(C_6H_4$-*p*-$OPh)_3\}_2$	CH_2Cl_2	−1739	60	106
trans-$Mo(CO)_4(PPh_2Et)_2$	toluene	−1705	110	106
cis-$Mo(CO)_4(PEt_3)_2$	CH_2Cl_2	−1764	20	105
cis-$Mo(CO)_4(PBu^n_2Ph)_2$	CH_2Cl_2	−1688	80	105
cis-[$Mo(CO)_4$(dppm)]	CH_2Cl_2	−1552	160	105
cis-[$Mo(CO)_4$(dppe)]	CH_2Cl_2	−1782	50	105
cis-[$Mo(CO)_4$(dppp)]	CH_2Cl_2	−1694	60	105
$Mo(CO)_4(Ph_2PCH_2PPr^i_2)$	CH_2Cl_2	−1612 (40°C)	150	33
$Mo(CO)_4(Ph_2PCH_2PBu^t_2)$	CH_2Cl_2	−1552 (40°C)	50	33
$Mo(CO)_4(Ph_2PCH_2PPhPr^i)$	CH_2Cl_2	−1588 (40°C)	50	33

$Mo(CO)_4\{CH_2(PPh_2)_2\}$	CH_2Cl_2	−1578 (40°C)	140	33
$Mo(CO)_4(Ph_2PCH{=}CHPPh_2)$	CH_2Cl_2	−1801 (40°C)	30	33
$Mo(CO)_4\{HC(PPh_2)_3\}$	CH_2Cl_2	−1538 (40°C)	100	33
$Mo(CO)_4\{Ph_2P(S)CH_2PPh_2\}$	CH_2Cl_2	−1468 (40°C)	400	33
$Mo(CO)_4\{Ph_2P(S)CH_2PPr^i_2\}$	CH_2Cl_2	−1545 (40°C)	400	33
cis-$Mo(CO)_4\{P(OMe)_3\}_2$	CH_2Cl_2/C_6D_6	−1827	20	33, 110, 105
trans-$Mo(CO)_4\{P(OMe)_3\}_2$	CH_2Cl_2/C_6D_6	−1844	60	33, 110
cis-$Mo(CO)_4\{P(OEt)_3\}_2$	CH_2Cl_2	−1807	20	105, 110
cis-$Mo(CO)_4\{P(OPr^i)_3\}_2$	CH_2Cl	−1762	20	105, 106
cis-$Mo(CO)_4\{P(OBu^n)_3\}_2$	CH_2Cl_2	−1808	30	105
cis-$Mo(CO)_4\{P(OPh)_3\}_2$	CH_2Cl_2	−1752	50	33, 105, 106, 124
trans-$Mo(CO)_4\{P(OPh)_3\}_2$	CH_2Cl_2	−1792	30	106
$Mo(CO)_4(PPh_2OMe)_2$	CH_2Cl_2	−1677 (40°C)	30	33
$Mo(CO)_4(PMe_2Ph)_2$	CH_2Cl_2	−1670 (40°C)	20	33
$Mo(CO)_4(pip)_2$	CH_2Cl_2	−1077 (40°C)	120	33
cis-$Mo(CO)_4(PPh_2Cl)_2$	CH_2Cl_2	−1522	70	111
cis-$Mo(CO)_4(PPh_2NH_2)_2$	CH_2Cl_2	−1652	50	111
cis-$Mo(CO)_4(PPh_2NHMe)_2$	CH_2Cl_2	−1622	100	111
cis-$Mo(CO)_4(PPh_2OMe)_2$	CH_2Cl_2	−1707	40	111
cis-$Mo(CO)_4(PPh_2SEt)_2$	CH_2Cl_2	−1540	150	111
cis-$Mo(CO)_4(PPh_2NHSiMe_3)_2$	CH_2Cl_2	−1563	80	111
cis-$Mo(CO)_4(PPh_2OSiMe_3)_2$	CH_2Cl_2	−1623	60	111
cis-$Mo(CO)_4(PPh_2NHC_6H_4$-*p*-$Me)_2$	CH_2Cl_2	−1571	80	111
cis-$Mo(CO)_4(PPh_2OC_6H_4$-*p*-$Me)_2$	CH_2Cl_2	−1654	90	111
cis-$Mo(CO)_4(PPh_2SC_6H_4$-*p*-$Me)_2$	CH_2Cl_2	−1537	100	111
$Mo(CO)_4(PPh_2NHSiMe_2NHPPh_2)$	CH_2Cl_2	−1610	40	111
$Mo(CO)_4(PPh_2OSiMe_2OPPh_2)$	CH_2Cl_2	−1700	90	111
$Mo(CO)_4(PPh_2NHSiMe(Ph)NHPPh_2)$	CH_2Cl_2	−1676	60	111
$Mo(CO)_4(PPh_2OSiMe(Ph)OPPh_2)$	CH_2Cl_2	−1685	50	111
$[Mo(CO)_4]_2\{(PPh_2)_2O_2SiO_2(PPh_2)_2\}$	CH_2Cl_2	−1710	50	111
$Mo(CO)_4(PPh_2NMeCH_2CH_2NMePPh_2)$	CH_2Cl_2	−1670	60	111
$K[Mo(CO)_4(S_2COEt)]$	Me_2SO	−1417	170	107
$Na[Mo(CO)_4(S_2CNMe_2)]$	Me_2SO	−1414	270	107
$Na[Mo(CO)_4(S_2CNEt_2)]$	Me_2SO	−1409	170	107

TABLE 19 (continued)

Compound	Solvent	Chemical shift (ppm)	Line-width (Hz)	Ref.
$(NH_4)[Mo(CO)_4\{S_2P(OEt)_2\}]$	Me_2SO	−1390	150	107
$K[Mo(CO)_4\{S_2CN(CH_2)_4\}]$	Me_2SO	−1388	250	107
$(NH_4)[Mo(CO)_4\{S_2CN(CH_2)_4\}]$	NMP	−1380	270	107
$Mo(CO)_4$(norbornadiene)	$CDCl_3$	−1591	25	101
cis-$Mo(CO)_4(py)_2$	pyridine	−1051	130	130

[a] ^{95}Mo–^{31}P spin–spin coupling constants appear in Table 26.

When L is a halogen ligand, replacement of Cl^- by Br^- by I^- causes more shielding, i.e. a normal halogen dependence. The available data also suggest that the ^{95}Mo shielding increases with the atomic number of the Group 15 donor atom: N < P < As < Sb.

(b) Tetracarbonyl compounds

The $Mo(CO)_4L_2$ complexes (Table 19) are similar to the pentacarbonyl complexes and become more deshielded when $P(OR)_3$ is replaced by PR_3, and an increase of the shielding from N to P to As to Sb is observed. The replacement of two carbonyl groups in $Mo(CO)_6$ causes greater chemical shift changes than the mono-substitution of the $Mo(CO)_5L$ series. A comparison of ten pairs of $Mo(CO)_5(PPh_2XR)$ and $Mo(CO)_4(PPh_2XR)_2$ complexes possessing identical XR groups showed that each $Mo(CO)_4(PPh_2XR)_2$ complex was less shielded than its $Mo(CO)_5(PPh_2XR)$ counterpart [109]. The correlation coefficient for all the pairs was 0.969. *trans*-$Mo(CO)_4L_2$ complexes are usually more shielded than the corresponding *cis*-$Mo(CO)_4L_2$ complexes [33,106].

(c) Tricarbonyl compounds

The ligand effects for $Mo(CO)_3L_3$ complexes (Table 20), where L is a monodentate ligand, are the same as those described above for the $Mo(CO)_5L$ and $Mo(CO)_4L_2$ complexes.

For the $Mo(CO)_3L'$ complexes, where L' is a ligand which can occupy three coordination sites of the metal, the ^{95}Mo nuclear shielding decreases with L' in the order Cp > tol > *o*-xyl > *p*-xyl > *m*-xyl > mes > triphos > cht > [9]aneS$_3$ > $HB(Me_2pz)_3$ > Me_3[9]aneN$_3$ > dien > [9]aneN$_3$. For the aromatic ligands in this series increasing ring methyl substitution, which is expected to increase the electron density in the aryl ring and presumably around the Mo nucleus, leads to shielding [112]. It is interesting to note that the $HB(Me_2pz)_3$ ligand deshields the molybdenum nucleus by nearly 1000 ppm relative to Cp.

The novel binuclear complex (**18**) contains two $Mo(CO)_3$([9]aneN$_3$) units linked by a $-CH_2CH_2-$ bridge between nitrogen atoms from each of the 1,4,7-triazacyclononane fragments. The chemical shift is intermediate between the shifts for $Mo(CO)_3$, (Me_3[9]aneN$_3$) and $Mo(CO)_3$([9]aneN$_3$) [87] as expected for alkylation of one nitrogen atom of each cyclic ligand. The large linewidth of **18** (850 Hz) presumably reflects the increased rotational correlation time for the larger binuclear species [114].

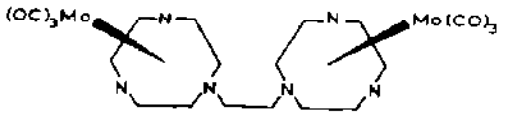

18

TABLE 20

Tricarbonyl compounds

Compound	Solvent	Chemical shift (ppm)	Line-width (Hz)	Ref.
$Na[CpMo(CO)_3]$	THF	−2123	20	112
$Mo(CO)_3(tol)$	CH_2Cl_2	−2034	<10	54, 112
$Mo(CO)_3(o\text{-xyl})$	CH_2Cl_2	−1988	<10	112
$Mo(CO)_3(p\text{-xyl})$	CH_2Cl_2	−1979	10	112
$Mo(CO)_3(m\text{-xyl})$	CH_2Cl_2	−1971	10	112
$Mo(CO)_3(mes)$	CH_2Cl_2	−1907	10	54, 112
$Mo(CO)_3(cht)$	CH_2Cl_2	−1684	10	54, 112
	$CDCl_3$	−1675	20	101
$Mo(CO)_3([9]aneS_3)$	$MeNO_2$	−1350	30	127
$(Et_4N)[Mo(CO)_3\{HB(Me_2pz)_3\}]$	$HCONMe_2$	−1149	80	87
$Mo(CO)_3(Me_3[9]aneN_3)$	Me_2SO	−1092	160	87
$Mo(CO)_3(dien)$	$HCONMe_2$	−1088	70	54
$Mo(CO)_3([12]aneN_3)$	CH_2Cl_2	−1001	13	87
$Mo(CO)_3([9]aneN_3)$	CH_2Cl_2	−866	20	87
fac-$Mo(CO)_3(py)_3$	pyridine	−800	7	185
fac-$Mo(CO)_3(PCl_3)_3$	$CDCl_3$	−1885	3	101
fac-$Mo(CO)_3(AsPh_3)_3$	$CDCl_3$	−1549	350	101
fac-$Mo(CO)_3(SbPh_3)_3$	$CDCl_3$	−1669	50	101
$Mo(CO)_3(triphos)$	CH_2Cl_2	−1760	40	106, 124
$\{Mo(CO)_3\}_2(dtne)$	Me_2SO	−1012	850	114
$Mo(CO)_3(PPh_2Me)_3$	CH_2Cl_2	−1427	10	124
fac-$Mo(CO)_3(MeCN)_3$	MeCN	−1114	10	106
fac-$Mo(CO)_3\{P(OMe)_3\}_3$	CH_2Cl_2/C_6D_6	−1756	10	33, 105, 110
mer-$Mo(CO)_3\{P(OMe)_3\}_3$	CH_2Cl_2/C_6D_6	−1780	200	33, 110
fac-$Mo(CO)_3\{P(OEt)_3\}_3$	CH_2Cl_2	−1721	4	54, 105, 110
fac-$Mo(CO)_3(bpy)\{P(OEt)_3\}_2$	CH_2Cl_2	−1097	50	105

Comparison of the data for *fac*- and *mer*-$Mo(CO)_3\{P(OMe)_3\}_3$ shows that the *mer* isomer is 24 ppm more shielded and has a substantially greater linewidth [33].

(d) Dicarbonyl and monocarbonyl compounds

Relatively few dicarbonyl and monocarbonylmolybdenum(0) complexes have been studied by ^{95}Mo NMR (Table 21). The data for *cis*- and *trans*-$Mo(CO)_2\{P(OMe)_3\}_4$, and $Mo(CO)\{P(OMe)_3\}_5$ and $Mo\{P(OMe)_3\}_6$ [33] complete the series $Mo(CO)_{6-n}\{P(OMe)_3\}_n$ for $n = 0$–6. Figure 22 shows that the molybdenum chemical shift exhibits a shallow minimum at $n = 1$ and then increases smoothly with increasing n. For $n = 2$ and $n = 4$

TABLE 21

Dicarbonyl and monocarbonyl compounds

Compound	Solvent	Chemical shift (ppm)	Line-width (Hz)	Ref.
cis-$Mo(CO)_2\{P(OMe)_3\}_4$	CH_2Cl_2/C_6D_6	−1660	100	33, 110
trans-$Mo(CO)_2\{P(OMe)_3\}_4$	CH_2Cl_2/C_6D_6	−1679	1600	33
$Mo(CO)_2(dptpe)_2$	THF	−1802 (57°C)	120	105
$Mo(CO)_2(C_7H_7)I$	$CDCl_3$	−1349	107	101
$[Mo(CO)_2(C_7H_7)(dppe)]PF_6$	CD_2Cl_2	−1083	250	101
$Mo(CO)\{P(OMe)_3\}_5$	CH_2Cl_2/C_6D_6	−1518	100	33, 110
$Mo\{P(OMe)_3\}_6$	[a]	−1358	15	33

[a] Light petroleum.

the *trans* isomer is more shielded than the *cis* isomer. The linewidths of *cis*-$Mo(CO)_2\{P(OMe)_3\}_4$ (100 Hz) and *trans*-$Mo(CO)_2\{P(OMe)_3\}_4$ (1600 Hz) differ enormously, reflecting the large electric field gradient (q) in the *trans* isomer (eqn. 1).

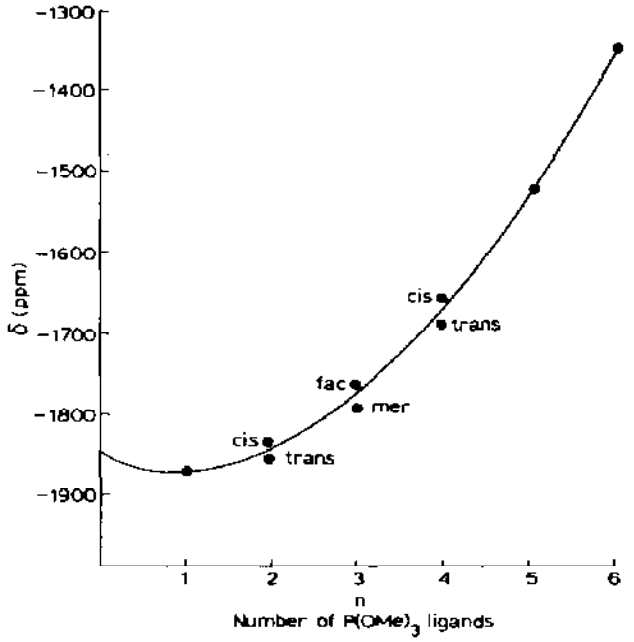

Fig. 22. Variation of $\delta(^{95}Mo)$ with n for species $Mo(CO)_{6-n}\{P(OMe)_3\}_n$. Adapted from data of refs. 33 and 110.

TABLE 22

Dinitrogen compounds [a]

Compound	Chemical shift (ppm)	Line-width (Hz)
trans-$Mo(N_2)_2(dptpe)_2$ [b]	−776 (55°)	~ 90
trans-$Mo(N_2)_2\{(4\text{-}C_6H_4OMe)_2PCH_2CH_2P(4\text{-}C_6H_4OMe)_2\}_2$	−798	~ 100
trans-$Mo(N_2)_2\{(4\text{-}C_6H_4Me)_2PCH_2CH_2P(4\text{-}C_6H_4Me)_2\}_2$	−793	~ 100
trans-$Mo(N_2)_2(dppe)_2$	−787	~ 100
trans-$Mo(N_2)_2\{(4\text{-}C_6H_4Cl)_2PCH_2CH_2P(4\text{-}C_6H_4Cl)_2\}_2$	−785	~ 100
trans-$Mo(N_2)_2\{(4\text{-}C_6H_4CF_3)_2PCH_2CH_2P(4\text{-}C_6H_4CF_3)_2\}_2$	−774	~ 100
trans-$Mo(N_2)_2\{(3\text{-}C_6H_4Me)_2PCH_2CH_2P(3\text{-}C_6H_4Me)_2\}_2$	−795	~ 100
trans-$Mo(N_2)_2(depe)_2$	−1022	~ 100
trans-$Mo(N_2)_2(dppe)(depe)$	−899	~ 100
trans-$Mo(N_2)_2(PMe_2Ph)_4$	−447	~ 100
trans-$Mo(N_2)_2(PPh_2Me)_4$	−464	~ 100

[a] In THF, data from ref. 115. [b] Ref. 105.

(e) Dinitrogen compounds

The ^{95}Mo NMR spectra of bis-dinitrogen complexes of the general formula $Mo(N_2)_2(PR_3)_4$ cover a chemical shift range of about 600 ppm (Table 22) [105,115]. A large number of these complexes have chelating $R_2PCH_2CH_2PR_2$ ligands. When R = Et the complex is more shielded than when R = aryl. The complexes with monodentate phosphine ligands have the most deshielded chemical shifts in this series (~ −450 ppm).

(viii) Mononitrosyl and thionitrosyl compounds

Data for several types of mononitrosylmolybdenum complexes appear in Table 23. So-called "piano-stool" complexes, such as $CpMo(CO)_2(NO)$ (**19**), contain the $\{MoNO\}^6$ group [119] and are formally isoelectronic with Mo(0) complexes. The shielding of the ^{95}Mo nucleus decreases in the order Cp > Me_5Cp > $HB(Me_2pz)_3$ > $HB(pz)_3$ > [9]aneN_3 > Me_3[9]aneN_3. This order parallels that for $Mo(CO)_3$ complexes of the same ligands except that the [9]aneN_3 and Me_3[9]aneN_3 complexes are reversed. Each $LMo(CO)_2(NO)$ complex is less shielded than its $LMo(CO)_3$ analogue (Table 20). For the Cp and Me_5Cp complexes ^{95}Mo–^{14}N spin–spin coupling is observed (Section E(xi)(d)) at room temperature [116].

Substitution of a nitrosyl group by a thionitrosyl group causes deshielding

TABLE 23

Mononitrosyl and thionitrosyl compounds

Compound	Solvent	Chemical shift (ppm)	Line-width (Hz)	Ref.
$CpMo(CO)_2(NO)$	MeCN	−1584	< 40	116
$(Me_5Cp)Mo(CO)_2(NO)$	MeCN	−1404	< 40	116
$LMo(CO)_2(NO)$ [a]	CH_2Cl_2	−743	60	117
$LMo(CO)_2(NS)$	CH_2Cl_2	−192	50	117
$\{HB(pz)_3\}Mo(CO)_2(NO)$	$MeCN/Me_2CO$	−672	70	116
$[([9]aneN_3)Mo(CO)_2(NO)]BF_4$	H_2O	−616	110	87
$[([12]aneN_3)Mo(CO)_2(NO)]ClO_4$	H_2O	−580	90	87
$[(Me_3[9]aneN_3)Mo(CO)_2(NO)]PF_6$	MeCN	−437	80	87
$[CpMo(NO)I_2]_2$	$HCONMe_2$	−26	750	118
$Cp(\sigma\text{-}Cp)Mo(NO)(S_2CNMe_2)$	$CDCl_3$	−369	390	101
$Mo(NO)(S_2CNMe_2)_3$	CH_2Cl_2	−212	900	30
$Mo(NS)(S_2CNMe_2)_3$	CH_2Cl_2	140	650	30
$Mo(NO)(S_2CNEt_2)_3$	CH_2Cl_2	−206	900	30
$Mo(NS)(S_2CNEt_2)_3$	CH_2Cl_2	142	850	30
$CpMo(NO)(SPh)_2$	$CDCl_3$	144	580	186
$LMo(NO)I_2$	CH_2Cl_2	2272	1800	118
$LMo(NO)Cl_2$	CH_2Cl_2	1811	1400	118
$LMo(NO)F_2$	CH_2Cl_2	1274	1490	118
$LMo(NO)I(NHC_6H_4Me)$	CH_2Cl	568	1350	118
LMo(NO)I(NHEt)	CH_2Cl_2	430	1200	118
LMo(NO)Cl(NHEt)	CH_2Cl_2	404	1000	118
LMo(NO)I(OPh)	CH_2Cl_2	1179	1600	118
LMo(NO)Cl(OPh)	CH_2Cl_2	1050	1750	118
LMo(NO)Cl(SPh)	CH_2Cl_2	1200	2340	118
$LMo(NO)Cl(NHC_6H_4Br)$	CH_2Cl_2	539	1500	118
$LMo(NO)Cl(NHC_6H_4Me)$	CH_2Cl_2	523	1700	118
$LMo(NO)(OEt)_2$	CH_2Cl_2	464	800	118
$LMo(NO)I(NHNMe_2)$	CH_2Cl_2	284	900	118
$LMo(NO)(SPh)_2$	CH_2Cl_2	990	1560	118
$LMo(NO)(OPh)_2$	CH_2Cl_2	624	1600	118
$LMo(NO)(NHPh)_2$	CH_2Cl_2	161	600	118

[a] L = Hydrotris(3,5-dimethyl-1-pyrazolyl)borate.

of about 500 ppm, a chemical shift change comparable with that seen in the replacement of a terminal oxo group by a terminal sulfido group in Mo(VI) complexes [19,68,71]. All of the $LMo(CO)_2(NX)$ piano stool complexes have

relatively narrow lines (40–110 Hz).

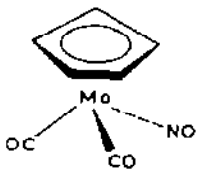

19

The $Mo(NO)(S_2CNR_2)_3$ complexes of Table 23 contain the $\{MoNO\}^4$ group and are formally related to seven-coordinate Mo(II) complexes. The chemical shift of $Mo(NO)(S_2CNMe_2)_3$ (−212 ppm) is substantially deshielded relative to the $\{MoNO\}^6$ complexes. The linewidths of these $\{MoNO\}^4$ complexes (900 Hz) are much larger than those for the piano stool molecules discussed above. Substitution of the nitrosyl group by a thionitrosyl group again causes deshielding, but by a smaller amount (350 ppm) [30].

Six-coordinate $\{MoNO\}^4$ complexes with the general formula $\{HB(Me_2pz)_3\}Mo(NO)XY$, where X and Y are monoanionic ligands, exhibit ^{95}Mo NMR resonances (160 to 2270 ppm) which are substantially deshielded [118] relative to the other types of mononitrosyl complexes in Table 23, and relative to monomeric Mo(II) (d^4) complexes (Tables 12–16). In addition these nitrosyl complexes show an inverse halogen dependence of the chemical shift, a phenomenon seen previously only for Mo(VI) complexes [73]. For the $\{HB(Me_2pz)_3\}Mo(NO)X_2$ compounds shielding increases in the order X = I < Cl < SPh < OPh < OEt < NHPh. The linewidths are large relative to other complexes of similar molecular size and shape. For example, the linewidth of $\{HB(Me_2pz)_3\}Mo(NO)Cl_2$ is 1400 Hz, whereas the linewidth of $\{HB(Me_2pz)_3\}Mo(CO)_2(NO)$ is only 60 Hz. These large differences in linewidth presumably arise from large differences in the asymmetry parameters for the two molecules.

(ix) Dinitrosyl compounds

The chemical shifts measured for six-coordinate $[Mo(NO)_2]^{2+}$ complexes which contain the $\{Mo(NO)_2\}^6$ unit range from +200 to −1000 ppm (Table 24). The chemical shifts generally decrease with the increasing ability of ancillary ligands to delocalize electrons from the metal atom. Substitution of Cl^- by Br^- and I^- in $CpMo(NO)_2X$ complexes results in a decrease of the chemical shift, i.e. these complexes show a normal halogen dependence. Figure 6 and Table 24 show that the linewidth of $Mo(NO)_2(acac)_2$ increases from 90 to 435 Hz with increasing viscosity of the solvent. The chemical shift varies by only 25 ppm in these solvents and shows no correlation with viscosity.

TABLE 24

Dinitrosyl compounds [a]

Compound	Solvent	Chemical shift (ppm)	Linewidth (Hz)
$CpMo(NO)_2I$	CH_2Cl_2	−985	70
$CpMo(NO)_2Br$	CH_2Cl_2	−883	70
$CpMo(NO)_2Cl$	CH_2Cl_2	−852	70
$(Me_5Cp)Mo(NO)_2Cl$	MeCN	−800	70
$Mo(NO)_2Cl_2(PPh_3)_2$	$HCONMe_2$	−500	430
$Mo(NO)_2(S_2CNMe_2)_2$	$HCONMe_2$	−438	90
	MeCN	−437	70
	Me_2CO	−438	60
	Me_2SO	−435	150
$Mo(NO)_2(S_2CNEt_2)_2$	$HCONMe_2$	−430	120
	MeCN	−430	80
	Me_2CO	−431	80
	Me_2SO	−425	170
$Mo(NO)_2\{HB(Me_2pz)_3\}Cl$	CH_2Cl_2	−384	180
$Mo(NO)_2(acac)_2$	$HCONMe_2$	−298	190
	MeCN	−298	90
	Me_2CO	−296	90
	Me_2SO	−282	315
	MeOH	−286	105
	CH_2Cl_2	−283	110
	CH_2ClCH_2Cl	−285	190
	benzene	−281	135
	toluene	−281	125
	iso-pentanol	−271	435
$Mo(NO)_2Cl_2(phen)$	$HCONMe_2$	−265	160
	MeCN	−265	170
	Me_2CO	−265, −280	90
$Mo(NO)_2Cl_2(bpy)$	$HCONMe_2$	−263	170
	MeCN	−255	120
	Me_2CO	−264, −280	100
$(Et_4N)_2[Mo(NO)_2(CN)_4]$	$HCONMe_2$	−104	20
	MeCN	−98	20
	H_2O	−105	20
$Cs_2[Mo(NO)_2Cl_4]$	HCl	+152	170
$(Et_4N)_2[Mo(NO)_2(ox)_2]$	$HCONMe_2$	+201	110

[a] Data from ref. 28.

The ^{95}Mo NMR spectra of $Mo(NO)_2Cl_2L$ (where L = *o*-phen or bpy) show one peak in $HCONMe_2$ and MeCN, but two peaks in acetone. This has been attributed to the partial dissociation of Cl^- from the parent

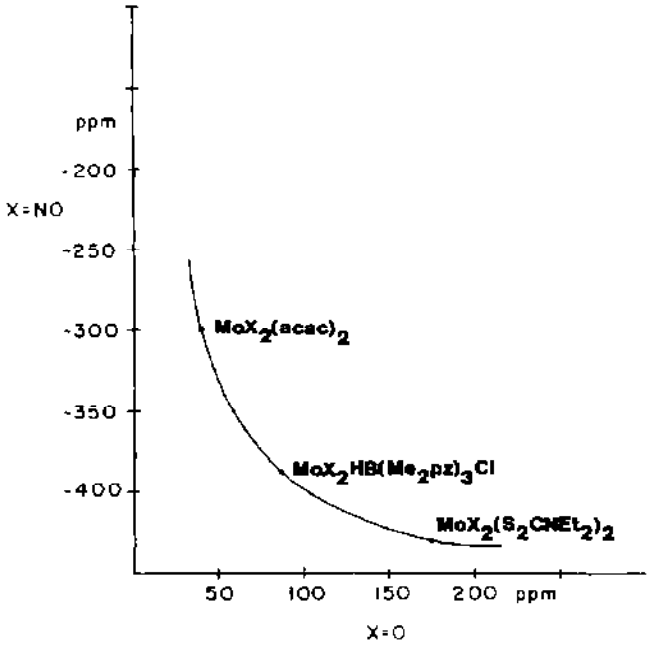

Fig. 23. Inverse correlation of $\delta(^{95}Mo)$ for $[MX_2]^{2+}$ species (X = NO, O).

complex in acetone. Addition of HCl to the acetone solution yields an NMR spectrum with only the parent species present [28].

The general response of the ^{95}Mo chemical shift of six-coordinate $[Mo(NO)_2]^{2+}$ complexes to the other four co-ligands is the opposite of that found for six-coordinate $[MoO_2]^{2+}$ complexes in which the Mo atom is in the +VI oxidation state (Tables 5 and 6). The differing chemical shift response of these two classes of compounds to the same co-ligands is illustrated in Fig. 23.

(x) Molybdenum–mercury compounds

A series of $Cp(CO)_2LMoHgX$ complexes has been studied and the chemical shifts found to vary from −1706 to −1939 ppm, depending on the nature of L and X (Table 25).

(xi) Spin–spin couplings between ^{95}Mo and other nuclei

Spin–spin couplings between ^{95}Mo and ^{31}P, ^{19}F, ^{17}O, ^{14}N and ^{1}H have been observed by ^{95}Mo NMR. Coupling between ^{13}C and ^{95}Mo has been observed by ^{13}C NMR for $Mo(CO)_6$; the ^{95}Mo–^{13}C coupling constant is 68 Hz [121–123].

TABLE 25

$Cp(CO)_2LMoHgX$ compounds [a]

L	X	Chemical shift (ppm)	Linewidth (Hz)
CO	$CpMo(CO)_3$	−1834	160
CO	Cl	−1826	160
CO	Br	−1815	180
CO	I	−1795	120
CO	S_2COEt	−1911	120
CO	S_2CNEt_2	−1939	120
CO	$S_2P(OEt)_2$	−1878	120
$P(OMe)_3$	Cl	−1745	260
$P(OMe)_3$	Br	−1727	230
$P(OMe)_3$	I	−1706	220
$P(OMe)_3$	S_2CNEt_2	−1844	180
$P(OMe)_3$	$S_2P(OEt)_2$	−1780	180

[a] In $CHCl_3$, data from refs. 93, 120.

(a) ^{95}Mo–^{31}P coupling

^{31}P has a nuclear spin of 1/2 (100% abundant) and ^{95}Mo–^{31}P spin–spin coupling has been observed for a large number of Mo(0) complexes with phosphorus ligands (Fig. 21). The coupling constants range from 117 to 290 Hz (Table 26) with the smaller values (117–145 Hz) being observed for phosphine ligands. Replacement of a phenyl group in the triphenylphosphine ligand by an alkoxy group increases the coupling constant by 12–15 Hz [33,105,108,110,111]. Replacement of the phenyl group by an $-NR_2$ or $-SR$ group changes J only slightly compared with triphenylphosphine [108,110,111]. For phosphite ligands coupling constants from 209 to 257 Hz are found [33,105,124]. The largest coupling constants are due to PF_3 ligands (279–290 Hz) [125]. For a given phosphine ligand (L) the ^{95}Mo–^{31}P coupling constants are relatively independent of the number of phosphorus ligands attached to the ^{95}Mo nucleus, and similar coupling constants are found for $Mo(CO)_5L$, $Mo(CO)_4L_2$ and $Mo(CO)_3L_3$ complexes.

(b) ^{95}Mo–^{19}F coupling

In complexes containing the PF_3 ligand second order coupling between ^{95}Mo and ^{19}F is also found. The coupling constant is 14 Hz [125].

(c) ^{95}Mo–^{17}O coupling

Spin–spin coupling between ^{17}O ($I = 5/2$) and ^{95}Mo has been observed

TABLE 26

$^{95}Mo-^{31}P$ coupling constants

Compound	Solvent	$J(^{95}Mo-^{31}P)$ (Hz)	Ref.
$Mo(CO)_5(PEt_3)$	[a]	133	105
$Mo(CO)_5(PBu^n_3)$	[a]	133	105
$Mo(CO)_5(PPh_3)$	CH_2Cl_2	144	101, 105
$Mo(CO)_5(PMe_2Ph)$	$CHCl_3$	131	105
$Mo(CO)_5(PEt_2Ph)$	CH_2Cl_2	132	105
$Mo(CO)_5(PBu^n_2Ph)$	CH_2Cl_2	133	105
$Mo(CO)_5(PCy_3)$	CH_2Cl_2	129	106, 124
$Mo(CO)_5(PBu^i_3)$	CH_2Cl_2	127	33, 105, 106, 124
$Mo(CO)_5\{P(OMe)_3\}$	[a]	218	33, 105
$Mo(CO)_5\{P(OEt)_3\}$	[a]	214	33, 54, 105
$Mo(CO)_5\{P(OPr^i)_3\}$	[a]	215	33, 105
$Mo(CO)_5\{P(OBu^n)_3\}$	[a]	216	105
$Mo(CO)_5\{P(OPh)_3\}$	$CHCl_3$	237	33, 105
$Mo(CO)_5\{P(C_6H_4\text{-}p\text{-}OMe)_3\}$	CH_2Cl_2	156	124
$Mo(CO)_5\{P(OCH_2)_3CEt\}$	CH_2Cl_2	227 (40°C)	33
$Mo(CO)_5\{PPh(OMe)_2\}$	CH_2Cl_2	183	33
$Mo(CO)_5(PPh_2Cl)$	$CDCl_3$	165	109
$Mo(CO)_5(PPh_2OMe)$	$CDCl_3$	156	108
$Mo(CO)_5(PPh_2OEt)$	$CDCl_3$	159	108
$Mo(CO)_5(PPh_2OPr^n)$	$CDCl_3$	159	108
$Mo(CO)_5(PPh_2SPr^n)$	$CDCl_3$	142	109
$Mo(CO)_5(PPh_2OPr^i)$	$CDCl_3$	156	108
$Mo(CO)_5(PPh_2SPr^i)$	$CDCl_3$	145	109
$Mo(CO)_5(PPh_2OBu^n)$	$CDCl_3$	159	108
$Mo(CO)_5(PPh_2OBu^s)$	$CDCl_3$	159	108
$Mo(CO)_5(PPh_2OBu^i)$	$CDCl_3$	159	108
$Mo(CO)_5(PPh_2OSiMe_3)$	$CDCl_3$	161	109
$Mo(CO)_5(PPh_2OPh)$	$CDCl_3$	161	109, 126

$Mo(CO)_5\{PPh_2(OC_6H_4\text{-}p\text{-}Bu^t)\}$	$CDCl_3$	164	126
$Mo(CO)_5\{PPh_2(OC_6H_4\text{-}p\text{-}Ph)\}$	$CDCl_3$	164	126
$Mo(CO)_5\{PPh_2(OC_6H_4\text{-}p\text{-}OMe)\}$	$CDCl_3$	162	126
$Mo(CO)_5\{PPh_2(OC_6H_4\text{-}p\text{-}OPh)\}$	$CDCl_3$	162	126
$Mo(CO)_5\{PPh_2(OC_6H_4\text{-}p\text{-}SMe)\}$	$CDCl_3$	161	126
$Mo(CO)_5\{PPh_2(OC_6H_4\text{-}p\text{-}Cl)\}$	$CDCl_3$	161	126
$Mo(CO)_5\{PPh_2(OC_6H_4\text{-}p\text{-}COPh)\}$	$CDCl_3$	164	126
$Mo(CO)_5\{PPh_2(OC_6H_4\text{-}p\text{-}CO_2Me)\}$	$CDCl_3$	164	126
$Mo(CO)_5\{PPh_2(OC_6H_4\text{-}p\text{-}COMe)\}$	$CDCl_3$	164	126
$Mo(CO)_5\{PPh_2(OC_6H_4\text{-}p\text{-}CHO)\}$	$CDCl_3$	164	126
$Mo(CO)_5\{PPh_2(OC_6H_4\text{-}p\text{-}CN)\}$	$CDCl_3$	165	126
$Mo(CO)_5\{PPh_2(OC_6H_4\text{-}p\text{-}NO_2)\}$	$CDCl_3$	165	126
$Mo(CO)_5\{PPh_2(OC_6H_4\text{-}p\text{-}Me)\}$	$CDCl_3$	162	109, 126
$Mo(CO)_5\{PPh_2(SC_6H_4\text{-}p\text{-}Me)\}$	$CDCl_3$	150	109, 126
$Mo(CO)_5(PPh_2NH_2)$	$CDCl_3$	148	109
$Mo(CO)_5(PPh_2NHMe)$	$CDCl_3$	146	108
$Mo(CO)_5(PPh_2NHEt)$	$CDCl_3$	146	108
$Mo(CO)_5(PPh_2NHPr^n)$	$CDCl_3$	146	108
$Mo(CO)_5(PPh_2NHPr^i)$	$CDCl_3$	146	108
$Mo(CO)_5(PPh_2NHBu^n)$	$CDCl_3$	149	108
$Mo(CO)_5(PPh_2NHBu^s)$	$CDCl_3$	151	108
$Mo(CO)_5(PPh_2NHBu^i)$	$CDCl_3$	146	108
$Mo(CO)_5(PPh_2NHSiMe_3)$	$CDCl_3$	149	109
$Mo(CO)_5(PPh_2NHPh)$	$CDCl_3$	150	109
$Mo(CO)_5\{PPh_2(NHC_6H_4\text{-}p\text{-}Me)\}$	$CDCl_3$	153	109
$Mo(CO)_5\{PPh(NEt_2)_2\}$	CH_2Cl_2	159 (40°C)	33
$Mo(CO)_5\{P(NMe_2)_3\}$	CH_2Cl_2	173 (40°C)	33
cis-$Mo(CO)_4(PEt_3)_2$	CH_2Cl_2	125	105
cis-$Mo(CO)_4(PBu^n_3)_2$	CH_2Cl_2	124	105
cis-$Mo(CO)_4(PBu^n_2Ph)_2$	CH_2Cl_2	140	105
$Mo(CO)_4(PPh_2OMe)_2$	CH_2Cl_2	161	33
cis-$Mo(CO)_4$(dppm)	CH_2Cl_2	119	33, 105
cis-$Mo(CO)_4$(dppe)	CH_2Cl_2	128–145	33, 105, 124
cis-$Mo(CO)_4$(dppp)	CH_2Cl_2	142	33, 105

TABLE 26 (continued)

Compound	Solvent	$J(^{95}Mo-^{31}P)$ (Hz)	Ref.
$Mo(CO)_4(Ph_2PCH_2PPr^i_2)$	CH_2Cl_2	117 (40°C)	33
$Mo(CO)_4(Ph_2PCH_2PBu^t_2)$	CH_2Cl_2	117 (40°C)	33
$Mo(CO)_4(Ph_2PCH_2PPhPr^i)$	CH_2Cl_2	124 (40°C)	33
$Mo(CO)_4\{CH_2{=}C(PPh_2)_2\}$	CH_2Cl_2	125 (40°C)	33
$Mo(CO)_4(Ph_2PCH{=}CHPPh_2)$	CH_2Cl_2	134 (40°C)	33
$Mo(CO)_4\{HC(PPh_2)_3\}$	CH_2Cl_2	127 (40°C)	33
cis-$Mo(CO)_4\{P(OMe)_3\}_2$	CH_2Cl_2	215	33, 105, 110
cis-$Mo(CO)_4\{P(OEt)_3\}_2$	CH_2Cl_2	213	105
cis-$Mo(CO)_4\{P(OPr^i)_3\}_2$	CH_2Cl_2	209	105
cis-$Mo(CO)_4\{P(OBu^n)_3\}_2$	CH_2Cl_2	212	105
cis-$Mo(CO)_4\{P(OPh)_3\}_2$	CH_2Cl_2	226	105
$Mo(CO)_4(PMe_2Ph)_2$	CH_2Cl_2	130 (40°C)	33
cis-$Mo(CO)_4\{P(OPh)_3\}_2$	CH_2Cl_2	250	106, 124
cis-$Mo(CO)_4(pip)\{P(OPh)_3\}$	CH_2Cl_2	257	106, 124
cis-$Mo(CO)_4(PPh_3)_2$	CH_2Cl_2	140	106, 124
cis-$Mo(CO)_4(PPh_2Me)_2$	CH_2Cl_2	133	106, 124
trans-$Mo(CO)_4\{P(OPh)_3\}_2$	CH_2Cl_2	225	124
trans-$Mo(CO)_4\{P(OMe)_3\}_2$	CH_2Cl_2/C_6D_6	235	33, 110
trans-$Mo(CO)_4(PPh_2Me)_2$	$C_6H_5CH_3$	134	124
cis-$Mo(CO)_4(PPh_2Cl)_2$	CH_2Cl_2	166	111
cis-$Mo(CO)_4(PPh_2NH_2)_2$	CH_2Cl_2	144	111
cis-$Mo(CO)_4(PPh_2NHMe)_2$	CH_2Cl_2	138	111
cis-$Mo(CO)_4(PPh_2OMe)_2$	CH_2Cl_2	153	111
cis-$Mo(CO)_4(PPh_2SEt)_2$	CH_2Cl_2	140	111
cis-$Mo(CO)_4(PPh_2NHSiMe_3)_2$	CH_2Cl_2	139	111
cis-$Mo(CO)_4(PPh_2OSiMe_3)_2$	CH_2Cl_2	162	111
cis-$Mo(CO)_4\{PPh_2(NHC_6H_4\text{-}p\text{-}Me)\}_2$	CH_2Cl_2	140	111
cis-$Mo(CO)_4\{PPh_2(OC_6H_4\text{-}p\text{-}Me)\}_2$	CH_2Cl_2	157	111
cis-$Mo(CO)_4\{PPh_2(SC_6H_4\text{-}p\text{-}Me)\}_2$	CH_2Cl_2	133	111

$Mo(CO)_4(PPh_2NHSiMe_2NHPPh_2)$	CH_2Cl_2	145	111
$Mo(CO)_4(PPh_2OSiMe_2OPPh_2)$	CH_2Cl_2	154	111
$Mo(CO)_4(PPh_2NHSiMe(Ph)NHPPh_2)$	CH_2Cl_2	144	111
$Mo(CO)_4(PPh_2OSiMe(Ph)OPPh_2)$	CH_2Cl_2	155	111
$[Mo(CO)_4]_2\{(PPh)_2O_2SiO_2(PPh_2)_2\}$	CH_2Cl_2	153	111
$Mo(CO)_4(PPh_2NMeCH_2CH_2NMePPh_2)$	CH_2Cl_2	153	111
fac-$Mo(CO)_3\{PBu^n_3\}_3$	CH_2Cl_2	124	105
fac-$Mo(CO)_3\{P(OMe)_3\}_3$	CH_2Cl_2	214	105
fac-$Mo(CO)_3\{P(OEt)_3\}_3$	CH_2Cl_2	210	105
fac-$Mo(CO)_3(bpy)\{P(OEt)_3\}$	CH_2Cl_2	240	105
$Mo(CO)_3$(triphos)	CH_2Cl_2	129	106, 124
$Mo(CO)_3(PPh_2Me)_3$	CH_2Cl_2	126	106, 124
$Mo(CO)_5(PF_3)$	[b]	284	125
cis-$Mo(CO)_4(PF_3)_2$	[b]	281	125
trans-$Mo(CO)_4(PF_3)_2$	[b]	288	125
fac-$Mo(CO)_3(PF_3)_3$	[b]	290	125
mer-$Mo(CO)_3(PF_3)_3$	[b]	290	125
fac-$Mo(CO)_3(PCl_3)_3$	$CDCl_3$	251	101
cis-$Mo(CO)_2\{P(OMe)_3\}_4$	CH_2Cl_2/C_6D_6	220	33
cis-$Mo(CO)\{P(OMe)_3\}_5$	CH_2Cl_2/C_6D_6	240	33
$[Mo(CO)(C_7H_7)(dppe)]PF_6$	CD_2Cl_2	160	101
$Mo\{P(OMe)_3\}_6$	CH_2Cl_2/C_6D_6	256	33
$Mo(PF_3)_6$	C_6F_6	279	125
trans-$Mo(N_2)_2$(dptpe)$_2$	THF	205 (55°C)	105
trans-$Mo(N_2)_2\{(4\text{-}C_6H_4OMe)_2PCH_2CH_2P(4\text{-}C_6H_4OMe)_2\}_2$	THF	190	115
trans-$Mo(N_2)_2\{(4\text{-}C_6H_4Me)_2PCH_2CH_2P(4\text{-}C_6H_4Me)_2\}_2$	THF	175	115
trans-$Mo(N_2)_2$(dppe)$_2$	THF	180	115
trans-$Mo(N_2)_2\{(4\text{-}C_6H_4Cl)_2PCH_2CH_2P(4\text{-}C_6H_4Cl)_2\}_2$	THF	180	115
trans-$Mo(N_2)_2\{(4\text{-}C_6H_4CF_3)_2PCH_2CH_2P(4\text{-}C_6H_4CF_3)_2\}_2$	THF	180	115
trans-$Mo(N_2)_2\{(3\text{-}C_6H_4Me)_2PCH_2CH_2P(3\text{-}C_6H_4Me)_2\}_2$	THF	ca. 165	115
trans-$Mo(N_2)_2$(depe)$_2$	THF	185	115
trans-$Mo(N_2)_2$(dppe)(depe)	THF	185	115
trans-$Mo(N_2)_2(PPh_2Me)_4$	THF	190	115

[a] The solvent is the ligand. [b] Not specified.

TABLE 27

$^{95}Mo-^{14}N$ coupling constants

Compound	Solvent	T (K)	$J(^{95}Mo-^{14}N)$ (Hz)	Ref.
$CpMo(CO)_2(NO)$	MeCN	293	46	116
$(Me_5Cp)Mo(CO)_2(NO)$	MeCN	343	46	116
$HB(Me_2Pz)_3Mo(CO)_2(NO)$	$HCONMe_2$	423	44	116
$[([9]aneN_3)Mo(CO)_2(NO)]BF_4$	H_2O	373	39	87

by both ^{95}Mo NMR and by ^{17}O NMR [39,55] in aqueous solutions of $[MoO_4]^{2-}$ enriched with ^{17}O. The coupling constant is 40 Hz.

(d) $^{95}Mo-^{14}N$ coupling

$^{95}Mo-^{14}N$ spin–spin coupling has been found in $\{MoNO\}^6$ "piano stool" complexes [116] (Section E(viii)) with the general formula $LMo(CO)_2(NO)$, where L = Cp, Me_5Cp, $HB(Me_2pz)_3$, $HB(pz)_3$ and $[9]aneN_3$ (Table 27).

The splitting can be seen at room temperature for the Cp and Me_5Cp complexes in low viscosity solvents. Elevated temperatures are needed in all the other cases in order to resolve the triplet due to the coupling of ^{95}Mo with one ^{14}N ($I = 1$) nucleus. It was not possible to observe a completely resolved 1 : 1 : 1 triplet since these complexes decompose at high temperatures (Fig. 24). The observed coupling constants are 44–46 Hz.

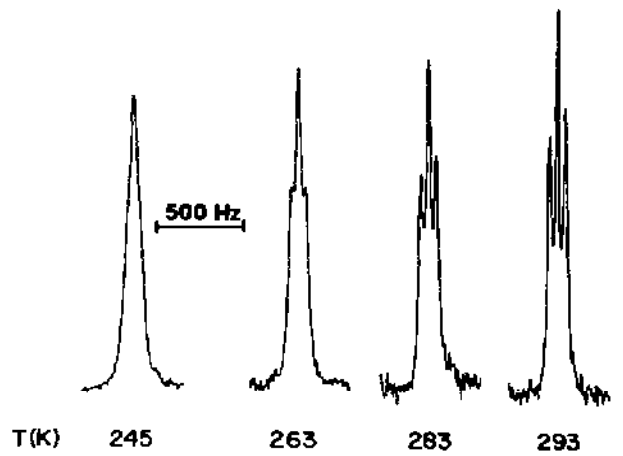

Fig. 24. Temperature dependence of the resolution of $^{95}Mo-^{14}N$ spin–spin coupling in $CpMo(CO)_2(NO)$ in MeCN. Adapted from ref. 116, with permission.

(e) ^{95}Mo–^{1}H coupling

A coupling constant of 15 Hz has been found for ^{95}Mo–^{1}H spin–spin coupling for the bridging H atom in $(Et_4N)[HMo_2(CO)_{10}]$ at room temperature [105]. There are as yet no reports of ^{95}Mo–^{1}H spin–spin coupling for a terminal H atom.

(xii) Relaxation time studies

Both ^{95}Mo and ^{97}Mo are spin 5/2 nuclei and, as briefly discussed in Section A, their relaxation processes are expected [15] to be controlled by the quadrupolar mechanism. As seen in eqn. 1, both the longitudinal and transverse relaxation times, T_1 and T_2, are inversely proportional to the linewidth $W_{1/2}$ and controlled by the magnitudes of the electric field gradient and the correlation time, τ_c. These influences are responsible for the wide range (0.4–4000 Hz) of observed ^{95}Mo linewidths, and consequently T_1 values varying from several seconds to microseconds are expected. In addition, since the ratio of the ^{95}Mo and ^{97}Mo nuclear quadrupole moments Q are known (Table 1), eqn. 1 requires $\{T_1(^{95}Mo)/T_1(^{97}Mo)\}^{1/2} = Q(^{97}Mo)/Q(^{95}Mo) = 11.4$.

Table 28 lists measured $T_1(^{95}Mo)$ values, observed linewidths and T_2 values (designated T_2^*) derived from those linewidths [129,130]. Adequate signal-to-noise ratios are attained using the inversion recovery method (Fig. 25).

The longest T_1 observed is just over 7 s for $Mo(CO)_6$. For a strictly octahedral molecule, the electric field gradient, q, is zero and it is possible for relaxation processes other than the quadrupolar mechanism to become important. In particular, the spin rotation mechanism can be quite efficient, especially for nuclei with large chemical shift ranges [131]. This possibility has been tested [129] in a detailed study of the relaxation properties of the ^{95}Mo, ^{97}Mo, ^{17}O and ^{13}C nuclei in $Mo(CO)_6$ in $CDCl_3$ solution. An experimental estimate of τ_c, $8.5(\pm 0.1)\times 10^{-2}$ s, can be obtained from the measurement of $T_1(^{13}C)$ as a function of magnetic field strength (eqn. 3, Section C(vi)(b) provides an order-of-magnitude estimate only). The results (a) confirm the presence of a small, but non-zero ^{95}Mo quadrupole-coupling constant $e^2q_{zz}Q/h = 133 \pm 15$ kHz, which is in excellent agreement with an estimate obtained in the solid state [132], and (b) indicate that ^{95}Mo and ^{97}Mo relaxation is entirely quadrupolar and caused by rotational reorientation of the small permanent electric field gradient.

If quadrupolar relaxation determines the ^{95}Mo relaxation rates in $Mo(CO)_6$ with a long T_1, then it can safely be assumed to dominate in molecules of lower symmetry. This is confirmed for a selection of molecules whose linewidths are greater than 20 Hz (Table 28) where there is good quantitative

TABLE 28

^{95}Mo relaxation times [a] and linewidths [b]

Compound	Conditions	T_1 (ms)	$W_{1/2}$ (Hz)	T_2^{*} [c] (ms)
$Mo(CO)_6$	0.39 M, $CDCl_3$, 40°C	7010	0.9	340
$CpMo(CO)_3(CH_2C_6H_5)$	0.5 M, $CHCl_3$	4.9	67	4.8
$K_4[Mo(CN)_8]$	0.5 M, H_2O	4.5	74	4.3
$H_2[Mo_3O_4(C_2O_4)_3(H_2O)_3]$	1 M in saturated oxalic acid	0.69	466	0.68
$[Mo_2(O_2CBu^n)_4]$ [d]	1 M, THF, 30°C	0.18	1720	0.19
$[MoS_4]^{2-}$ [e]	0.5 M, H_2O	5370	2.0	160
$[MoO_4]^{2-}$ [e]	0.2 M, H_2O (pH 11), 30°C	1560	2.0	160
	2 M, H_2O (pH 11), 30°C	778	0.7	450
	1 M, (3 M NaCl, H_2O (pH 9–12), 29°C) [f]	840	–	–
$Mo(CO)_3(mes)$	0.5 M, CH_2Cl_2	77.6	6	55
	0.5 M, $CDCl_3$	70.1	7	45
$Mo(CO)_3(p\text{-xyl})$	0.5 M, CH_2Cl_2	104	5	64
	0.5 M, $CDCl_3$	86	5	64
$Mo(CO)_3(tol)$	0.5 M, CH_2Cl_2	165	3	110
	0.5 M, $CDCl_3$	140	4	80
$Mo(CO)_5(PEt_3)$	0.5 M, neat PEt_3	41.4	11	28.9
$Mo(CO)_5(PBu^n_3)$	0.5 M, neat PBu^n_3	5.9	53	6.0
$Mo(CO)_3\{P(OEt)_3\}_3$	0.5 M, CH_2Cl_2	268	3	110
cis-$Mo(CO)_4(py)_2$	0.5 M, $CDCl_3$	3.0	104	3.1

[a] T_1 values were measured using the inversion recovery method on a JEOL FX-200 spectrometer operating at 13 MHz at 20°C using unlocked, non-spinning samples, unless otherwise noted. [b] Refs. 129 and 130. [c] Derived from $W_{1/2}$ values: see text. [d] Measured with the transverse probe described in Section C(vi)(d). [e] Locked, spinning sample. [f] Ref. 18.

agreement between the inversion recovery T_1 values and the linewidth T_2^* values, as required by eqn. 1. The compounds with a linewidth of less than 20 Hz listed in Table 28 exhibit T_2^* values consistently smaller than T_1. This is an artifact of the experimental conditions (unlocked, non-spinning sample) chosen to facilitate the inversion recovery measurements, and which add up to 3 Hz to the observed linewidths. The derived T_2^* values are included in Table 28 as a qualitative guide only. However, the predictions of eqn. 1 qualitatively rationalize existing experimental data. Thus the experimental linewidths (Table 2, Section E(i)(b)) of the ^{95}Mo and ^{97}Mo resonances of the series $[MoO_{4-n}S_n]^{2-}$ ($n = 0, 2, 3, 4$) [53] are in qualitative agreement.

In general, narrow linewidths and long relaxation times are associated with small molecules of high symmetry (small q and τ_c) and broad lines and short relaxation times with a combination of large molecules or low site

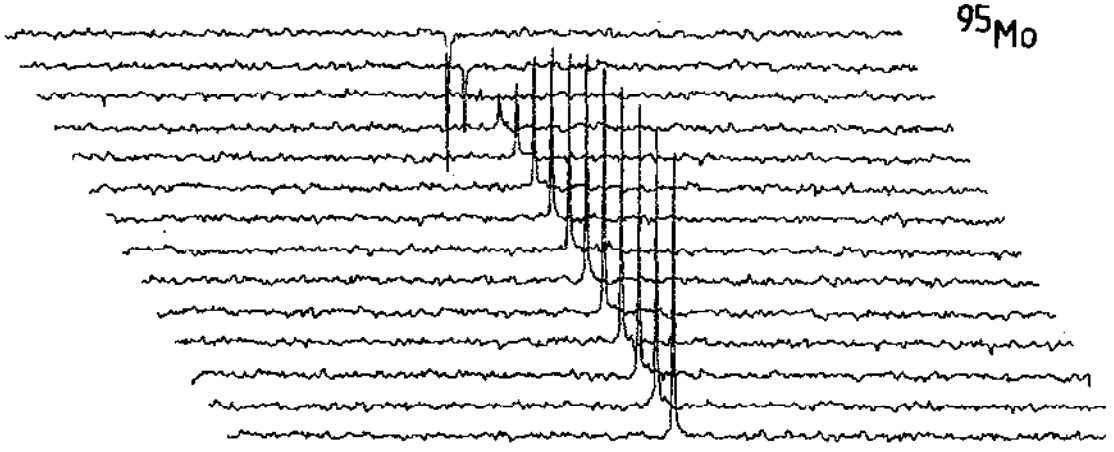

Fig. 25. ^{95}Mo inversion recovery $(180°-\tau-90°-T)_n$ experiment for $Mo(CO)_3$(*p*-xyl) (0.5 M, CH_2Cl_2, 20°C). Spectral width, 5000 Hz; 16 K data points; 4992 points sampled; T, 500 ms; n, 200; accumulation time, 32 min. Reproduced from ref. 130, with permission.

symmetry (larger q or τ_c). Specific features of quantitative relaxation time measurements are listed below (Table 28):

(a) Very long ^{95}Mo relaxation times of 5.4 and 1.6 s are observed for the tetrahedral molecules $[MoS_4]^{2-}$ and $[MoO_4]^{2-}$ in aqueous solution as expected from the high point symmetry. The relative magnitudes are not those expected from simple size considerations and are most likely related to the influence of hydrogen-bonding between coordinated oxo and solvent water leading to a longer correlation time. This effect also rationalizes the dependence of the T_1 value on $[MoO_4]^{2-}$ concentration.

(b) Substitution of the more viscous solvent $CDCl_3$ for CH_2Cl_2 in arene molybdenum tricarbonyl species shortens T_1 values, as expected (eqns. 1 and 3).

(c) An increase in the effective size of $Mo(CO)_5(PR_3)$ by substituting R = Bu^n for R = Et increases τ_c and reduces T_1 from 41.4 to 5.9 ms. On the other hand, although $Mo(CO)_3\{P(OEt)_3\}_3$ is considerably larger than these molecules, T_1 is 268 ms, pointing to a much smaller q.

Besides being useful as a probe of symmetry and correlation times, relaxation time studies reveal optimum acquisition parameters and sample conditions (solvent, temperature) for the collection of ^{95}Mo spectra. This is particularly important for "difficult" samples, i.e. those exhibiting broad lines which must be measured at low concentrations.

(xiii) Experiments with the enzyme xanthine oxidase

An obvious application for ^{95}Mo NMR would be as a probe for the diamagnetic states of the various molybdo–enzymes and their cofactors [7].

Such an application has prompted detailed examination of species containing the *cis*-$[Mo^{VI}OS]^{2+}$ and $-[MoO_2]^{2+}$ structural units (Tables 5 and 6) which appear [78,79] to be present in certain of those enzymes which feature a mononuclear molybdenum active site.

Milk xanthine oxidase (300 000 daltons, α_2, 2 Mo, 4 Fe_2S_2, 2 FAD) whose oxidized active and inactive (desulfo) forms are thought to feature the above structural units, can be isolated in large quantities. A series of measurements on both forms of the enzyme (including samples enriched with ^{95}Mo) have been undertaken independently in the authors' laboratories [133,134]. A resonance has not been observed to date. To assist further development, one of the experiments is outlined. A sample of xanthine oxidase (1.0 g; enriched to 75 atom % ^{95}Mo; 5.1×10^{-4} M ^{95}Mo in active enzyme; 1.8×10^{-4} M in desulfo enzyme) was examined using the transverse probe described in Section C(vi)(d). Sensitivity testing indicated that a resonance of linewidth < 1500 Hz was detectable at 5×10^{-4} M ^{95}Mo. In three separate accumulations, a total chemical shift range of -380 to $+3400$ ppm was scanned.

The combined experiments [133,134] suggest that (a) the linewidth $W_{1/2}$ for the active form of the enzyme is > 1500 Hz under the present conditions or (b) its chemical shift lies outside the -380 to $+3400$ ppm range suggested by the model compounds.

A broad signal might be expected for Mo sites of low symmetry in a large molecule such as xanthine oxidase. Indeed, if the correlation time, τ_c, is assumed to be ca. 10^{-8} to 10^{-9} s for the large molecule, it might be suggested that a ^{95}Mo resonance for xanthine oxidase in solution will be unobservable according to eqn. 1. However, recent studies [17(b), 26(b)] of other quadrupolar nuclei, ^{43}Ca ($I = 7/2$) and ^{17}O ($I = 5/2$), in proteins of molecular weight up to 20 000 d have demonstrated that it is difficult to estimate a realistic correlation time, τ_c, for the local environment of the observed nucleus, and that it is not possible to calculate τ_c assuming a rigid spherical model (eqn. 3). These recent studies have clearly demonstrated that NMR signals of quadrupolar nuclei bound to macromolecules can be observed in cases where simple predictions using eqns. 1 and 3 suggest that linewidths would be too broad for detection.

Nevertheless, the most promising biological systems for ^{95}Mo study are the lower molecular weight cofactors [7], FeMoco and Moco, provided that diamagnetic samples of sufficient concentration can be generated.

F. TUNGSTEN-183 NMR

Early investigations concentrated on the solid state and aimed to determine μ by direct observation of the nucleus in metallic tungsten [135], tungsten–cobalt alloys [136] and tungsten bronzes [137]. This aim was

frustrated by the need to know the magnitude of the Knight shift, which could not be calculated accurately. Initial direct measurements in solution were reported in 1975 by Banck and Schwenk [138] who examined liquid WF_6, aqueous $[WO_4]^{2-}$ and WCl_6 in CS_2. However, indirect double and triple resonance techniques had been used earlier to obtain chemical shifts [32,139,140] and such techniques remain valuable [33,141].

The sensitivity of commercial spectrometers has steadily increased in recent years, and direct observation of the low-frequency resonance of the insensitive ^{183}W ($I = 1/2$) nucleus (Table 1) is becoming more routine. At the present time the chemical shifts of about 140 tungsten compounds (mainly W(0), W(II) and W(VI) species including about 50 polyoxotungstates) have been recorded in solution. The reported chemical shift range covers some 11 000 ppm ($W_2(O_2CCF_3)_4$, 6760; WCp_2H_2, −4663 ppm).

The sharp lines in ^{183}W NMR spectra enable spin–spin couplings to other kinds of nuclei and to other ^{183}W nuclei to be detected. Such couplings provide a powerful technique for assigning the stereochemistries of iso- and heteropolytungstates (Section F(i)). The recent successful application of two-dimensional NMR techniques to investigating ^{183}W resonances at natural abundance [149] promises to play a major role in understanding heteropolytungstate anions (Section F(i)(b)).

(i) Tungstate and the polyoxotungstates

The ^{183}W chemical shift for the tetrahedral $[WO_4]^{2-}$ anion shows little dependence on concentration or counterion [138]. The chemical shift for 2.31 molal $Na_2[WO_4]$ shows a small temperature dependence (ca. 0.16 ppm K^{-1} in the range 274–332 K). Relaxation times for this anion have not been reported, although in comparison with other W(VI) species of high symmetry (Section F(ii)), they are likely to be greater than 5 s.

The rich and subtle chemistry of isopoly- and heteropolytungstate species based on the $[WO_4]^{2-}$ anion has attracted continuing interest [6]. The potential of ^{183}W NMR for structural characterization of these compounds was first demonstrated by Baker et al. [142] in 1979 and recently progress has been rapid. For many individual species, rearrangements involving W-sites are slow on the ^{183}W NMR time scale and structurally inequivalent W atoms exhibit separate narrow resonances. Consequently, relative signal intensities and coupling patterns due to spin–spin interactions with other magnetic nuclei (in particular, with other ^{183}W nuclei via ^{183}W–O–^{183}W units: $N(^{183}W) = 14.40$ atom % (Table I)) can allow unambiguous assignment of structurally inequivalent W atoms.

Data for polyoxotungstate species are collected in Table 29. Observed chemical shifts for diamagnetic species range from +58.9 ppm for $[W_6O_{19}]^{2-}$

TABLE 29

Polyoxotungstates

Anion	Solvent	Chemical shift [a,b,c] (ppm)	Comments	Ref.
$[W_6O_{19}]^{2-}$	$HCONMe_2$	+58.9		143
$[(PhPO_3)_2W_5O_{15}]^{4-}$	CD_3CN	−155.9	1:2:1 triplet; $^2J_{W-O-P}$, 1.95 Hz	144
α-$[PW_{12}O_{40}]^{3-}$	D_2O	−99.4	doublet; $^2J_{W-O-P}$, 1.17 Hz	145
α-$[AsW_{12}O_{40}]^{3-}$	$HCONMe_2$/ $(CD_3)_2CO$	−64.6		146
α-$[SiW_{12}O_{40}]^{4-}$	D_2O	−103.8		145
	CD_3CN/ $HCONMe_2$	−92.1		143
β-$[SiW_{12}O_{40}]^{4-}$	D_2O	−109.7(1), −114.7(2), −129.8(1)	$^2J_{W-O-W}$, ca. 8 and 20 Hz	147
	D_2O	−109.1(1), −114.0(2), −129.2(1)	$^2J_{W-O-W}$, 8.3 and 20.5 Hz	146
	CD_3CN/ $HCONMe_2$	−103.5(1), −104.0(2), −120.5(1)		143
α-$[GeW_{12}O_{40}]^{4-}$	D_2O	−81.9		145
	D_2O	−79.8		146
β-$[GeW_{12}O_{40}]^{4-}$	D_2O	−89.5(1), −91.6(2), −104.0(1)	$^2J_{W-O-W}$, 8.3 and 20.3 Hz	147
α-$[BW_{12}O_{40}]^{5-}$	D_2O	−130.8		145
α-$[ZnW_{12}O_{40}]^{6-}$	D_2O	−95.8		145
α-$[(H_2)W_{12}O_{40}]^{6-}$	D_2O	−113.0		145
α-$[(D_2)W_{12}O_{40}]^{6-}$	D_2O	−120.0		145
β-$[(H_2)W_{12}O_{40}]^{6-}$	D_2O	−107.2(1), −120.9(2), −130.6(1)		147
α-$[(H_2)W_{12}O_{39}F]^{5-}$	D_2O	−94.3(1), −104.1(2), −108.6(1)	$^1J_{W-F}$, 32 H_z; $^2J_{W-O-W}$, ca. 5 and 22 Hz	147
α-$[CoW_{12}O_{40}]^{6-}$	D_2O	−882 [c]		148
α-$[CoW_{12}O_{40}]^{5-}$	D_2O	−1955 [c]		148
α-$[PW_{11}O_{39}]^{7-}$	D_2O	−102.0(2), −102.4(2), −106.3(2), −124.2(1), −134.5(2), −154.5(2)	Li^+ salt with added $LiClO_4$ (0.5 M); $^2J_{W-O-P}$, 1.20 to 1.71 Hz	145
	D_2O	−97.3(2), −102(2), −108.9(2), −116.6(1), −132.0(2), −152.1(2)	Na^+ salt; $^2J_{W-O-P}$, 0.9 to 2.1 Hz, $^2J_{W-O-W}$, 5.6 to 10.1 and 16.8 to 27.8 Hz	149
	D_2O	−98.1(2), −98.8(2), −103.6(2), 121.4(1), −132.4(2), −152.2(2)	Li^+ salt; $^2J_{W-O-P}$, 0.9 to 1.8 Hz	149

α-$[SiW_{11}O_{39}]^{8-}$	D_2O	$-100.9(2), -116.1(2), -121.3(1), -127.9(2), -143.2(2), -176.2(2)$		142, 145
	D_2O	$-100.8(2), -116.1(2), -121.3(1), -127.9(2), -143.2(2), -176.1(2)$	A second set of peaks (ca. 9% of main spectrum) occurs at $-139.8, -142.1, -144.7, -145.7, -166.7$ ppm. An expected sixth peak is obscured by the main spectrum.	149
α-$[PbPW_{11}O_{39}]^{5-}$	D_2O (60°C)	$-74.4(2), -82.7(2), -102.8(2), -111.5(1), -127.4(2), -146.3(2)$	$^2J_{W-O-P}$, 0.95 to 2.20 Hz	149
α-$[GaW_{11}O_{39}]^{9-}$	D_2O	species 1: $-16.2(1), -101.2(2), -126.9(2), -133.8(2), -137.3(2), -155.9(2)$ species 2: $-67.4, -81.3, -97.1, -119.2, -125.5, -185.0$		149
α-$[GeGa(OH)W_{11}O_{39}]^{6-}$	D_2O	$-37.2(2), -87.2(2), -115.1(2), -118.6(1), -123.7(2), -184.9(2)$		149
α-$[GaGe(OH)W_{11}O_{39}]^{6-}$	D_2O	$-51.6(2), -82.3(2), -118.8(2), -122.7(2), -127.5(1), -225.0(2)$		149
$[Ce(PW_{11}O_{39})_2]^{11-}$	D_2O	$+349, +193, -114.8, -116.7, -141.5$		150
$[Ce(PW_{11}O_{39})_2]^{10-}$	D_2O	$-105.8, -110.3, -116.6, -120.5, -138.0, -142.3, -152.3, -175.7$		150
α-$[TiPW_{11}O_{40}]^{5-}$	CH_3CN/CD_3CN	$-57.2(2), -92.6(2), -101.9(1), -106.7(2), -109.2(2), -118.0(2)$	$^2J_{W-O-P}$, 1.0 to 1.6 Hz, $^2J_{W-O-W}$, 9 ± 2 and 20 ± 4 Hz	151
α-$[ClTiPW_{11}O_{39}]^{4-}$	$HCOMe_2/MeCN\text{-}d_3$	$-88.3(1), -92.3(2), -96.5(2), -108.3(2), -108.5(2), -108.8(2)$		151
α-$[(CpFe(CO)_2Sn)PW_{11}O_{39}]^{4-}$	D_2O	$-106.5(2), -108.8(2), -123.4(1), -127.4(2), -127.9(2), -192.7(2)$		151

TABLE 29 (continued)

Anion	Solvent	Chemical shift [a,b,c]	Comments	Ref.
α-$[CpTiPW_{11}O_{39}]^{4-}$	MeCN-d_3	−78.3(2), −93.6(1), −94.8(2), −100.4(2), −112.3(2), −117.7(2)	$^2J_{W-O-P}$, ca. 1Hz	143
	$HCOMe_2$/MeCN-d_3	−76.7(2), −90.9(1), −92.3(2), −97.7(2), −109.5(2), −115.1(2)	$^2J_{W-O-P}$, ca. 1 Hz	143
$[Ti_2PW_{10}O_{40}]^{7-}$	H_2O/D_2O (35°C)	−73.7(2), −112.5(2), −125.5(2), −127.0(2), −143.0(2)	$^2J_{W-O-P}$, 1.19 to 1.75 Hz; $^2J_{W-O-W}$, 6.4 to 7.8 and 1.75 to 21.0 Hz	152
$[(CpFe(CO)_2Sn)_2PW_{10}O_{38}]^{5-}$	H_2O/D_2O (60°C)	−108.1(2), −127.8(2), −146.6(2), −209.0(2), −218.7(2)		152
$\alpha[P_2W_{18}O_{62}]^{6-}$	D_2O	−128.1(1), −173.8(2)	$^2J_{W-O-P}$, 1.17 and 1.61 Hz	142, 145, 153, 154
β-$[P_2W_{18}O_{62}]^{6-}$	D_2O	−111.6(1), −131.1(1) −171.1(2), −191.2(2)	$^2J_{W-O-P}$, 1.17 to 1.61 Hz	145, 153, 154
α-$[As_2W_{18}O_{62}]^{6-}$	D_{2O}	−121.8(1), −145.3(2)		154
γ-$[As_2W_{18}O_{62}]^{6-}$	D_2O	−110.0(1), −166.0(2)		154
α-$[P_2W_{12}Mo_6O_{62}]^{6-}$	D_2O	−130.3(1), −166.6(1), −179.9(1)	$^2J_{W-O-P}$, 1.17 to 1.61 Hz	154
α-$[P_2W_{15}Mo_3O_{62}]^{6-}$	D_2O	−134.1(1), −179.3(2), −180.1(2)	$^2J_{W-O-P}$, 1.10 to 1.61 Hz	154
"polymeric" 6:1 tungstophosphate	D_2O	−207.6(2), −209.7(2), −275.5(1), −287.8(1)	$^2J_{W-O-P}$, 1.17 to 1.47 Hz	154
α_2-$[P_2W_{17}O_{61}]^{10-}$	D_2O	−127.9(2), −140.8(2), −159.6(2), −175.8(2), −179.6(1), −218.9(2), −222.7(2), −255.0(2), −242.3(2)	$^2J_{W-O-P}$, 0.95 to 2.20 Hz	145, 153

α_2-$[P_2W_{17}VO_{62}]^{7-}$	D_2O	−142.0(2), −182.5(2), −184.4(1), −220.0(2), −221.6(2), −225.4(2), −244.8(2)	$^2J_{W-O-P}$, 1.17 to 2.05 Hz	145
$[As_2W_{21}O_{69}(H_2O)]^{6-}$	Me_2SO-d_6	7 resonances ca. −33 to ca. −192 (2:4:4:4:4:2:1)		183
B-$[P_2W_{18}Zn_4(H_2O)O_{68}]^{10-}$	D_2O	−90.3(1), −105.4(2), −115.0(2), −128.4(2), −134.2(2)	$^2J_{W-O-P}$ for the resonances at −90.3 and −128.4 ppm are 1.1 and 1.6 Hz respectively	155
B-$[P_4W_{30}Zn_4(H_2O)_2O_{112}]^{16-}$	D_2O (40°C)	−150.4(1), −160.5(2), −162.0(2), −180.0(2), −185.0(2), −238.2(2), −243.4(2), −244.7(2)		156

[a] All shifts are relative to external aqueous Na_2WO_4. However, different concentrations and pH of this reference have been used by various authors. Correction of tabulated chemical shifts relative to 2M Na_2WO_4 in D_2O at apparent pH 11 leads to minor changes only. [b] Values in parentheses are the relative intensities of the W signals. [c] Linewidths are generally <1 Hz except for the paramagnetic anions α-$[CoW_{12}O_{40}]^{6-}$ (34 Hz) and α-$[CoW_{12}O_{40}]^{5-}$ (14 Hz).

to -244.8 ppm for α_2-$[P_2W_{17}VO_{62}]^{7-}$ and for paramagnetic species from $+349$ ppm for $[Ce(PW_{11}O_{39})_2]^{11-}$ to -1955 ppm for α-$[CoW_{12}O_{40}]^{5-}$. Linewidths are generally < 0.5 Hz except in unusual circumstances (vide infra).

The only isopolytungstate examined to date is $[W_6O_{19}]^{2-}$. A single resonance is observed [143] consistent with O_h symmetry in solution.

A single fluxional polyoxotungstate, $(Bu^n_3NH)_4[(PhPO_3)_2W_5O_{15}]$ has been reported [144]. The anion has idealized C_2 symmetry (Fig. 26) in the solid state and three signals of relative intensity 2 : 2 : 1 modified by complex $^{183}W-^{31}P$ coupling are predicted for a static structure in solution. However,

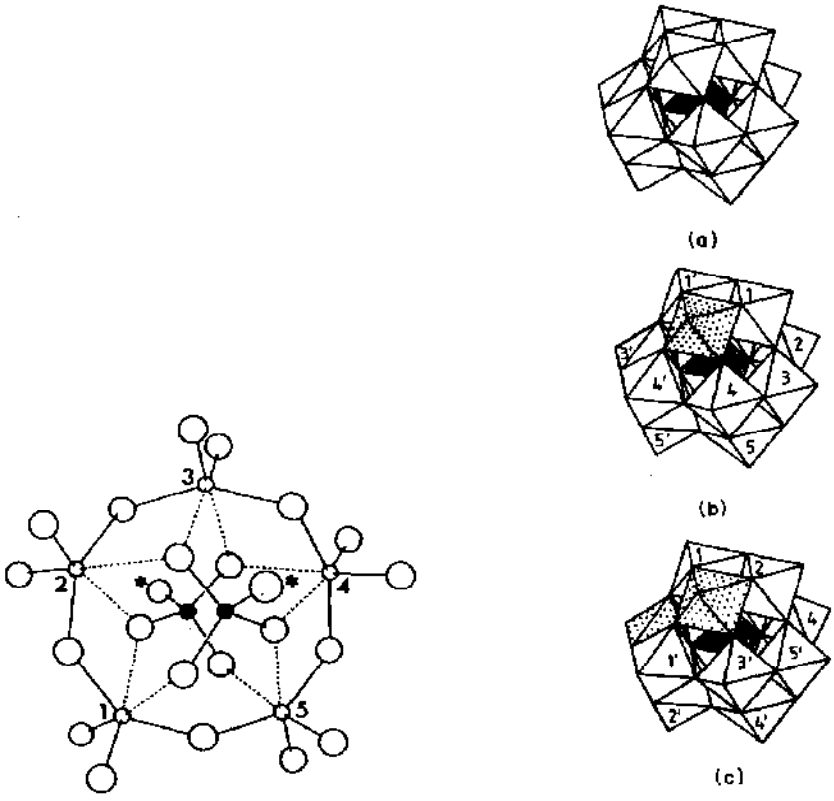

Fig. 26. Ball-and-stick model of the anion $[(PhPO_3)_2W_5O_{15}]^{4-}$: small circles, W; dark circles, P; large circles, O; starred circles, C of phenyl groups. Reproduced from ref. 144, with permission.

Fig. 27. Condensed polyhedron models for: (a) Keggin anions, α-$[X^{n+}W_{12}O_{40}]^{(8-n)-}$. The heteroatom X occupies the central tetrahedral site (hatched), when $X^{n+} = H_2^{2+}$ or D_2^{2+}, the protons or deuterons lie off-center on opposite edges of the tetrahedron; (b) α-$[X^{n+}W_{11}O_{39}]^{(12-n)-}$. The spotted octahedron is missing. Pairs of W atoms (e.g. 1,1′) are structurally equivalent. The unique W atom, 6, is obscured: (c) α-$[Ti_2PW_{10}O_{40}]^{7-}$ and α-$[\{CpFe(CO)_2Sn\}_2PW_{10}O_{38}]^{5-}$. The Ti and Sn atoms occupy the spotted octahedral sites.

the ^{183}W spectrum observed in dry CH_2Cl_2 or in wet MeCN consists of a single line split into a 1 : 2 : 1 triplet by coupling to two equivalent ^{31}P nuclei (J, 1.95 Hz). The ^{17}O spectrum also indicates the presence of intramolecular processes. The ring of five W atoms is a topological analogue of cyclopentane, and an exchange mechanism analogous to the facile interconversion of the "envelope" (four coplanar atoms and one atom out of the plane) conformers of cyclopentane via a ring pseudorotation is proposed [144] in the present case.

(a) Hetero-12-tungstate anions

The isomorphous series $[X^{n+}W_{12}O_{40}]^{(8-n)-}$ exhibits the so-called Keggin structure which includes a number of isomeric forms (α, β, γ, δ, and ϵ). The α-form (Fig. 27(a)) has T_d point symmetry and consists of four equivalent W_3O_{13}-units (some of the O atoms are shared by different units). The β-form has one of the W_3O_{13}-units rotated by 60°. Similar rotations of two, three and four units give rise to the γ, δ and ϵ isomers [157]. The heteroatom, X^{n+}, occupies the central tetrahedral site. ^{183}W NMR studies have so far involved the α- and β-forms only.

A single sharp resonance arises from the twelve equivalent W atoms of an α-isomer unless, of course, X is a magnetic nucleus and ^{183}W–O–X spin–spin coupling is resolved. The magnitude of the ^{183}W chemical shifts of a series of α-anions (Table 29) varies linearly with the wavelength of the electronic absorption maximum of lowest energy [145] (Fig. 28). Such a relationship is expected if the localized paramagnetic term of the Ramsay equation [158,159] dominates the shielding and if the absorption maximum is a measure of $\Delta\epsilon$, the average energy of excitation from the ground state to excited states which can mix into the ground state (see Section G(i)(b)). For this series of α-$[X^{n+}W_{12}O_{40}]^{(8-n)-}$ anions, it is apparent that the anisotropy of the electric field around the ^{183}W nucleus is constant and that the $\Delta\epsilon$ term controls the shielding.

Similar correlations have been observed previously in ^{59}Co and ^{51}V shielding studies for octahedral d^6 complexes and rationalized by crystal field theory [160]. Figure 28 does not show a monotonic dependence of $\delta(^{183}W)$ with the oxidation state of X and attempts to correlate overall anionic charge and resultant electron density with ^{183}W nuclear shielding appear to be invalid [143].

An interesting species is $H_5[H_2W_{12}FO_{39}]$. The anion has an α-type structure with the fluorine atom occupying one of the vertices of the central X tetrahedral site. The effective point symmetry is C_{3v} and the ^{183}W spectrum shows three signals in the expected 1 : 2 : 1 intensity ratio [147]. In this case ^{183}W–O–^{183}W coupling is observed and the $^2J_{W-O-W}$ coupling constants fall into two distinct classes: (a) 5 ± 1 Hz between W atoms of edge-sharing

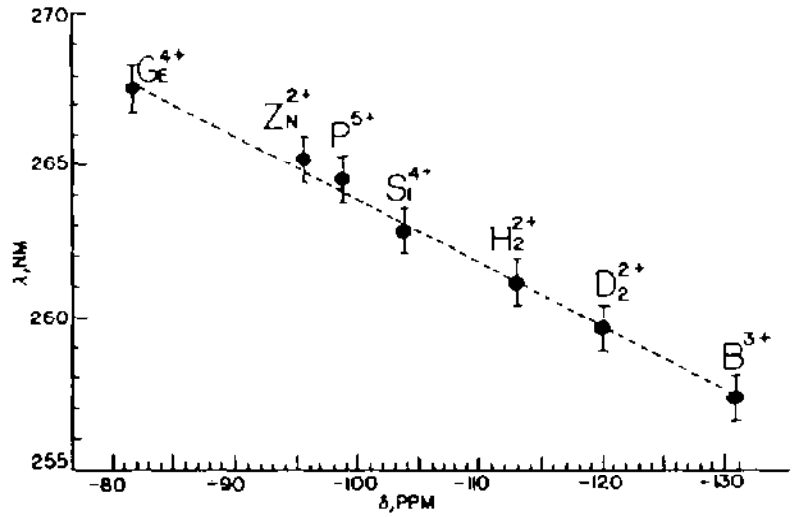

Fig. 28. Variation of $\delta(^{183}W)$ for α-$[X^{n+}W_{12}O_{40}]^{(8-n)-}$ with the wavelength of their lowest energy optical absorption maxima. Reproduced from ref. 145, with permission.

octahedra and (b) 22 ± 1 Hz between W atoms of corner-sharing octahedra. These observations are of particular importance in assigning ^{183}W resonances to separate W atoms in a variety of structures in the polyoxotungstates. The $^2J_{W-O-W}$ values are dependent on W–O–W bond angles for the limited number of cases where precise correlation has been attempted [147]. More detailed examples of the application of $^2J_{W-O-W}$ values in structural correlations are given later (Section F(i)(b)).

The more highly shielded ^{183}W nuclei observed in the paramagnetic α-$[Co^{III}W_{12}O_{40}]^{5-}$ and α-$[Co^{II}W_{12}O_{40}]^{6-}$ anions [148], are a result of a contact contribution to the isotropic chemical shifts. These shifts have been interpreted in terms of direct delocalization of cobalt spin density on to the W atoms [161]. ^{183}W NMR has obvious potential as a probe in such species.

The β-$[X^{n+}W_{12}O_{40}]^{(8-n)-}$ anions exhibit C_{3v} point symmetry and so three ^{183}W resonances in the intensity ratio 1 : 2 : 1 are expected. This is indeed found for the limited number of β-anions so far examined [143,146,147]. Spin–spin coupling has been resolved for β-$[XW_{12}O_{40}]^{4-}$ (X = Si, Ge) [140,146,147] and the coupling constants $^2J_{W-O-W}$ of 8 ± 1 and 20 ± 1 Hz allow, by analogy with $H_5[H_2W_{12}FO_{39}]$, unambiguous assignment of the inequivalent W atoms.

(b) Heteropoly-11-tungstate anions

If one or more of the W-centered octahedral units are removed from a Keggin anion, "lacunary" anions are formed. For example, removal of a $[WO]^{4+}$ unit from α-$[X^{n+}W_{12}O_{40}]^{(8-n)-}$ results in α-$[X^{n+}W_{11}O_{39}]^{(12-n)-}$

(Fig. 27(b)) which features one structurally unique W atom and five inequivalent pairs of W atoms as imposed by the C_s point symmetry. The structural integrity of these species ($X = P^{5+}$, Si^{4+}) in aqueous solution is demonstrated [142,145,149] by the observation of six separate ^{183}W resonances in the intensity ratio 2 : 2 : 2 : 1 : 2 : 2 (Fig. 29(a)). Each ^{183}W resonance in the phosphorus species is a doublet due to $^{183}W-O-^{31}P$ coupling and satellites due to $^{183}W-O-^{183}W$ coupling are clearly visible.

Brevard [149] has demonstrated that the assignment of ^{183}W signals to individual W atoms can be straightforward when two-dimensional (2D) NMR techniques are used to establish the connectivity of various W atoms via their $^{183}W-O-^{183}W$ couplings. The work employed the 2D COSY 90 and 2D INADEQUATE sequences. The 2D COSY 90 experiment for $Na_7[PW_{11}O_{39}]$ in D_2O is represented as a contour plot in Fig. 29(b). The larger contours on the diagonal represent the normal 1D spectrum, while the off-diagonal contours (about 14% of the main signal) result from $^{183}W-O-^{183}W$ coupling between the various edge-and corner-shared octahedra.

Using the atom numbering system of Fig. 27(b) it is clear that the following coupling patterns should be observed as off-diagonal peaks in the contour plot: W_1 coupled to W_3, W_2; W_2 coupled to W_1, W_3, W_6; W_3 coupled to W_1, W_2, W_4, W_5; W_4 coupled to W_3, W_5; W_5 coupled to W_3, W_4, W_6; W_6 coupled to W_5, W_2. Systematic examination of Fig. 29(b) shows that all connectivities are present for $Na_7[PW_{11}O_{39}]$. In addition, the fact that $^{183}W-O-^{183}W$ coupling via corner-sharing of octahedra ($^2J_{W-O-W}$, 16.8–27.8 Hz; e.g. W_6-O-W_5) is stronger than that via edge-sharing ($^2J_{W-O-W}$, 5.6–10.1 Hz; e.g. W_6-O-W_2) is confirmed (vide supra: Section F(i)(a)). The coupling patterns were confirmed by the 2D INADEQUATE sequence [149].

Each experiment takes about 30 h but the unambiguous identification of the coupling patterns is worth the expenditure of spectrometer time. The power of these and other 2D methods will find increasing use in the structural characterization of the polyoxotungstates. Consideration could be given to isotope enrichment with ^{183}W to improve the sensitivity of the 2D methods.

Previous assignments of W atoms in the α-$[X^{n+}W_{11}O_{39}]^{(12-n)-}$ series were based partially on the premise that W atoms closest to the vacancy give rise to the most deshielded ^{183}W resonance signals [145]. Although this can be the case [149] it is not necessarily so and other structural factors must be considered. For example, the resonances due to W_1, W_4 and W_5 in α-$[PW_{11}O_{39}]^{7-}$ are deshielded markedly when the cation changes from Na^+ to Li^+. It is suggested [149] that the cations occupy the "vacancy" and differentially modify the anionic structures. In $Na_9GaW_{11}O_{39}$, two species are detected. These are assigned tentatively to the lacunary α-$[GaW_{11}O_{39}]^{9-}$ anion and to $[NaGaW_{11}O_{39}]^{8-}$ (with an associated Na^+ ion).

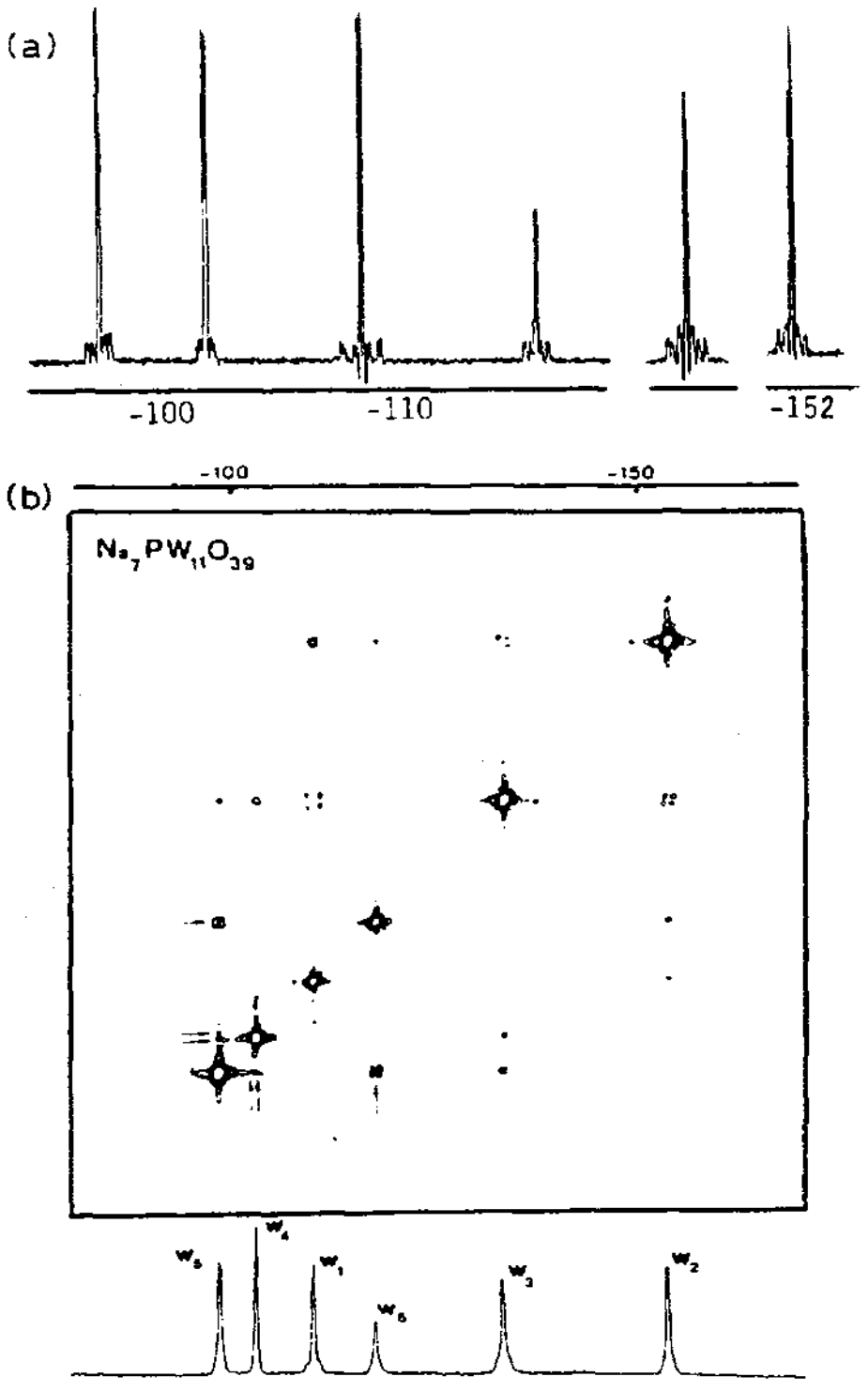

Fig. 29. (a) ^{183}W NMR spectrum of $Na_7[PW_{11}O_{39}]$ (1 M in D_2O; 16.67 MHz; T, 333 K). Satellite peaks due to ^{183}W–O–^{183}W and ^{183}W–O–^{31}P coupling are clearly visible after Gaussian deconvolution of the FID: (b) ^{183}W 2D COSY 90 contour plot. Conditions as for (a) except T, 303 K. Adapted from ref. 149, with permission.

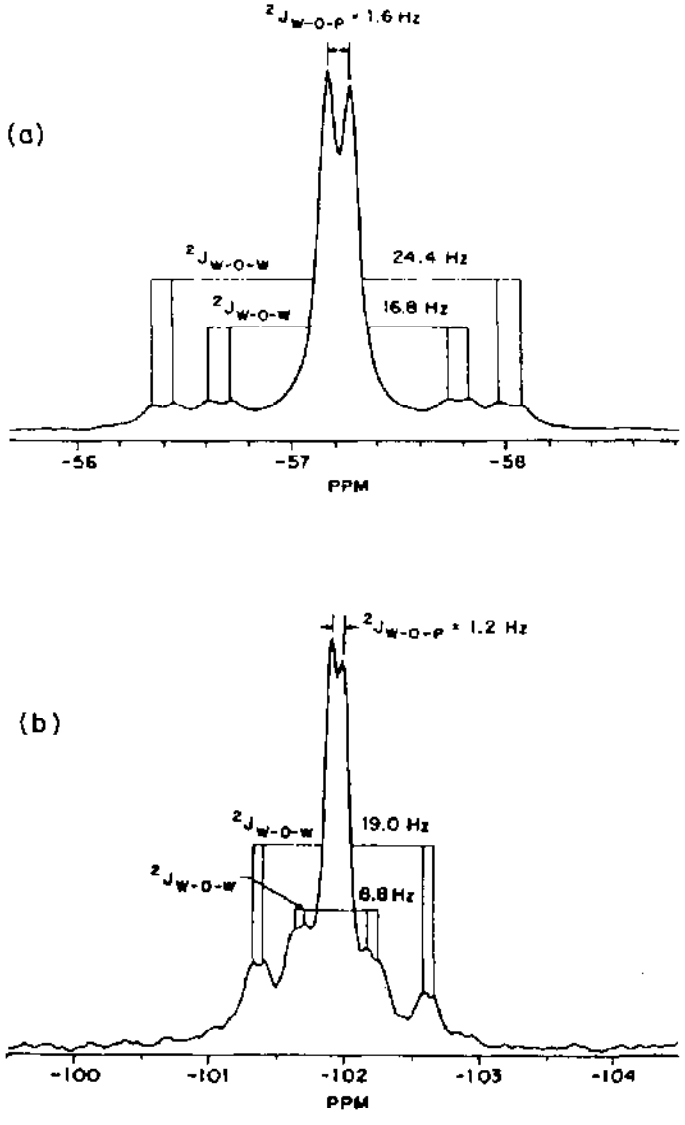

Fig. 30. Expanded regions of the ^{183}W spectrum of α-$(Bu^n_4N)_5[TiPW_{11}O_{40}]$ shown in Fig. 2. The expansions show the ^{183}W–O–^{31}P couplings and ^{183}W–O–^{183}W couplings of two different isotopomers: (a) ^{183}W resonance 1; (b) ^{183}W resonance 6. Reproduced from ref. 151, with permission.

The vacancy is certainly occupied in species such as α-$[Y^{m+}PW_{11}O_{39}]^{(7-m)-}$ ($Y^{m+} = TiO^{2+}$, $TiCl^{3+}$, $CpTi^{3+}$, $CpFe(CO)_2Sn^{3+}$). Qualitative features [151,162] of the spectra are similar to those of $[PW_{11}O_{39}]^{7-}$ and analysis of the W–O–W fine structure observed at the base

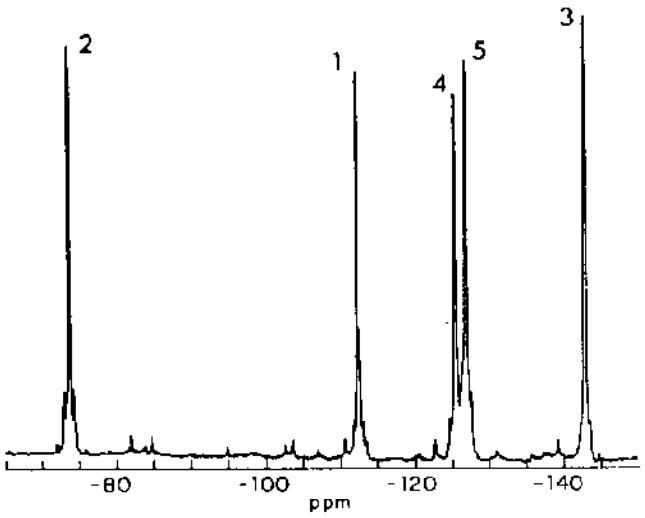

Fig. 31. ^{183}W NMR spectrum of α-$Li_7[Ti_2PW_{10}O_{40}]$ in H_2O/D_2O, (T, 35°C). The numbering system is that of Fig. 27(c). Reproduced from ref. 162, with permission.

of the major peaks (Figs. 2, 27(b) and 30) in α-$(Bu^n_4N)_5[TiPW_{11}O_{40}]$ allow assignment of the individual resonances, assuming (Section F(i)(a)) that $^2J_{W-O-W} = 9 \pm 2$ Hz and $^2J_{W-O-W} = 20 \pm 4$ Hz, respectively, correspond to edge- and corner-sharing between two tungsten-centered octahedra of oxygen atoms. The method is restricted if there is overlap of resonances, as in $(Bu^n_4N)_5[ClTiPW_{11}O_{39}]$ [151].

Disubstitution of a Keggin anion leads to the possibility of five structural isomers of C_s (two cases), C_1, C_2 and C_{2v} point symmetries. That the C_2 isomer (Fig. 27(c)) is present in the α-$[Ti_2PW_{10}O_{40}]^{7-}$ and α-$[\{CpFe(CO)_2Sn\}_2PW_{10}O_{38}]^{5-}$ anions is proven by the observation of five resonances of equal intensity (Fig. 31). A structural assignment [162] based on the $^2J_{W-O-W}$ coupling constants was possible and confirmed by a 2D-INADEQUATE experiment which clearly substantiated the proposed connectivities.

(c) Heteropoly-18-tungstates and related species

The structures of these anions are derived formally from those of the Keggin anions by removal of a W_3O_9-unit followed by fusing of two of the resulting fragments. The structure of α-$[P_2W_{18}O_{62}]^{6-}$ is shown in Fig. 32(a). Note the tetrahedral sites occupied by the P atoms. The β-isomer is derived by rotation by 60° of one of the W_3 caps. The ^{183}W NMR spectra of the α- and β-$[P_2W_{18}O_{62}]^{6-}$ isomers in D_2O exhibit the two (1 : 2) and four (1 : 1 : 2 : 2) resonances respectively predicted from the static solid-state structures [142,145,153]. Each ^{183}W nucleus is coupled to one ^{31}P nucleus.

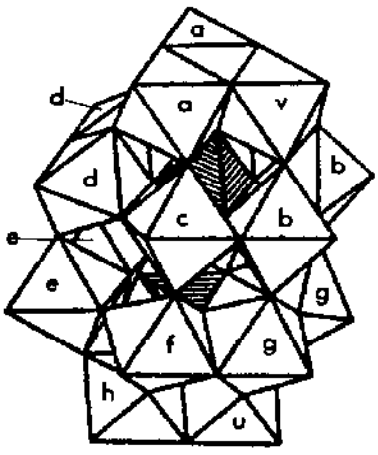

(a)

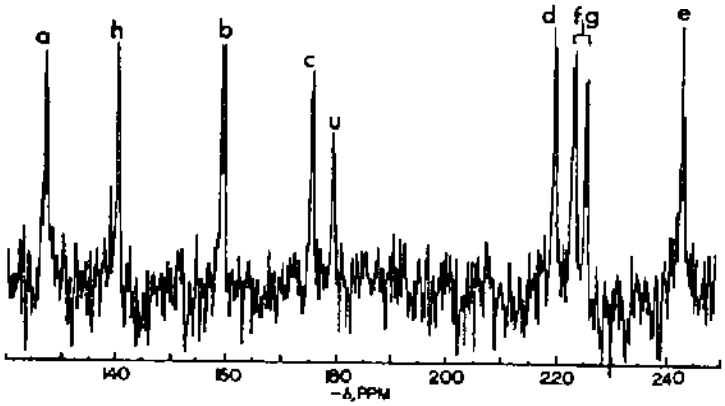

(b)

Fig. 32. (a) Condensed polyhedron model of the Wells–Dawson anion, α-$[P_2W_{18}O_{62}]^{6-}$. The P atoms occupy the hatched tetrahedral sites. The structure of α_2-$[P_2W_{17}O_{61}]^{10-}$ is derived by removal of the $[WO]^{4+}$ unit associated with site v; (b) ^{183}W NMR spectrum of α_2-$Na_{10}[P_2W_{17}O_{61}]$ (0.6 M in D_2O; 3.75 MHz). The labels are those of (a). Reproduced from ref. 145, with permission.

The ^{183}W NMR spectra of the α-$[As_2W_{18}O_{62}]^{6-}$ and γ-$[As_2W_{18}O_{62}]^{6-}$ ions both consist of two resonances in the ratio 1 : 2. The large downfield and upfield shifts of the resonances in the γ-isomer are consistent with a 60° rotation of both the W_3 caps in the α-isomer [154].

The observation [145,153] of nine doublets of relative intensities 2 : 2 : 2 : 2 : 1 : 2 : 2 : 2 : 2 (Fig. 32(b)) shows that α_2-$[P_2W_{17}O_{61}]^{10-}$ is derived from the parent α-$[P_2W_{18}O_{62}]^{6-}$ anion by removal of the $[WO]^{4+}$ unit labelled v in Fig. 32(a). The weaker resonance is assigned to the resultant

unique W atom in the opposing W_3 capping unit. When a $[VO]^{3+}$ unit is inserted into the vacancy v to yield α_2-$[P_2VW_{17}O_{62}]^{7-}$ the spectrum is similar to that of α_2-$[P_2W_{17}O_{61}]^{10-}$ except that two of the signals are missing. It is suggested [145] that the nuclear quadrupole moment of ^{51}V ($I = 7/2$) provides a mechanism for the rapid relaxation of certain ^{183}W nuclei (labelled a and b in Fig. 32(a)) which broadens their resonances beyond detection. Unambiguous confirmation of these assignments would be provided by 2D methods which would establish the connectivities of the W atoms.

(d) Trivacant heteropolytungstate derivatives

Removal of $[W_3O_6]^{6+}$ units from $[PW_{12}O_{40}]^{3-}$ and $[P_2W_{18}O_{62}]^{6-}$ anions generate [163,164] the so-called trivacant anions $[PW_9O_{34}]^{9-}$ and $[P_2W_{15}O_{56}]^{12-}$. Reaction of β-$[PW_9O_{34}]^{9-}$ with ions M^{2+} (M = Co, Cu, Zn) allows isolation of $K_{10}[P_2W_{18}M_4(H_2O)_2O_{68}]\cdot 20H_2O$ [155]. The observed solid-state structure of the anion (Fig. 33(a)) is of C_{2h} point symmetry and features two $[PW_9O_{34}]^{9-}$ units acting as ligands to a central array of four M-centered octahedra. The ^{183}W NMR spectrum of the Zn^{2+} derivative exhibits five resonances of relative intensities 1 : 2 : 2 : 2 : 2, consistent with the presence of the same structure in aqueous solution.

A similar synthesis [156] based upon $[P_2W_{15}O_{56}]^{12-}$ produces $Na_{16}[P_4W_{30}M_4(H_2O)_2O_{112}]$ whose solid-state structure also features an anion of C_{2h} symmetry (Fig. 33(b)). The ^{183}W NMR spectrum of the Zn^{2+} derivative consists of eight resonances of relative intensity 1 : 2 : 2 : 2 : 2 : 2 : 2 : 2 and, in conjunction with ^{31}P NMR, strongly suggests the presence in solution of the isomer shown in Fig. 33(b). There are in fact 16 possible isomeric forms of which four have C_{2h} point symmetry.

(e) General comments

The ^{183}W chemical shifts in the polyoxotungstates are dependent on factors such as ionic strength of the solutions. Detailed studies on α-$[SiW_{12}O_{40}]^{4-}$, α-$[PW_{12}O_{40}]^{3-}$ and α-$[P_2W_{18}O_{62}]^{6-}$ showed that the ^{183}W chemical shifts were not sensitive to the pH (pD) of the solution but increases in ionic strength (including that due to an increase in concentration of the polyoxotungstate itself) caused upfield chemical shifts of ca. 1 ppm. The shift is not necessarily the same for all signals [145] and, in some cases, changes in ionic strength can be used to shift overlapping ^{183}W resonances differentially to achieve better dispersion of the signals [145]. The chemical shifts are often counterion dependent, a fact which must be carefully considered when assigning ^{183}W resonance signals to separate W atoms [149] (see Section F(i)(b)).

The collection of ^{183}W data is very time-consuming and spectra with

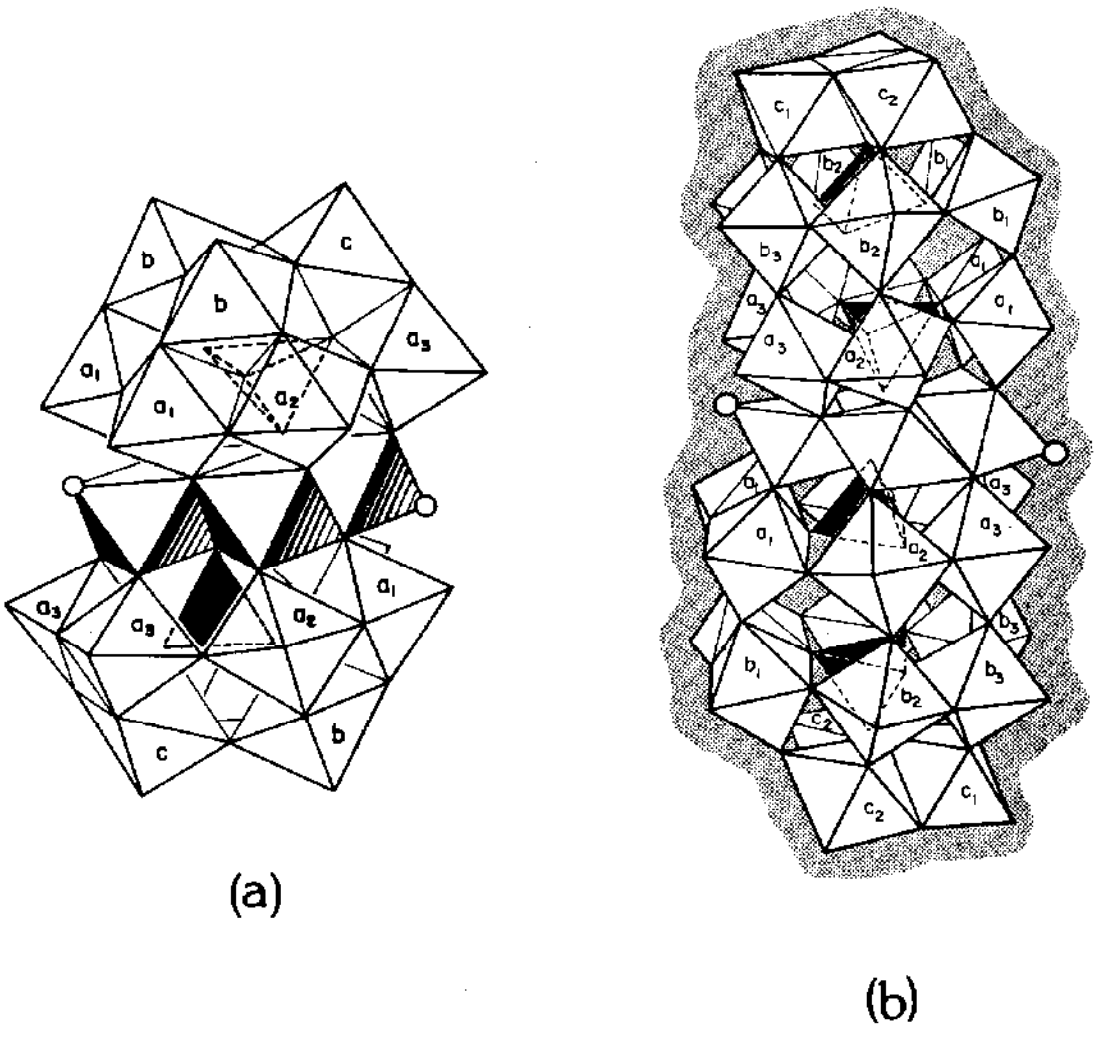

Fig. 33. Condensed polyhedron models of: (a) B-$[P_2W_{18}M_4(H_2O)_2O_{68}]^{10-}$ (M = Co^{2+}, Cu^{2+}, Zn^{2+}). The four M atoms occupy the four central edge-linked octahedral sites; the two P atoms occupy the internal tetrahedral (dashed) sites; the circles represent the H_2O ligands. The model has C_{2h} point symmetry and the five different W sites are labelled a_1, a_3, a_2, b and c. Reproduced from ref. 155, with permission; (b) B-$[P_4W_{30}M_4(H_2O)_2O_{112}]^{16-}$ (M = Co^{2+}, Cu^{2+}, Zn^{2+}). The M, P and H_2O sites are represented as in (a). The model has C_{2h} point symmetry and the eight different W sites are labelled a_1, a_2, a_3, b_1, b_2, b_3, c_1 and c_2. Reproduced from ref. 156, with permission.

acceptable S/N ratios are often achieved only after three to four days accumulation. Nevertheless, the potential sensitivity of the method to distinguish very minor structural changes in a wide range of polyoxotungstates (as illustrated in the examples discussed in this section) justifies the commitment of spectrometer time. The application of 2D NMR methods is an exciting development in the unambiguous assignment of ^{183}W resonances to

particular W atoms in these species. Rapid progress should occur in this area.

(ii) Other tungsten(VI) compounds

Detailed relaxation time measurements on the ^{183}W nucleus have been reported (T_1, 4.2 ± 0.6 s; T_2, 2.1 ± 0.4 s) for only one compound, WF_6 [138]. Their magnitude indicates that relaxation times are likely to be relatively long for this nucleus in other W-containing species. A recent study of $W(CO)_6$ suggests that T_1 is in excess of 80 s for this compound in CH_2Cl_2 [35].

The ^{183}W chemical shifts for the W(VI) compounds collected in Table 30 span ca. 4900 ppm, with the resonance position being strongly affected by the nature of the coordinated ligand. The most highly shielded compound is

TABLE 30

Tungsten(VI) compounds

Compound	Solvent	Chemical shift (ppm)	Ref.
WF_6	neat liquid	−1117	138
$WF_5(OMe)$	C_6F_6	−1065	32
$WF_5(OPh)$	C_6F_6	−916	32
$[WOF_5]^-$	CD_3CN	−502	32
$[(WOF_4)_2F]^-$	$OS(OMe)_2$	−490	32
cis-$WF_4(OMe)_2$	neat liquid	−946	32
cis-$WF_4(OPh)_2$	C_6F_6	−850	32
trans-$WOF_4(OMe_2)$	neat liquid	−541	32
trans-$WOF_4\{OPMe(OMe)_2\}$	CD_3CN	−574	32
trans-$WOF_4\{OS(OMe)_2\}$	$OS(OMe)_2$	−578	32
mer-$WF_3(OMe)_3$	C_6F_6	−643	32
cis-$WF_2(OMe)_4$	C_6F_6	−503	32
WCl_6	CS_2	+2181	138
$WO_2(ONEt_2)_2$	$CDCl_3$	−330	165
$WO_2(ONC_5H_{10})_2$	$CDCl_3$	−338	165
$(NH_4)_2[WS_4]$	D_2O	+3769	56
$K_2[WOS_3]$	D_2O	+2760	56
$(NH_4)_2[WO_2S_2]$	D_2O	+1787	56
$(NH_4)_2[WO_3S]$	D_2O	+841	56
$(Pr^n_4N)_2[(NCCu)WS_4]$	$HCONMe_2$	+3084	56
$(Pr^n_4N)_2[(NCAg)WS_4]$	$HCONMe_2$	+3185	56
$(Pr^n_4N)_2[(NCCu)_2WS_4]$	$HCONMe_2$	+2641	56
$(Et_4N)_2[(NCCu)WOS_3]$	$HCONMe_2$	+1994	56
$W(CCMe_3)(CH_2CMe_3)_3$	toluene	+2282	102

WF_6. Substitution of fluorine atoms by ligands containing oxygen donors causes progressive deshielding of the ^{183}W nucleus. Similarly, substitution of fluorine atoms in WF_6 by chlorine atoms causes significant deshielding.

In the series $[WO_{4-n}S_n]^{2-}$ ($n = 0$–4), a systematic decrease in shielding occurs [56] with successive substitution of ligand O by S (Fig. 14). The decrease is 841–1009 ppm per S and the trend parallels that of the molybdenum analogues (Section E(i)(b)). The ^{183}W resonance in $(NH_4)_2[WS_4]$ appears to be solvent dependent (cf. $[MoS_4]^{2-}$) as a difference of 100 ppm in the ^{183}W chemical shift is observed between D_2O and $HCONMe_2$. The ^{183}W chemical shifts of the binuclear anions $[(CN)MS_2WS_2]^{2-}$ (M = Cu, Ag), $[(CN)CuS_2WOS]^{2-}$, and the trinuclear anions $[(CN)CuS_2WS_2Cu(CN)]^{2-}$ are all shielded with respect to the corresponding $[WS_4]^{2-}$ or $[WOS_3]^{2-}$ anions. The CuCN moiety is more shielding than is AgCN.

The most striking feature of the ^{183}W and ^{95}Mo chemical shifts (Section E(i)(b) and Tables 2, 4 and 30) in the $[MS_4]^{2-}$ anions and species derived from them, is the constancy of the shielding sensitivity $\delta(W)/\delta(Mo) = 1.67 \pm 0.03$ (Fig. 34). This ratio has been useful for monitoring reaction mixtures for likely products in these systems and in searching for ^{183}W signals, a process which can consume many hours of spectrometer time. It should be stressed, however, that the shielding sensitivity can vary significantly in other systems (Section G(i)(d)).

Linewidths of ^{183}W resonances in W(VI) compounds are usually less than 1 Hz. However, in binuclear and trinuclear tungsten species containing CuCN units, the $^{63,65}Cu$ quadrupolar nucleus causes appreciable broadening of the ^{183}W linewidth [56], e.g. in $[(NCCu)WS_4]^{2-}$ $W_{1/2} = 5$ Hz; in $[(NCCu)_2WS_4]^{2-}$ $W_{1/2} = 60$ Hz.

(iii) Tungsten(IV) and (III) compounds

The single reported ^{183}W chemical shift for a compound of formal oxidation state(IV) is that of Cp_2WH_2 (−4663 ppm, CH_2Cl_2) [141]. A similar situation holds for oxidation state (III): $W_2(OBu^t)_6$ (4408 ppm, toluene) [102].

(iv) Tungsten(II) compounds

With one exception, the compounds examined are mononuclear organotungsten species containing cyclopentadienyl and carbonyl ligands [141,152]. Their ^{183}W chemical shifts (Table 31) span 1600 ppm, with all resonances being shielded with respect to the $[WO_4]^{2-}$ reference. As observed for the molybdenum analogues, the series $CpW(CO)_3X$ (X = Cl, Br, I) follows a normal halogen dependence.

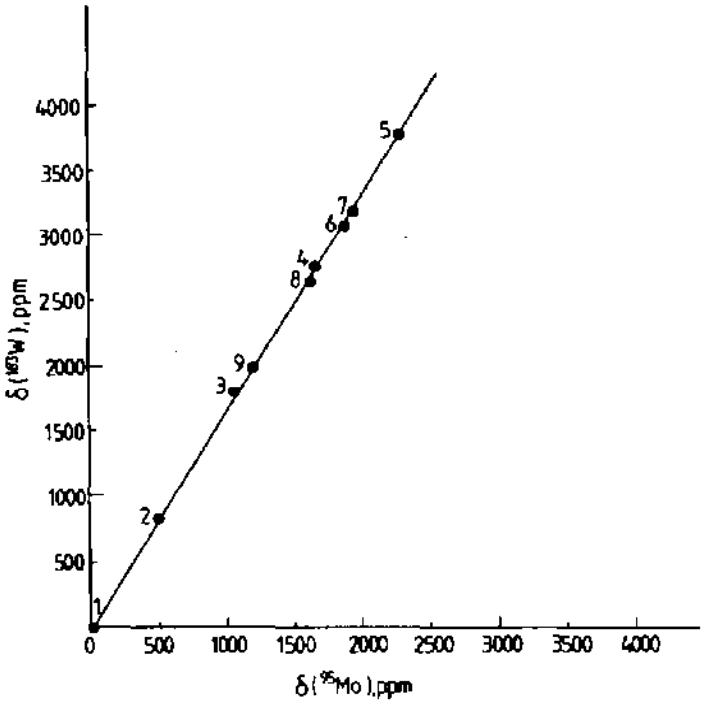

Fig. 34. Plot of $\delta(^{183}W)$ versus $\delta(^{95}Mo)$ for the following molecules: M = Mo, W: 1, $[MO_4]^{2-}$; 2, $[MO_3S]^{2-}$; 3, $[MO_2S_2]^{2-}$; 4, $[MOS_3]^{2-}$; 5, $[MS_4]^{2-}$; 6, $[(NCCu)MS_4]^{2-}$; 7, $[(NCAg)MS_4]^{2-}$; 8, $[(NCCu)_2MS_4]^{2-}$; 9, $[(NCCu)MoOS_3]^{2-}$. Reproduced from ref. 56, with permission.

The dimer $W_2(O_2CCF_3)_4$, which features a quadruple W–W bond, has a chemical shift of 6760 ppm in THF solution [166]. This large positive shift is well outside the range for the mononuclear species and parallels the behavior of the analogous Mo(II) species (Section E(v)(e)). Interestingly, $\delta(^{183}W)/\delta(^{95}Mo) = 1.68$ (see Section F(ii)).

(v) Tungsten(0) compounds

A total of 52 species have been examined (Table 32) and the chemical shifts found to span the range −3486 to −2641 ppm. The majority contain phosphorus-donor ligands observed via multiple resonance experiments (see Section C(vii)). $W(CO)_6$ and $W(CO)_5L$ ($L = PPh_3$, $PPh_2(CH{=}CH_2)$, $PPh(CH{=}CH_2)_2$) were measured directly and it is to be expected that such experiments will become more commonplace.

The most highly shielded W(0) compound is $W(CO)_6$. Replacement of a single CO ligand by a monodentate P-donor ligand causes deshielding of up to 211 ppm. Further substitution of CO by P donors causes additional

TABLE 31

Tungsten(II) compounds

Compound	Solvent	Chemical shift (ppm)	Ref.
$[CpW(CO)_3(PPh_2Me)]I$	CD_3NO_2	−3327	152
$CpW(CO)_2H(P(OMe)_3)$	C_6H_6	−3886	141
$CpW(CO)_2H(PMe_2Ph)$	C_6H_6	−3673	141
$CpW(CO)_2H(PPh_2Me)$	C_6H_6	−3674	141
$CpW(CO)_3H$	C_6H_6	−4010	141
$CpW(CO)_3D$	C_6H_6	−4021	141
$CpW(CO)_3Me$	C_6H_6	−3542	141
$CpW(CO)_3Et$	C_6H_6	−3461	141
$CpW(CO)_3Cl$	C_6H_6	−2400	141
$CpW(CO)_3Br$	C_6H_6	−2578	141
$CpW(CO)_3I$	C_6H_6	−2990	141
$CpW(CO)_3(SnMe_3)$	C_6H_6	−4037	141
$CpW(CO)_3(PPh_2)$	C_6D_6 (−80°C)	−3542	152
$CpW(CO)_2(PPh_2)(PMe_3)$	C_6D_6	−3232	152
$CpW(CO)_3(P(S)Ph_2)$	$CH_2Cl_2/CDCl_3$	−3201	152
$CpW(CO)_2(P(S)Ph_2)(PMe_3)$	$CDCl_3$	−3019	152
$[CpW(CO)_3]_2$	C_6H_6	−4033	141
$[W(CNCH_2Ph)_5(bpy)](PF_6)_2$	Me_2CO	−1192	29
$[W(CNCMe_3)_5(bpy)](PF_6)_2$	Me_2CO	−1131	29
$W_2(O_2CCF_3)_4$	THF	+6760	166

deshielding, but the effects are not simply additive. Substitution of $P(OMe)_3$ by N-donors on *cis*-$W(CO)_4\{P(OMe)_3\}_2$ also causes deshielding.

In the series of compounds *cis*-$W(CO)_4\{Ph_2P(CH_2)_nPPh_2\}$ and related species containing bidentate P ligands, the ^{183}W chemical shift is sensitive to the size of the chelate ring. Arguments relating to the chelate ring size and the associated interbond angles have been used to rationalize the trends [33,167].

(vi) Spin–spin coupling between ^{183}W and other nuclei

There have been many reports of spin–spin coupling of the ^{183}W nucleus to other nuclei. The majority of these couplings have been observed as weak satellite peaks which arise from coupling of the observed nucleus having close to 100 atom % natural abundance (e.g. ^{31}P, ^{19}F, ^{1}H) to the ^{183}W atom (N, 14.4 atom %). Sometimes coupling to ^{183}W is observed in ^{13}C spectra despite the low natural abundance of that nucleus. The coupling constants J_{W-X} ($X = {}^{31}P$, ^{19}F, ^{13}C, ^{1}H) have been used in a number of studies to obtain useful stereochemical information.

TABLE 32

Tungsten(0) compounds

Compound	Solvent	Chemical shift (ppm)	Ref.
$W(CO)_6$	THF (55°C)	−3483	33
	CH_2Cl_2	−3486	35
$W(CO)_5(PPh_3)$	CH_2Cl_2	−3276	35
$W(CO)_5\{PPh_2(CH{=}CH_2)\}$	CH_2Cl_2	−3314	35
$W(CO)_5\{PPh(CH{=}CH_2)_2\}$	CH_2Cl_2	−3341	35
$W(CO)_5(PBu^n_3)$	CH_2Cl_2	−3408	33
$W(CO)_5(PPh_2Me)$	CH_2Cl_2	−3308	141
$W(CO)_5(PMe_2Ph)$	CH_2Cl_2	−3320	141
$W(CO)_5(PPhH_2)$	C_6H_6	−3414	141
$W(CO)_5\{P(OMe)_3\}$	neat liquid	−3469	33
$W(CO)_5(P(OPr^i)_3)$	CH_2Cl_2	−3410	33
$W(CO)_5\{P(OPh)_3\}$	CH_2Cl_2	−3410	33
$W(CO)_5\{PCl_2(OMe)\}$	C_6H_6	−3133	141
$W(CO)_5\{P(OMe)(OPh)_2\}$	$CDCl_3$	−3427	141
$W(CO)_5\{P(OMe)((OCH_2)_2CMe_2)\}$		−3456	141
$W(CO)_5\{PPh(OMe)_2\}$	C_6H_6	−3386	141
$W(CO)_5\{PPh_2(OMe)\}$	CH_2Cl_2	−3340	141
$W(CO)_5\{P(NMe_2)_3\}$	CH_2Cl_2	−3385	141
$W(CO)_5\{PPh_2(SnMe_3)\}$	C_6H_6	−3275	141
$W(CO)_5\{PPh(SnMe_3)_2\}$	C_6H_6	−3282	141
$W(CO)_5\{P(SnMe_3)_3\}$	C_6H_6	−3295	141
$(NEt_3H)[W(CO)_5\{P(O)(OMe_2)_2\}]$	C_6H_6	−3431	141
trans-$W(CO)_4\{P(OMe)_3\}_2$	CH_2Cl_2	−3427	141
cis-$W(CO)_4\{P(OMe)_3\}_2$	CH_2Cl_2/C_6D_6	−3401	33
cis-$W(CO)_4(py)\{P(OMe)_3\}$	C_6H_6	−2641	141
cis-$W(CO)_4(NCPh)\{P(OMe)_3\}$	C_6H_6	−2963	141
cis-$W(CO)_4(Mepy)\{P(OMe)_3\}$	C_6H_6	−2654	141
cis-$W(CO)_4\{P(OMe)_3\}\{S(SnMe_3)_2\}$	C_6H_6	−2918	141
trans-$W(CO)_4(PBu^n_3)_2$	CH_2Cl_2	−3125	140
cis-$W(CO)_4(PMe_2Ph)_2$	CH_2Cl_2	−3111	141
cis-$W(CO)_4(PBu^n_3)_2$	CH_2Cl_2	−2812	141
trans-$W(CO)_2\{P(OMe)_3\}_4$	CH_2Cl_2/C_6D_6	−3207	33
fac-$W(CO)_3(PMe_2Ph)$	CH_2Cl_2	−2812	141
fac-$W(CO)_3\{PPh(CH_2CH_2PPh_2)_2\}$	CH_2Cl_2/C_6D_6	−3255	33
fac-$W(CO)_3\{P(OMe)_3\}_3$	CH_2Cl_2/C_6D_6	−3297	33
cis-$W(CO)_4(Ph_2PNHPPh_2)$	CH_2Cl_2/C_6D_6	−3002	167
cis-$W(CO)_4$(dppm)	CH_2Cl_2/C_6D_6	−2957	33, 167
cis-$W(CO)_4$(dppe)	CH_2Cl_2/C_6D_6	−3291	33, 167
cis-$W(CO)_4$(dppp)	CH_2Cl_2/C_6D_6	−3158	33, 167
cis-$W(CO)_4(Ph_2P(CH_2)_4PPh)$	CH_2Cl_2/C_6D_6	−3117	167
cis-$W(CO)_4(Ph_2PCH_2PPr^i_2)$	CH_2Cl_2/C_6D_6	−3060	33
cis-$W(CO)_4(Ph_2PCH_2PBu^t_2)$	CH_2Cl_2/C_6D_6	−2980	33
cis-$W(CO)_4(Ph_2PCH_2PPhPr^i)$	CH_2Cl_2/C_6D_6	−3015	33

TABLE 32 (continued)

Compound	Solvent	Chemical shift (ppm)	Ref.
cis-$W(CO)_4(Ph_2PCH_2PMe_2)$	CH_2Cl_2/C_6D_6	−2979	33
cis-$W(CO)_4(Ph_2PCH_2PMePh)$	CH_2Cl_2/C_6D_6	−2987	33
cis-$W(CO)_4\{CH_2{=}C(PPh_2)_2\}$	CH_2Cl_2/C_6D_6	−3007	33, 167
cis-$W(CO)_4(Ph_2PCH{=}CHPPh_2)$	CH_2Cl_2/C_6D_6	−3333	33, 167
cis-$W(CO)_4\{CH(PPh_2)_3\}$	CH_2Cl_2/C_6D_6	−2929	33
cis-$W(CO)_4\{Ph_2P(S)CH_2PPh_2\}$	CH_2Cl_2/C_6D_6	−2859	33
cis-$W(CO)_4\{Ph_2P(S)CH_2PMe_2\}$	CH_2Cl_2/C_6D_6	−2878	33
cis-$W(CO)_4\{Ph_2P(S)CH_2PPr^i_2\}$	CH_2Cl_2/C_6D_6	−2933	33
cis-$W(CO)_4\{Ph_2P(S)CH_2PPhPr^i\}$	CH_2Cl_2/C_6D_6	−2898	33
cis-$W(CO)_4\{Ph_2P(Se)CH_2PPh_2\}$	CH_2Cl_2/C_6D_6	−2910	33

The recent direct measurement of the ^{183}W resonances in the polyoxotungstate species (Section F(i)) has highlighted the use of $^2J_{W-O-W}$ coupling constants to define the structures of certain of these compounds in solution. However, very few coupling constants have been derived from direct observation of the ^{183}W resonance. The discussion which follows is not intended to afford an exhaustive compilation of the coupling constants of ^{183}W to other nuclei. The ranges of various one-bond ^{183}W–X couplings (X = H, C, F, P) which were observed prior to 1978 have been reviewed [168].

(a) ^{183}W–^{31}P coupling

A large number of $^1J_{W-P}$ coupling constants have been measured. Several comprehensive reviews cover the literature through 1978 [168–171]. $^1J_{W-P}$ is normally in the range of 200 to 500 Hz but there are several compounds whose coupling constants are outside this range [141,172]. For example, the unusually small values of 155 Hz (R = Ph) and 145 Hz ($R = CO_2Me$) for $W(C{=}CHR)(CO)_3(dppe)$ are attributed to the strong *trans* influence of the vinylidene ligands.

A recent comprehensive study of a series of W(0)– and Mo(0)–phosphine complexes indicated that $^1J_{W-P}$ closely parallels $^1J_{Mo-P}$ in that the same trends are observed in corresponding series of compounds. The experimental ratio $^1J_{W-P}/^1J_{Mo-P}$ is 1.76 which corresponds to a ratio for the reduced coupling constants $^1K(WP)/^1K(MoP)$ of 2.76 [33]. $^1J_{W-P}$ is positive in octahedral W(0) compounds [173].

(b) ^{183}W–^{19}F coupling

The ^{183}W NMR spectrum of WF_6 consists of a septet (1 : 6 : 15 : 20 : 15 : 6 : 1) as expected for coupling between the ^{183}W nucleus and the six equivalent

^{19}F atoms, with $^1J_{W-F} = 40.7$ Hz [138]. Several studies of compounds in which one or more of the fluorine atoms in WF_6 are replaced by ligands containing oxygen donor atoms has shown that $^1J_{W-F}$ varies from 12 to 71 Hz and is dependent on the number of fluorine atoms replaced, the stereochemistry of the resulting species, and the nature of the coordinated ligand [32,174]. For other systems, values outside this range are observed. For example, $^1J_{W-F}$ in $(NF_4)[W_2O_2F_9]$ is 84 Hz [175].

(c) $^{183}W-^{13}C$ coupling

A recent comprehensive review on ^{13}C NMR spectroscopy gives an excellent coverage of J_{W-C} coupling constants in W compounds which contain direct W–C bonds [176]. For $W(CO)_6$, $^1J_{W-C}$ has been reported as 124.5 and 126 Hz while it varies in substituted species from 102.5 Hz for a *trans* CO group in $W(CO)_5(CR_2)$ to 202.6 Hz for the carbonyl ligands of $CpW(CO)_2(CR)$. The tabulation [176] also includes $^1J_{W-C}$ couplings of W to the carbon atom in coordinated alkyls, coordinated carbenes ($^1J_{W-C}$ ranges from ca. 70 to 120 Hz, the value being dependent on the nature of other ligands) and carbynes ($^1J_{W-C}$ ranges from 168 to 230 Hz).

More recently the presence of bridging carbene and carbyne ligands has been established by the use of $^1J_{W-C}$ coupling constants, which appear to be in the approximate range 29–160 Hz for these species [177]. The $^1J_{W-C}$ couplings for $K_4[W(CN)_7H]$ and $K_5[W(CN)_7]$ are 62.9 and 57.3 Hz, respectively [178].

(d) $^{183}W-^1H$ coupling

$^1J_{W-H}$ couplings in the tungsten hydrides for bridging and terminal hydride ligands are normally observed in the range 28–80 Hz [168]. However, recent studies [179,180] have indicated that $^1J_{W-H}$ for bridging hydrides can lie outside this range.

G. CONCLUSION

(i) Chemical shifts

(a) General comments

Sections E and F present and discuss ^{95}Mo and ^{183}W NMR data for about 450 molybdenum and 140 tungsten compounds. Both nuclei are very sensitive to changes in chemical environment with the existing chemical shift ranges covering 7000 and 11000 ppm for ^{95}Mo (Fig. 9) and ^{183}W respectively.

Generally the chemical shift increases as the metal oxidation state increases. However, there is considerable overlap in the center of the chemical shift ranges. For ^{95}Mo in the range -1000 to $+1000$ ppm, there is at least one example for each oxidation state from Mo(0) to Mo(VI), with the

exception of Mo(III). Clearly, ^{95}Mo and ^{183}W NMR are not simple probes of oxidation state, but the growing data bases are providing starting points for empirical correlations. In several instances, the influence of solvent, temperature, concentration and pH have been assessed. Sufficient preliminary information is available to allow careful design of experiments to test existing theories of nuclear shielding for heavy nuclei.

(b) Nuclear shieldings of heavy nuclei

The factors contributing to the chemical shifts of heavy nuclei have been recently reviewed [159]. The effective field, B, experienced by a nucleus is related to the applied field, B_0, by eqn. (7) where σ, the shielding constant, represents the difference between the environment of the nucleus under examination and a bare nucleus. Thus σ is determined by the electronic distribution about the nucleus.

$$B = B_0(1 - \sigma) \tag{7}$$

A number of theoretical approaches to calculating the nuclear shielding tensor have been taken. The Ramsey equation (8) which separates the shielding into diamagnetic (σ^d) and paramagnetic (σ^p) components is the most common starting point [158], but this approach has the disadvantage that the values of σ^d and σ^p are origin dependent, and that a knowledge of all the excited states is required.

$$\sigma = \sigma^d + \sigma^p \tag{8}$$

Several molecular methods have been developed within the framework of an independent electron model to produce atomic shielding relationships which contain localized and non-localized diamagnetic and paramagnetic terms. The localized terms are by far the largest so that

$$\sigma = \sigma_A^d(\text{loc}) + \sigma_A^p(\text{loc}) \tag{9}$$

with

$$\sigma_A^d(\text{loc}) = \left(\frac{\mu_0 e^2}{12\pi m}\right) \sum_B^A P_{\mu\mu} \langle \mu | r_{A\mu}^{-1} | \mu \rangle \tag{10}$$

In eqn. (10) $P_{\mu\mu}$ is the charge density in atomic orbital μ that is an average distance r_A from nucleus A.

$$\sigma_A^p(\text{loc}) = \left(\frac{-\mu_0 e^2 \hbar^2}{6\pi m^2 \Delta\epsilon}\right)\left(\langle r^{-3}\rangle_{np} P_\mu + \langle r^{-3}\rangle_{nd} D_\mu\right) \tag{11}$$

In eqn. (11) *np* and *nd* refer to the valence p and d electrons and P_μ and D_μ represent, respectively, the p and d electron imbalance about nucleus A. For heavy nuclei, such as ^{95}Mo and ^{183}W, eqn. (11) is the dominant factor in the

changes in total nuclear shielding, i.e. chemical shift differences among compounds [184]. Note that σ_A^p(loc) has a negative sign, and hence deshields the nucleus.

The complexities of making molecular orbital calculations on atoms as large as molybdenum have precluded detailed calculations of the nuclear shielding for these molecules. However, analysis of the form of eqn. (11) suggests how the trends in chemical shifts might be analyzed if the explicit assumption (not necessarily justified) is made that the $\Delta\epsilon$ term can be separated from $(\langle r^{-3}\rangle_{np} P_\mu + \langle r^{-3}\rangle_{nd} D_\mu)$.

Since σ_a^p(loc) is inversely dependent upon the average excitation energy, $\Delta\epsilon$, the nuclear shielding for a series of related molecules will decrease as $\Delta\epsilon$ decreases. Such behavior is found for the $[MO_{4-n}S_n]^{2-}$ ions (M = Mo, W; n = 0–4; Tables 2 and 30) where the chemical shift increases with increasing n and the ions become increasingly highly colored, indicating a decrease in $\Delta\epsilon$. A more quantitative correlation holds for α-$[X^{n+}W_{12}O_{40}]^{(8-n)-}$ (Fig. 28). For these M(VI) complexes softer donor and X atoms lead to deshielding of the metal nucleus, and an increase in the chemical shift.

For several other series of compounds, however, the chemical shift changes show no correlation with $\Delta\epsilon$. For example, the six-coordinate complexes containing the $\{Mo(NO)_2\}^6$ group (Table 24) show small variations in $\Delta\epsilon$ that are not correlated with changes in the chemical shift. The chemical shifts of these compounds decrease as the ancillary ligands become softer and more effective at delocalizing electrons, thereby decreasing $\langle r^{-3}\rangle_{np}$ and $\langle r^{-3}\rangle_{nd}$.

It should be apparent from the above examples that addition of soft polarizable ligands can result in either chemical shift increases or decreases (Fig. 23), depending upon the type of complex being studied. For compounds in different oxidation states the p and d electron imbalance (P_μ and D_μ respectively) may also differ, even though the ligands are similar. The chemical shift responses for several different classes of molybdenum compounds have been explicitly demonstrated by observing the dependence of the chemical shift to substitution of a single halogen atom.

(c) Halogen dependence of the chemical shift

Kidd [11] introduced the term halogen dependence to describe the response of the chemical shift to the sequential substitution of Cl by Br and I. Nuclear shielding which follows the order Cl < Br < I is called "normal halogen dependence", whereas the shielding order I < Br < Cl is called "inverse halogen dependence". An unusual feature of molybdenum compounds is that both kinds of halogen dependence are found. *cis*-Dioxomolybdenum(VI) complexes (Table 6) and six-coordinate $\{MoNO\}^4$ complexes (Table 23) exhibit inverse halogen dependence. Most other compounds,

TABLE 33

Summary of current ^{95}Mo NMR data

Class of complex	Oxidation state	Chemical shift range (ppm)	Linewidth range (Hz)	Halogen dependence	Table
$[MoX_4]^{2-}$ (X = O, S, Se)	+6	0 to 3150	0.3 to 10	–	2
Polyoxomolybdates	+6	−18 to 140	16 to 720	–	3
$[MoX_4(M'L)_n]^{2-}$ (M' = Cu^I, Ag^I)	+6	470 to 1925	15 to 1400	–	4
$MoX_2(ONR_2)_2$	+6	−230 to 1285	65 to 530	–	5
cis-$[MoO_2]^{2+}$	+6	−155 to 630	40 to 1170	inverse	6
$[MoO]^{4+}$	+6	−610 to 185	20 to 500	inverse	7
$[MoN]^{3+}$	+6	−120 to 1110	< 20 to 80	–	7
$[MoNPh]^{4+}$	+6	−295 to −220	400 to 480	inverse	7
$[MoO_3]$	+6	55 to 80	120 to 500	–	8
$[Mo_2O_2X_2]^{2+}$	+5	320 to 985	150 to 670	–	9
$[Mo_3O_4]^{4+}$	+4	990 to 1165	250 to 1400	–	10
$[Mo \equiv Mo]^{6+}$	+3	2420 to 3625	120 to 1320	–	11
$[Mo(CO)_3]^{2+}$	+2	−2075 to 200	25 to 300	normal	12, 13
$[Mo(CO)_2]^{2+}$	+2	−885 to 314	50 to 600	–	14, 15
$[Mo(CNR)_n]^{2+}$	+2	−1005 to +70	35 to 1100	normal	16
$[Mo \equiv Mo]^{4+}$	+2	3225 to 4150	220 to 1440	[a]normal	17
$[Mo(CO)_5]$	0	−1940 to −1385	5 to 190	normal	18
$[Mo(CO)_4]$	0	−1850 to −1050	5 to 400	–	19
$[Mo(CO)_3]$	0	−2125 to −865	4 to 850	–	20
$[Mo(CO)_2]$ and [Mo(CO)]	0	−1805 to −1080	100 to 1600	–	21
$[Mo(N_2)_2]$	0	−1025 to −445	90 to 100	–	22
$\{MoNO\}^4$	–	−370 to 2275	390 to 2000	inverse	23
$\{MoNO\}^6$	–	−1585 to −435	< 40 to 110	–	23
$\{Mo(NO)_2\}^6$	–	−985 to +205	20 to 435	normal	24

[a] Mainly elevated *T*.

including those of Mo(II) and Mo(0), show normal halogen dependence. Table 33 and Fig. 9 summarize the ^{95}Mo chemical shift data for various classes of molybdenum compounds. Table 33 also gives the halogen dependence for each class, if known.

Kidd [11] has suggested that inverse halogen dependence of the chemical shift occurs for elements with valence shell electron configurations which are less than half-filled, whereas normal halogen dependence will occur for other elements. It is interesting to note that the $5s^14d^5$ electron configuration of molybdenum would have both the *s* and *d* orbitals exactly half-filled.

(d) Shielding sensitivity

The shielding sensitivity is defined [11] as the ratio of chemical shifts for

analogous compounds of two different elements, and should be given by eqn. 12 for ^{183}W and ^{95}Mo.

$$\frac{\delta(W)}{\delta(Mo)} = \frac{\Delta\epsilon(Mo)}{\Delta\epsilon(W)} \left[\frac{\langle r^{-3} \rangle 6p_W P_{\mu W} + \langle r^{-3} \rangle 5d_W D_{\mu W}}{\langle r^{-3} \rangle 5p_{Mo} P_{\mu Mo} + \langle r^{-3} \rangle 4d_{Mo} D_{\mu Mo}} \right] \quad (12)$$

It is striking that this ratio is remarkably constant at 1.7 ± 0.2 for an extensive and disparate series [33,56] of M(0) and M(VI) species (e.g. Fig. 34) and some M(II) derivatives. Attempts to rationalize this constancy using eqn. (12) have not been particularly successful, and it may be that the assumptions introduced to produce the working equation are simply not justified in the present systems [33,56]. In addition, it has recently been observed that the ratio ranges from 1.1 to 20 for M(II)-isocyanide complexes and is highly dependent upon the reference chosen for the chemical shift comparisons [29].

In summary, while the assumption that the ratio is between 1 and 2 has been useful in searching for new ^{183}W signals, especially in reaction mixtures, it seems unwise to predict ^{183}W chemical shifts from the ^{95}Mo shifts for species of intermediate oxidation state.

(ii) Spin–spin coupling constants

The use of ^{183}W–O–^{183}W coupling observed in 1D and 2D ^{183}W spectra to provide definitive structural assignments in solution (Sections F(i)(a) and F(i)(b)) is a major development in polyoxometallate chemistry. Well-resolved coupling of ^{95}Mo to ^{31}P (Section E(xi)(a) and Fig. 21, for example) is of similar utility in organometallic chemistry. Theoretical rationalization of trends and magnitudes of coupling constant data is at an early stage of development.

(iii) Linewidths and relaxation times

It has been confirmed experimentally (Section E(xii)) that the quadrupole relaxation mechanism determines the ^{95}Mo relaxation rate in $Mo(CO)_6$ and it can safely be assumed to dominate in molecules of lower symmetry. This legitimizes previous rationalizations of experimental linewidths.

Detailed relaxation time data for the ^{183}W nucleus are available for WF_6 only [138].

(iv) Solid-state NMR

High resolution solid state measurements on molybdenum and tungsten compounds have yet to be reported in the literature. A recent experiment

[181] indicates that line-broadening due to chemical-shift anisotropy in solid $W(CO)_6$ is not excessive (δ, -3440 ppm; $W_{1/2}$, 500 Hz at 16.67 MHz). Recently considerable progress has been made [182] in the development of high resolution solid-state NMR of quadrupole nuclei such as ^{17}O, ^{23}Na, ^{27}Al and ^{51}V, and prospects are good for extension to ^{95}Mo despite its relatively low sensitivity and resonance frequency.

ACKNOWLEDGEMENTS

M.M. and J.H.E. thank Dr. K. Christensen for helpful technical discussions, Dr. C.G. Young for critically reading the manuscript, A. Cisco for technical assistance and R. Redmond and L. Ruiz for some of the drawings. Support by the U.S. Department of Agriculture (Grant No. 81-CRCR-1-0626) is gratefully acknowledged. Samples of molybdenum compounds were generously supplied by Professors Brunner, Dehnicke, Garner, McCleverty, Spence, Walton and Wieghardt and by Drs. C. Jones, E. Kober and J. Wachter. R.T.C.B., M.J.O.'C. and A.G.W. thank the Australian Research Grants Scheme and the Australian Wool Corporation for generous support and B.P. Shehan for many helpful discussions.

Note Added in Proof, September 1985

Several papers on the nuclear magnetic resonance properties of Group 6 metals have appeared since the original compilation of data for this review. Some features of Group 6 NMR are discussed in two more general reviews [187,188]. Probe ringing has been removed from ^{95}Mo NMR spectra by making the measurements at two different radiofrequency fields [189]. Comparison of the relaxation times of $[M(CO)_6]^{0,-}$ (M = Cr, Mo) species has permitted construction of a self-consistent set of quadrupole moments for ^{53}Cr, ^{95}Mo and ^{97}Mo. The results confirm the values for ^{95}Mo and ^{97}Mo listed in Table 1, but suggest that for ^{53}Cr, $|Q| = 0.041 \times 10^{-28}$ m^2 [190]. The binding of MoS_4^{2-} to bovine serum albumin decreases the ^{95}Mo chemical shift and increases the linewidth from < 1 to ca. 100 Hz. [190]. Several compounds containing the $[Mo_2O_5]^{2+}$ core have been characterized by ^{95}Mo NMR [192–194], supplementing the single result in Table 6 [128]. A ^{95}Mo NMR survey of polyoxomolybdates in aqueous solution [195] complements earlier results [60]; broad lines (250-2610 Hz) were observed [194]. The first detailed ^{95}Mo NMR study of mononuclear oxo–Mo(IV) complexes has revealed broad lines and chemical shifts in the range 1000–3200 ppm [70], several thousand ppm more deshielded than previously suggested [16,86]. The conformational isomers of CpMo(X)(Y)(allyl) compounds in solution have been established by ^{95}Mo NMR [196]. The ^{95}Mo NMR chemical shifts

of $[Mo(CO)_5X]^-$ anions show normal halogen dependence as X is varied [197]. Diamagnetic tetranuclear homo- and heterometallic cubane complexes containing molybdenum [198] exhibit sharp ^{95}Mo resonances in the -130 to -1620 ppm region [92]. The ^{95}Mo and ^{97}Mo spectra of MoF_6 have been investigated in both the liquid and solid phases. The liquid spectra are septets with $J_{Mo-F} = 47.2$ Hz [199]. The solid state structure of the first mercury(I)-containing polytungstate, $[(Hg_2)_2WO(H_2O)(AsWgO_{33})_2]^{10-}$ was confirmed in Me_2SO solution by ^{183}W NMR [200]. The ^{183}W spectra of the two-electron reduced diamagnetic heteropoly blue anions, α-$[P_2Mo_3W_{15}O_{62}]^{8-}$ and α-$[P_2W_{18}O_{62}]^{8-}$, have shown that these anions retain the Wells–Dawson structure (Fig. 32(a)) of their oxidized parents. The extra electrons are delocalized over the Mo_3O_{13} cap and the twelve "belt" tungsten atoms, respectively. Also reported are the first ^{183}W relaxation times for polyoxotungstate systems. For α-$[P_2W_{18}O_{62}]^{8-}$ at 26°C the relaxation time of the capping tungsten atoms (276 ms) is 12 times larger than that for the belt tungsten atoms (23.4 ms) [201].

REFERENCES

1 F.A. Cotton and G. Wilkinson, Advanced Inorganic Chemistry, 4th edn., Wiley-Interscience, New York, 1980, pp. 719, 844.
2 C.L. Rollinson, in A.F. Trotman-Dickenson, (exec. Ed.), Comprehensive Inorganic Chemistry, Pergamon, Oxford, Vol. 3, 1973, p. 623.
3 G. Wilkinson, F.G.A. Stone and E.W. Abel (eds.), Comprehensive Organometallic Chemistry, Pergamon, New York, Vol. 3, 1982.
4 E.I. Stiefel, Prog. Inorg. Chem., 22 (1977) 1.
5 Z. Dori, Prog. Inorg. Chem., 28 (1981) 239.
6 M.T. Pope, Heteropoly and Isopoly Oxometalates, Springer-Verlag, Berlin, 1983.
7 M. Coughlan (Ed.), Molybdenum and Molybdenum-containing Enzymes, Pergamon, Oxford, 1980.
8 S.P. Cramer and K.O. Hodgson, Prog. Inorg. Chem., 25 (1979) 1.
9 R.G. Kidd and R.J. Goodfellow, in Harris, R.K. and B.E. Mann (Eds.), NMR and the Periodic Table, Academic Press, London, 1978, p. 212.
10 F.W. Wehrli, Annu. Rep. NMR Spectrosc., 9A (1979) 146.
11 R.G. Kidd, Annu. Rep. NMR Spectrosc., 10A (1979) 19.
12 P.L. Rinaldi, G.C. Levy and G.R. Choppin, Rev. Inorg. Chem., 2 (1980) 53.
13 J.H. Enemark, in A. Müller and W.E. Newton (Eds.), Nitrogen Fixation: The Chemical–Biochemical–Genetic Interface, Plenum Press, New York, 1983, p. 329.
14 R.G. Kidd, in J.B. Lambert and F.G. Riddell (Eds.), The Multinuclear Approach to NMR Spectroscopy, Reidel, Dordrecht, 1983, p. 445.
15 (a) A. Abragam, The Principles of Nuclear Magnetism, Oxford University Press, London, 1961, p. 314.
(b) R.K. Harris, in R.K. Harris and B.E. Mann (Eds.), NMR and the Periodic Table, Academic Press, London, 1978, p. 17.
16 S.F. Gheller, T.W. Hambley, R.T.C. Brownlee, M.J. O'Connor, M.R. Snow and A.G. Wedd, J. Am. Chem. Soc., 105 (1983) 1527.

17 (a) W.G. Klemperer, Angew. Chem. Int. Ed. Engl., 17 (1978) 246.
(b) J.A. Gerlt, P.C. Demou and S. Mehdi, J. Am. Chem. Soc., 104 (1982) 2848.
(c) S. Forsen and B. Lindman, Annu. Rep. NMR Spectrosc., 11A (1981) 183.
(d) R.T.C. Brownlee, M. Sadek and D.J. Craik, Org. Magn. Reson., 21 (1983) 616.
18 R.R. Vold and R.L. Vold, J. Magn. Reson., 19 (1975) 365 and references therein.
19 O. Lutz, A. Nolle and P. Kroneck, Z. Naturforsch., Teil A, 32 (1977) 505.
20 P.B. Shehan, R.T.C. Brownlee, M. Kony, M.J. O'Connor and A.G. Wedd, J. Magn. Reson., 63 (1985) 343.
21 C. Brevard in P. Laszlo (Ed.), NMR of Newly Accessible Nuclei, Academic Press, New York, Vol. 1, 1983, p. 3.
22 T.C. Farrar and E.D. Becker, Pulse and Fourier Transform NMR, Academic Press, New York, 1971.
23 K.A. Christensen, P.E. Miller, M. Minelli, T.W. Rockway and J.H. Enemark, Inorg. Chim. Acta, 56 (1981) L27.
24 K.A. Christensen, M. Minelli and J.H. Enemark, unpublished results.
25 E. Fukushima and S.B.W. Roeder, Experimental Pulse NMR, A Nuts and Bolts Approach, Addison-Wesley, Reading, MA, 1981, p. 463.
26 (a) S. Forsen and B. Lindman, Ion Binding in Biological Systems Measured by Nuclear Magnetic Resonance, in D. Glick, (Ed.), Methods of Biochemical Analysis, Wiley, New York, 1981.
(b) T. Andersson, T. Drakenberg, S. Forsen, E. Thulin and M. Swärd, J. Am. Chem. Soc., 104 (1982) 576.
27 (a) E. Hofer, W. Holzbach and K. Wieghardt, Angew. Chem., Int. Ed. Engl., 20 (1981) 282.
(b) K. Wieghardt, M. Hahn, J. Weiss and W. Swiridoff, Z. Anorg. Allg. Chem., 492 (1982) 164.
28 M. Minelli, J.L. Hubbard and J.H. Enemark, Inorg. Chem., 23 (1984) 970.
29 M. Minelli, A. Bell, J.H. Enemark and R.A. Walton, J. Organomet. Chem., 284 (1985) 25.
30 M. Minelli, C.G. Young and J.H. Enemark, Inorg. Chem., 24 (1985) 1111.
31 D.I. Hoult in G.C. Levy (Ed.), Topics in C-13 NMR Spectroscopy, Vol. III, Wiley, New York, 1979, p. 16.
32 W. McFarlane, A.M. Noble and J.M. Winfield, J. Chem. Soc. A, (1971) 948.
33 G.T. Andrews, I.J. Colquhoun, W. McFarlane and S.O. Grim, J. Chem. Soc. Dalton Trans., (1982) 2353.
34 C. Brevard and R. Schimpf, J. Magn. Reson., 47 (1982) 528.
35 R.L. Keiter and D.G. Van der Velde, J. Organomet. Chem., 258 (1983) C34.
36 Y. Egozy and A. Loewenstein, J. Magn. Reson., 1 (1969) 494.
37 B.W. Epperlein, H. Krüger, O. Lutz, A. Nolle and W. Mayr, Z. Naturforsch., Teil A, 30 (1975) 1237.
38 E. Haid, D. Köhnlein, G. Kössler, O. Lutz and W. Schich, J. Magn. Reson., 55 (1983) 145.
39 O. Lutz, W. Nepple, and A. Nolle, Z. Naturforsch., Teil A, 31 (1976) 1046.
40 R.G. Kidd, J. Magn. Reson., 45 (1981) 88.
41 W. Ertmer, U. Johann and R. Mosmann, Z. Phys. A, 309 (1982) 1.
42 (a) W.G. Proctor and F.C. Yu, Phys. Rev., 81 (1951) 20.
(b) S.I. Aksenov, Soviet Phys. JETP, 8 (1959) 207.
43 T.J. Rowland, Prog. Math. Sci., 1 (1961) 9.
44 J. Kaufmann, Z. Phys., 182 (1964) 217.

45 A. Narath and D.W. Alderman, Phys. Rev., 143 (1966) 328.
46 H. Krüger, O. Lutz, A. Nolle and A. Schwenk, Z. Naturforsch., Teil A, 28 (1973) 119.
47 A. Narath, K.C. Brog and W.H. Jones, Jr., Phys. Rev. B, 2 (1970) 2618.
48 G.F. Lynch and S.L. Segal, Can. J. Phys., 50 (1972) 567.
49 W.D. Kautt, H. Krüger, O. Lutz, H. Maier and A. Nolle, Z. Naturforsch., Teil A, 31 (1976) 351.
50 O. Lutz, A. Nolle and P. Kroneck, Z. Naturforsch., Teil A, 31 (1976) 454.
51 K.U. Buckler, A.R. Haase, O. Lutz, M. Müller and A. Nolle, Z. Naturforsch., Teil A, 32 (1977) 126.
52 O. Lutz, A. Nolle and P. Kroneck, Z. Phys. A, 282 (1977) 157.
53 P. Kroneck, O. Lutz and A. Nolle, Z. Naturforsch., Teil A, 35 (1980) 226.
54 A.F. Masters, R.T.C. Brownlee, M.J. O'Connor, A.G. Wedd and J.D. Cotton, J. Organomet. Chem., 195 (1980) C17.
55 R.R. Vold and R.L. Vold, J. Chem. Phys., 61 (1974) 4360.
56 S.F. Gheller, T.W. Hambley, J.R. Rodgers, R.T.C. Brownlee, M.J. O'Connor, M.R. Snow and A.G. Wedd, Inorg. Chem., 23 (1984) 2519.
57 S.F. Gheller, P.A. Gazzana, A.F. Masters, R.T.C. Brownlee, M.J. O'Connor, A.G. Wedd, J.R. Rogers and M.R. Snow, Inorg. Chim. Acta, 54 (1981) L131.
58 M.T. Pope, Heteropoly and Isopoly Oxometalates, Springer Verlag, Berlin, 1983, pp. 42–44.
59 M.A. Freeman, F.A. Schultz and C.N. Reilley, Inorg. Chem., 21 (1982) 567.
60 S.F. Gheller, M. Sidney, A.F. Masters, R.T.C. Brownlee, M.J. O'Connor and A.G. Wedd, Aust. J. Chem., 37 (1984) 1825.
61 M. Filowitz, R.K.C. Ho, W.G. Klemperer and W. Shum, Inorg. Chem., 18 (1979) 93.
62 A.F. Masters, S.F. Gheller, R.T.C. Brownlee, M.J. O'Connor and A.G. Wedd, Inorg. Chem., 19 (1980) 3866.
63 A. Müller, E. Diemann, R. Jostes and H. Bögge, Angew. Chem. Int. Ed. Engl., 20 (1981) 934.
64 A.G. Wedd, in A. Müller and R. Krebbs (Eds.), Sulfur: Its Significance for Chemistry, the Geo-, Bio- and Cosmo-spheres and Technology, Elsevier, Amsterdam, 1984, p. 181.
65 L. Maier and L.C.D. Groenweghe, J. Chem. Eng. Data, 7 (1962) 307.
66 S.R. Acott, C.D. Garner, J.R. Nicholson, and W. Clegg, J. Chem. Soc. Dalton Trans., (1983) 713.
67 M. Minelli, J.H. Enemark, J.R. Nicholson and C.D. Garner, Inorg. Chem., 23 (1984) 4384.
68 S.F. Gheller, T.W. Hambley, P.R. Traill, R.T.C. Brownlee, M.J. O'Connor, M.R. Snow and A.G. Wedd, Aust. J. Chem., 35 (1982) 2183.
69 S. Bristow, D. Collison, C.D. Garner and W. Clegg, J. Chem. Soc. Dalton Trans., (1983) 2495.
70 C.G. Young and J.H. Enemark, Inorg. Chem., in press.
71 M. Minelli, J.H. Enemark, K. Wieghardt and M. Hahn, Inorg. Chem., 22 (1983) 3952.
72 P.R. Traill, M.J. O'Connor and A.G. Wedd, unpublished observations.
73 M. Minelli, K. Yamanouchi, J.H. Enemark, P. Subramanian, B.B. Kaul and J.T. Spence, Inorg. Chem., 23 (1984) 2554.
74 E.C. Alyea and J. Topich, Inorg. Chim. Acta, 65 (1982) L95.
75 I. Buchanan, C.G. Garner and W. Clegg, J. Chem. Soc. Dalton Trans., (1984) 1333.
76 R.W.K. Lee, N.C. Howlader, G.P. Haight and E. Oldfield, unpublished results.
77 I. Buchanan, M. Minelli, M.T. Ashby, T.J. King, J.H. Enemark and C.D. Garner, Inorg. Chem., 23 (1984) 495.

78 S.P. Cramer, R. Wahl and K.V. Rajagopalan, J. Am. Chem. Soc., 103 (1981) 7721.
79 S.P. Cramer, L.P. Solomonson, M.W.W. Adams and L.E. Mortenson, J. Am. Chem. Soc., 106 (1984) 1467.
80 K. Yamanouchi and J.H. Enemark, Inorg. Chem., 18 (1979) 1626.
81 D.L. Kepert, Prog. Inorg. Chem., 23 (1977) 1.
82 E.I. Stiefel, K.F. Miller, A.E. Bruce, J.L. Corbin, J.M. Berg and K.O. Hodgson, J. Am. Chem. Soc., 102 (1980) 3624.
83 S. Bristow, J.H. Enemark, C.D. Garner, M. Minelli, G.A. Morris and R.B. Ortega, Inorg. Chem., in press.
84 M. Postel, C. Brevard, H. Arzoumanian and J.G. Riess, J. Am. Chem. Soc., 105 (1983) 4922.
85 S.F. Gheller, M.J. O'Connor and A.G. Wedd, unpublished results.
86 S.F. Gheller, R.T.C. Brownlee, M.J. O'Connor and A.G. Wedd, in H.F. Barry and P.C.H. Mitchell (Eds.), Proceedings of the Fourth International Conference on the Chemistry and Uses of Molybdenum, Climax Molybdenum Co., Ann Arbor, MI, 1982, p. 67.
87 K. Wieghardt, M. Guttmann, P. Chaudhuri, W. Gebert, M. Minelli, C.G. Young and J.H. Enemark, Inorg. Chem., in press.
88 I. Buchanan, W. Clegg, C.D. Garner and G.M. Sheldrick, Inorg. Chem., 22 (1983) 3657.
89 K. Wieghardt, M. Hahn, W. Swiridoff and J. Weiss, Inorg. Chem., 23 (1984) 94.
90 R.K. Murmann and M.E. Shelton, J. Am. Chem. Soc., 102 (1980) 3984.
91 S.P. Cramer, P.K. Eidem, M.T. Paffett, J.R. Winkler, Z. Dori and H.B. Gray, J. Am. Chem. Soc., 105 (1983) 799.
92 C.G. Young, M. Minelli, J.H. Enemark, G. Miessler, N. Janietz, H. Kauermann and J. Wachter, Polyhedron, in press.
93 J.Y. LeGall, M.M. Kubicki and F.Y. Petillon, J. Organomet. Chem., 221 (1981) 287.
94 R.T.C. Brownlee, A.F. Masters, M.J. O'Connor, A.G. Wedd, H.A. Kimlin and J.D. Cotton, Org. Magn. Reson., 20 (1982) 73.
95 G. Backes-Dahmann, W. Hermann, K. Wieghardt and J. Weiss, Inorg. Chem., 24 (1985) 485.
96 S. Lincoln, S.-L. Soong, S.A. Koch, M. Sato and J.H. Enemark, Inorg. Chem., 24 (1985) 1355.
97 H. Brunner, P. Beier, E. Frauendorfer, M. Muschiol, D.K. Rastogi, J. Wachter, M. Minelli and J.H. Enemark, Inorg. Chim. Acta, 96 (1985) L5.
98 H. Brunner, Adv. Organomet. Chem., 19 (1980) 151.
99 M. Minelli, T.W. Rockway, J.H. Enemark, H. Brunner and M. Muschiol, J. Organomet. Chem., 217 (1981) C34.
100 H. Brunner and D.K. Rastogi, Inorg. Chem., 19 (1980) 891.
101 S. Dysart, I. Georgii and B.E. Mann, J. Organomet. Chem., 213 (1981) C10.
102 M. Minelli, J.H. Enemark and E. Kober, unpublished results.
103 R.J. Klinger, W. Butler and M.D. Curtis, J. Am. Chem. Soc., 97 (1975) 3535.
104 R.D. Adams, D.M. Collins and F.A. Cotton, Inorg. Chem., 13 (1974) 1086.
105 A.F. Masters, G.E. Bossard, T.A. George, R.T.C. Brownlee, M.J. O'Connor and A.G. Wedd, Inorg. Chem., 22 (1983) 908.
106 E.C. Alyea, A. Somogyvari, in H.F. Barry and P.C.H. Mitchell (Eds.), Proceedings of the Climax Fourth International Conference on the Chemistry and Uses of Molybdenum, Climax Molybdenum Company, Ann Arbor, MI, 1982, p. 46.
107 E.C. Alyea and A. Somogyvari, Inorg. Chim. Acta, 83 (1984) L49.
108 G.M. Gray and R.J. Gray, Organometallics, 2 (1983) 1026.

109 G.M. Gray, Inorg. Chim. Acta, 81 (1984) 157.
110 P. Jaitner and M. Wohlgenannt, Monatsh. Chem., 113 (1982) 699.
111 G.M. Gray and C.S. Kraihanzel, Inorg. Chem., 22 (1983) 2959.
112 A.F. Masters, R.T.C. Brownlee, M.J. O'Connor and A.G. Wedd, Inorg. Chem., 20 (1981) 4183.
113 M. Minelli, C.G. Young, J.H. Enemark and K. Wieghardt, unpublished results.
114 M. Minelli, J.H. Enemark and K. Wieghardt, unpublished results.
115 S. Donovan-Mtunzi, M. Hughes, G.J. Leigh, H.M. Ali, R.L. Richards and J. Mason, Organomet. Chem., 246 (1983) C1.
116 M. Minelli, J.L. Hubbard, K.A. Christensen and J.H. Enemark, Inorg. Chem., 22 (1983) 2652.
117 M. Minelli, J.L. Hubbard, D.L. Lichtenberger and J.H. Enemark, Inorg. Chem., 23 (1984) 2721.
118 C.G. Young, M. Minelli, J.H. Enemark, W. Hussain, C.J. Jones and J.A. McCleverty, manuscript in preparation.
119 J.H. Enemark and R.D. Feltham, Coord. Chem. Rev., 13 (1974) 305.
120 M.M. Kubicki, R. Kergoat, J.Y. LeGall, J.E. Guerchais, J. Douglade and R. Mecier, Aust. J. Chem., 35 (1982) 1543.
121 P.S. Braterman, D.W. Milne, E.W. Randall and E. Rosenberg, J. Chem. Soc. Dalton Trans., (1973) 1027.
122 O.A. Gansow, B.Y. Kimura, G.R. Dobson and R.A. Brown, J. Am. Chem. Soc., 93 (1971) 5922.
123 B.E. Mann, J. Chem. Soc. Dalton Trans. (1973) 2012.
124 E.C. Alyea, R.E. Lenkinski, A. Somogyvari, Polyhedron, 1 (1982) 130.
125 J.T. Bailey, R.J. Clark and G.C. Levy, Inorg. Chem., 21 (1982) 2085.
126 G.M. Gray, R.J. Gray and D.C. Berndt, J. Magn. Reson., 57 (1984) 347.
127 M.T. Ashby and D.L. Lichtenberger, Inorg. Chem., 24 (1985) 636.
128 B. Piggott, R.N. Sheppard and D.J. Williams, Inorg. Chim. Acta, 86 (1984) L65.
129 R.T.C. Brownlee, M.J. O'Connor, B.P. Shehan and A.G. Wedd, J. Magn. Reson., 61 (1985) 22.
130 R.T.C. Brownlee, M.J. O'Connor, B.P. Shehan and A.G. Wedd, J. Magn. Reson., 61 (1985) 516.
131 C. Deverell, Mol. Phys., 18 (1970) 319.
132 A. Nolle, Z. Phys. A, 280 (1977) 231.
133 G.R. Hanson, G.R. Pullen, S.F. Gheller, G.R. Wilson, T.D. Bailey, C.R. Rodrigues, R.S. Scopes, R.T.C. Brownlee, M.J. O'Connor and A.G. Wedd, unpublished observations.
134 M. Minelli, J.H. Enemark and R.C. Bray, unpublished observations.
135 P.B. Sogo and C.D. Jeffries, Phys. Rev., 98 (1955) 1316.
136 A. Narath, K.C. Brog and W.H. Jones, Jr., Phys. Rev., B2 (1970) 2618.
137 A. Narath and D.C. Wallace, Phys. Rev., 127 (1962) 724.
138 J. Banck and A. Schwenk, Z. Physik., Teil B, 20 (1975) 75.
139 M.P. Klein and J. Happe, Bull. Am. Phys. Soc., 6 (1961) 104.
140 P.J. Green and T.H. Brown, Inorg. Chem., 10 (1971) 206.
141 H.C.E. McFarlane, W. McFarlane and D.S. Rycroft, J. Chem. Soc. Dalton Trans., (1976) 1616.
142 R. Acerete, C.F. Hammer and L.C.W. Baker, J. Am. Chem. Soc. 101 (1979) 267.
143 O.A. Gansow, R.K.C. Ho and W.G. Klemperer, J. Organomet. Chem., 187 (1980) C27.
144 P.R. Sethuraman, M.A. Leparulo, M.T. Pope, F. Zonnevijlle, C. Brevard and J. Lemerle, J. Am. Chem. Soc., 103 (1981) 7665; 104 (1982) 3782.

145 R. Acerete, C.F. Hammer and L.C.W. Baker, J. Am. Chem. Soc., 104 (1982) 5384.
146 R. Thouvenot, M. Fournier, R. Franck and C. Rocchiccioli-Deltcheff, Inorg. Chem., 23 (1984) 598.
147 J. Lefebvre, F. Chauveau, P. Doppelt and C. Brevard, J. Am. Chem. Soc., 103 (1981) 4589.
148 (a) R. Acerete, Ph.O. Thesis, Georgetown University, 1981.
(b) Ref. 6, p. 13.
149 C. Brevard, R. Schimpf, G. Tourne and C.M. Tourne, J. Am. Chem. Soc., 105 (1983) 7059.
150 L.P. Kazansky and M.A. Fedotov, J. Chem. Soc. Chem. Commun., (1983) 417.
151 W.H. Knoth, P.J. Domaille and D.C. Roe, Inorg. Chem., 22 (1983) 198.
152 W. Malisch, R. Maisch, I.J. Colquhoun and W. McFarlane, J. Organomet. Chem., 220 (1981) C1.
153 R. Acerete, S. Harmalker, C.F. Hammer, M.T. Pope and L.C.W. Baker, J. Chem. Soc. Chem. Commun., (1979) 777.
154 R. Acerete, C.F. Hammer and L.C.W. Baker, Inorg. Chem., 23 (1984) 1478.
155 R.G. Finke, M. Droege, J.R. Hutchinson and O. Gansow, J. Am. Chem. Soc., 103 (1981) 1587.
156 R.G. Finke and M.W. Droege, Inorg. Chem., 22 (1983) 1006.
157 Ref. 6, pp. 25–27.
158 (a) N.F. Ramsey, Phys. Rev. 77 (1950) 567; 78 (1950) 699.
(b) C.J. Jameson and H.S. Gutowsky, J. Chem. Phys., 40 (1964) 1714.
(c) J.S. Griffith and L.E. Orgel, Trans. Faraday Soc., 53 (1957) 601.
159 G.A. Webb, in P. Laszlo (Ed.), NMR of Newly Accessible Nuclei, Vol. 1, Chemical and Biochemical Applications, Academic Press, New York, 1983, p. 3.
160 (a) R. Freeman, G.R. Murray and R.E. Richards, Proc. R. Soc. London, Ser. A, 242 (1957) 455.
(b) N. Juranic, M.B. Celap, D. Vucelic, M.J. Malinar and N. Radivojsa, J. Magn. Reson., 35 (1979) 319.
(c) D. Rehder, Bull. Magn. Reson., 4 (1982) 33.
(d) R. Bramley, M. Bronson, A.M. Sargeson and C.E. Schäffer, J. Am. Chem. Soc., 107 (1985) 2780.
161 R. Acerete, J.C. Bas, N. Casan, C.F. Hammer and L.C. W. Baker, 187th ACS National Meeting, St. Louis, Missouri, April 1984, Abstract 116.
162 P.J. Domaille and W.H. Knoth, Inorg. Chem., 22 (1983) 818.
163 Ref. 6, p. 59.
164 R. Massart, R. Contant, J-M. Fruchart, J-P. Ciabrini and M. Fournier, Inorg. Chem., 16 (1977) 2916.
165 A. McDonell, S. Vasudevan, M.J. O'Connor and A.G. Wedd, Aust. J. Chem., (1985) 38 (1985) 1017.
166 D.J. Santure, K.W. McLaughlin, J.C. Huffman and A.P. Sattelberger, Inorg. Chem., 22 (1983) 1877.
167 G.T. Andrews, I.J. Colquhoun and W. McFarlane, Polyhedron, 2 (1983) 783.
168 Ref. 15(b), pp. 216–217.
169 J.G. Verkade, Coord. Chem. Rev., 9 (1972) 1.
170 T.G. Appleton, H.C. Clark and L.E. Manzer, Coord. Chem. Rev., 10 (1973) 335.
171 P.S. Pregosin and R.W. Kunz, in P. Diehl, E. Fluck and R. Kosfeld (Eds.), NMR: Basic Principles and Progress, vol. 16, Springer Verlag, 1979.
172 K.R. Birdwhistell, S.J.N. Burgmayer and J.L. Templeton, J. Am. Chem. Soc., 105 (1983) 7789.

173 W. McFarlane and D.S. Rycroft, J. Chem. Soc. Chem. Commun., (1973) 336.
174 V.O. Leitzke and F. Sladky, Z. Anorg. Allgem. Chem., 480 (1981) 7.
175 W.W. Wilson and K.O. Christe, Inorg. Chem., 20 (1981) 4139.
176 B.E. Mann and B.F. Taylor, ^{13}C NMR Data for Organometallic Compounds, Academic Press, London, 1981.
177 (a) L. Busetto, J.C. Jeffery, R.M. Mills, F.G.A. Stone, M.J. Went and P. Woodward, J. Chem. Soc. Dalton Trans., (1983) 101 and references therein.
(b) M. Green, S.J. Porter and F.G.A. Stone, J. Chem. Soc. Dalton Trans., (1983) 513.
(c) G.M. Dawkins, M. Green, K.A. Mead, J-Y. Salaün, F.G.A. Stone and P. Woodward, J. Chem. Soc. Dalton Trans., (1983) 527 and references therein.
178 A.M. Soares, P.M. Kiernan, D.J. Cole-Hamilton and W.P. Griffith, J. Chem. Soc. Chem. Commun., (1981) 84.
179 (a) C-Y. Wei, M.W. Marks, R. Bau, S.W. Kirtley, D.E. Bisson, M.E. Henderson and T.F. Koetzle, Inorg. Chem., 21 (1982) 2556.
(b) J.T. Lin, G.P. Hagen and J.E. Ellis, J. Am. Chem. Soc., 105 (1983) 2296.
(c) J.T. Lin and J.E. Ellis, J. Am. Chem. Soc., 105 (1983) 6252.
180 (a) P.S. Pregosin, A. Togni and L.M. Venanzi, Angew. Chem. Intl. Ed. Engl., 20 (1981) 668.
(b) N.W. Alcock, O.W. Howarth, P. Moore and G.E. Morris, J. Chem. Soc. Chem. Commun., (1979) 1160.
(c) P.M. Boorman, K.J. Moynihan and K.A. Kerr, J. Chem. Soc. Chem. Commun., (1981) 1286.
181 C. Brevard, private communication.
182 (a) M.D. Meadows, K.A. Smith, R.A. Kinsey, T.M. Rothgeb, R.P. Skarjune and E. Oldfield, Proc. Natl. Acad. Sci. USA, 79 (1982) 1351.
(b) S. Schramm, R.J. Kirkpatrick and E. Oldfield, J. Am. Chem. Soc., 105 (1983) 2483.
183 Y. Jeannin and J. Martin-Frère, J. Am. Chem. Soc., 103 (1981) 1664.
184 H. Nakatsuji, K. Kanda, K. Endo and T. Yonezawa, J. Am. Chem. Soc., 106 (1984) 4653; K. Kanda, H. Nakatsuji and T. Yonezawa, J. Am. Chem. Soc., 106 (1984) 5888.
185 R.T.C. Brownlee, M.J. O'Connor, B.P. Shehan and A.G. Wedd, J. Magn. Reson., 64 (1985) 142.
186 M.T. Ashby and J.H. Enemark, J. Am. Chem. Soc., in press.
187 D. Rehder, Magn. Reson. Rev., 9 (1984) 125.
188 J.J. Dechter, Prog. Inorg. Chem., 33 (1985) 393.
189 G.A. Morris and M.J. Toohey, J. Magn. Reson., in press.
190 R.T.C. Brownlee and B.P. Shehan, J. Magn. Reson., in press.
191 S. Bristow, C.D. Garner, S.K. Hagyard, G.A. Morris, J.R. Nicholson and C.F. Mills, J. Chem. Soc. Chem. Commun., (1985) 479.
192 B. Piggott, S.D. Thorpe and R.N. Sheppard, Inorg. Chim. Acta, 103 (1985) L3.
193 M.V. Capparalli, B. Piggott, S.D. Thorpe, S.F. Wong and R.N. Shepard, Inorg. Chim. Acta, 106 (1985) 19.
194 B. Piggott, S.F. Wong and R.N. Shepard, Inorg. Chim. Acta, 107 (1985) 97.
195 M.A. Fedotov, Izv. Akad. Nauk. SSSR, Ser. Khim., (1984) 1166.
196 J.W. Faller and B.C. Whitmore, Organometallics, in press.
197 E.C. Alyea, A. Malek and J. Malito, Inorg. Chim. Acta, 101 (1985) 147.
198 H. Brunner, N. Janietz, J. Wachter, T. Zahn and M.L. Ziegler, Angew. Chem., Int. Ed. Engl., 24 (1985) 133.
199 F. Brunet, H. LeBail and J. Virlet, Ann. Chim. Fr., 9 (1984) 771.
200 J. Martin-Frère and Y. Jeannin, Inorg. Chem., 23 (1984) 3394.
201 M. Kozik, C.F. Hammer and L.C.W. Baker, J. Am. Chem. Soc., in press.